Title
Cosserat Curves: Descriptions of Peristalsis and a Discrete Model

Author
Hemingway, Evan

Publication Date
2020

Peer reviewed|Thesis/dissertation

Cosserat Curves: Descriptions of Peristalsis and a Discrete Model

by

Evan Grant Hemingway

A dissertation submitted in partial satisfaction of the

requirements for the degree of

Doctor of Philosophy

in

Engineering - Mechanical Engineering

in the

Graduate Division

of the

University of California, Berkeley

Committee in charge:

Professor Oliver O'Reilly, Chair
Professor James Casey
Professor Alexander Givental

Spring 2020

Cosserat Curves: Descriptions of Peristalsis and a Discrete Model

Abstract

Cosserat Curves: Descriptions of Peristalsis and a Discrete Model

by

Evan Grant Hemingway

Doctor of Philosophy in Engineering - Mechanical Engineering

University of California, Berkeley

Professor Oliver O'Reilly, Chair

In this work, problems and developments in the mechanics of slender, or rod-like bodies, are presented. We begin by offering a modern perspective on Green and Naghdi's developments of the latter half of the 20th century for a directed rod. This review serves as background material to the more novel parts of this dissertation, which include applications and a discretization of the continuous theory. Governing equations for rods are developed by derivation from three-dimensional continuum mechanics and by direct approach. A treatment of constraints is also presented.

After the background material is reviewed, we thoroughly describe a model for peristaltic locomotion using Green and Naghdi's directed rod theory. The resulting model is applied to simulating motions of a compressible soft robot which uses Poisson's effect for peristalsis. In addition, a calibration of parameters results in a validation of the model for use in biomimetic modeling of earthworm locomotion. Incompressibility of the worm is enforced as an internal constraint of the directed rod. In addition, a pair of muscle actuation models for a single continuum is included in our discussion.

Finally, a discrete model for elastic rods undergoing planar motions is presented based on the theory of the directed rod. Discrete edge vectors and directors are used to capture cross section deformations including stretch, stretch gradients, shear, shear gradients, and the Poisson effect. In addition, deformations such as longitudinal stretch and bending are also incorporated. The model is validated with the help of known analytical solutions to benchmark problems from Green and Naghdi's continuous rod theory.

To my family: James, Debra, Alexander, and Andrew.

Contents

List of Figures

List of Tables

Acknowledgments

I am grateful to my parents, James and Debra, for working tirelessly in a variety of jobs to support me during my childhood. They have set a model for me in their value for work ethic. My mother's job in the airline industry afforded me the opportunity to travel and see firsthand the diversity of ideas around the globe. This invaluable perspective has carried me through my time in graduate school and will continue to hold worth for me as I turn to the next chapter in life. I want to thank my brother Drew for his high expectations and incessantly pushing me to excel and become the best version of myself. In addition, I would like to thank my other brother, Alex, for his open mind and sharing his perspective when I needed it most. My entire family has especially supported me in times where I have found myself needing to deal with hardship during my graduate studies.

I want to thank my advisor, Oliver O'Reilly, for opening doors for me and allowing me to study under his guidance at UC Berkeley. When I first discovered Oliver's publications as a senior at Virginia Tech, I knew immediately that I would enjoy working with him. I remember feeling so privileged when I began my first year pursuing a Ph.D. at Berkeley in his lab. My experience has been everything that I wanted and more. The knowledge that I have absorbed from the professors at UC Berkeley is mine now. In addition to Professor O'Reilly, Professors James Casey and David Steigmann have revealed to me many of the fundamentals of mechanics. Nowhere in the industry would I have been able to be paid to learn at such depth. Thank you as well to Professor William Kier for the helpful dialogue on worm locomotion. I am grateful to UC Berkeley and the National Science Foundation for supporting my graduate studies as I was the recipient of fellowships from both institutions.

When I found myself facing mental roadblocks while pursuing my Ph.D., I would often seek out other graduate students to help me clarify an idea in my head. I am grateful to Paul Drazin and Christopher Daily-Diamond for providing me mentorship in my starting years at Berkeley as they would always be available to answer my, what probably seemed to them, simple questions. Thank you to Erden Yildizdag for studying with me before our qualifying exams and revealing to me your own curiosity and thoughtfulness. In my later years, Hyung-Taek Kim and Nathaniel Goldberg were always willing to listen to my ideas when we were in the lab together. I also want to thank Zacharias Vangelatos for his company during the many times we chose to "indulge" ourselves by eating out and sharing a meal in Berkeley.

Finally, I want to thank Roger Chang, an instructor in mechanics at Virginia Tech. I had Roger for several classes, including dynamics, as I pursued my undergraduate degree in Engineering Science and Mechanics. He is arguably the most respected person in Blacksburg, and the most devoted teacher that I know. Without his mentorship, I would not be where I am today.

Chapter 1

Introduction

The work presented in this dissertation makes use of a directed rod model due to Green and Naghdi that was developed in the late 20th century. A directed rod is sometimes also referred to as a Cosserat curve, an acknowledgement of the Cosserat brothers' impressive work on the mechanics of materials in the early 20th century. In their endeavor to properly model a continua comprised of a polar material, the Cosserats employed the use of a vector called a director to give the sense of direction of the couple stresses and body couples acting in the body (see [69] for a historical background). Eventually, the Cosserat brothers extended the concept of the director to additionally have a kinematical meaning for non-polar continua [34]. They then applied this perspective to their work on theories of rods and shells. Continuum models that employ the use of a director to capture observed phenomena have come to be called Cosserat continua. A model for rods that utilizes directors is called a Cosserat curve. Green and Naghdi picked up on the Cosserat's kinematical perspective of the director when they developed a thorough derivation for rods from three-dimensional continuum mechanics [25] and an alternative approach, called the direct approach, where the directed curve was simply postulated [26]. In this work, we will frequently refer to a Cosserat curve as a directed rod.

In Chapter 2 of this dissertation, we use Green and Naghdi's rod theory to develop a continuous description of peristaltic locomotion (Figure 1.1). Our description for peristalsis is motivated by the growing field of soft robotics in the 21st century. Many bio-inspired soft robots are making use of peristalsis as inspiration for a locomotion scheme. In Chapter 2, we design a scheme for peristalsis and apply Green and Naghdi's rod model to a description of the rod-like body that comprises the soft robot. In order to validate the model, kinematical and kinetic data on earthworm locomotion is gathered from the biological literature. A biomimetic model of the earthworm is then applied, and we show that our description of peristalsis is valid.

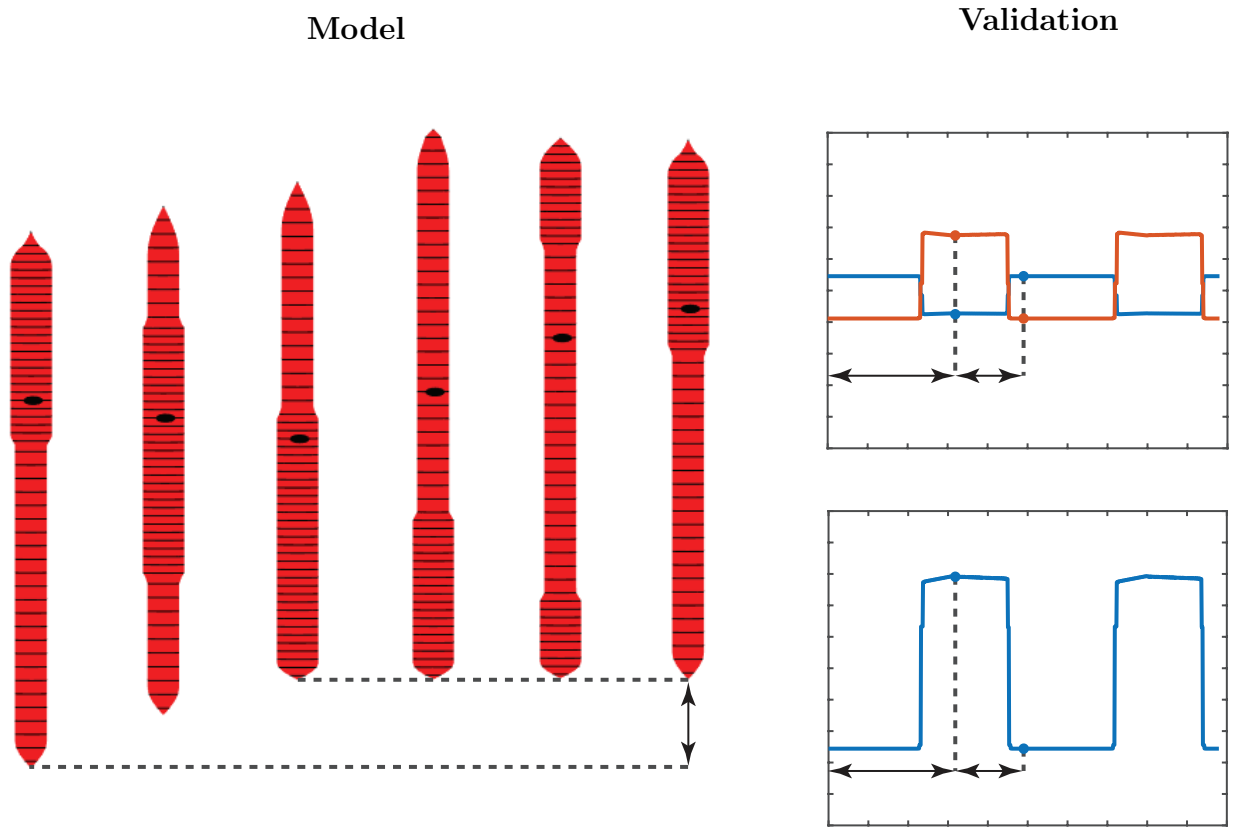

Figure 1.1: *The continuous biomimetic model for peristalsis and its validation that is presented in Chapter 2.*

In Chapter 3 of this dissertation, we develop a discrete model for rod-like bodies (Figure 1.2). The theory uses the concept of the director as a relative position vector to the lateral boundary of a rod, and a set of discrete edge vectors make up the rod's centerline. Inspired by Green and Naghdi's work, a balance of director momentum is postulated to help establish the governing equations for the discrete rod. A strain energy for non-linear deformations is put down, and the resulting equations are validated against known solutions for linearly elastic rods. Following a calibration of stiffnesses, the discrete model is dynamically validated by comparing with the expected natural frequency of vibration for a first mode shape of a Bernoulli-Euler beam.

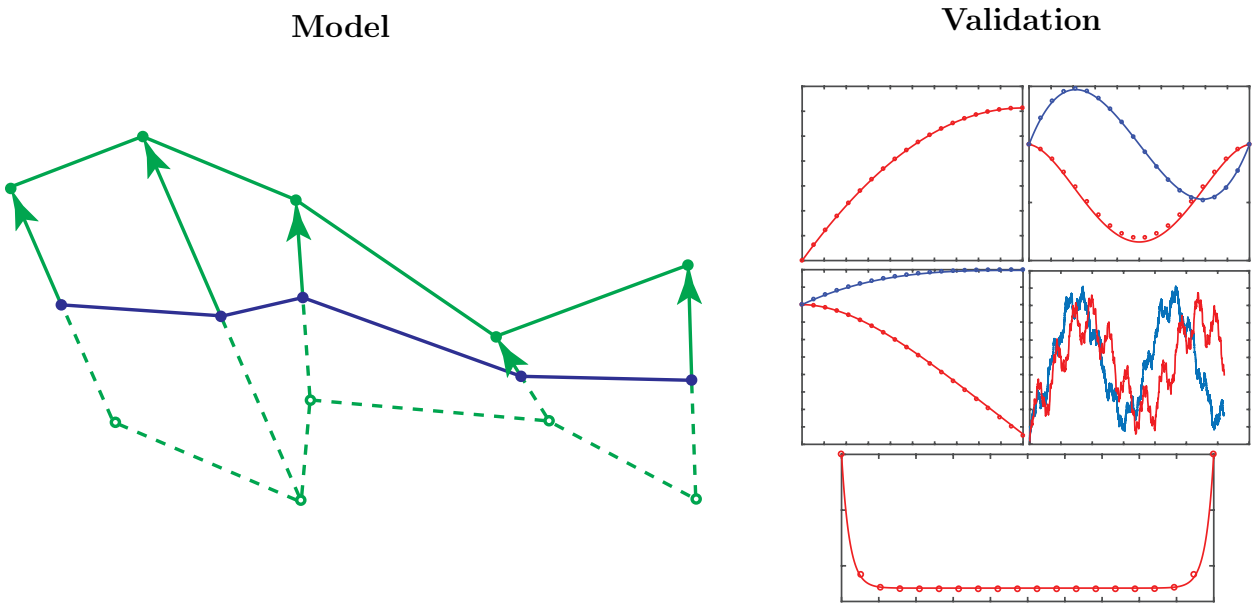

Figure 1.2: *The discrete directed rod model and its validation that is presented in Chapter 3.*

In this introductory chapter, we seek to establish the main equations from the mechanics of rods that are used in the research presented in later chapters. We begin with an overview of classical three-dimensional continuum mechanics, which serves as the basis of knowledge from which our rod models are developed. A reduced model for rod-like bodies is then presented as an approximation of three-dimensional continuum mechanics. We proceed by contrasting the developed equations with the direct approach, where an abstract directed curve is postulated. Following the presentation of the overall theory, we demonstrate how to treat internal and external constraints when using the directed rod model.

1.1 Background from continuum mechanics

In this section, classical continuum mechanics will be built until we reach the constitutive equations of linear elasticity for isotropic materials, which is the basis of the model for peristaltic locomotion that is presented in Chapter 2 and the inspiration for the non-linear discrete strain energy of Chapter 3. In what follows, lowercase and uppercase Latin indices are assumed to range from 1 to 3. Einstein's summation convention applies to any repeated indices, unless otherwise stated.

Material points in space

Continuum mechanics aims to describe how a body $\mathcal{B}$ distributes its material in space. We define a body as a collection of material points, with a given point being denoted by $X \in \mathcal{B}$.

A part $\mathcal{P} \subseteq \mathcal{B}$ is defined as a sub-body of the body. We assume the presence of a Euclidean three-space $\mathcal{E}^3$ into which material points are placed.

To define some of the ensuing kinematical quantities, it is necessary to identify a reference configuration of the body. The bounded region of $\mathcal{E}^3$ that the body $\mathcal{B}$ occupies in its reference configuration is called $\mathcal{R}_0 \subset \mathcal{E}^3$. A given part $\mathcal{P}$ occupies the region $\mathcal{V}_0 \subseteq \mathcal{R}_0$ in its reference configuration. In its current configuration, the body is assumed to occupy the region $\mathcal{R} \subset \mathcal{E}^3$ while the sub-part that occupies $\mathcal{V}_0$ is assumed to occupy $\mathcal{V} \subset \mathcal{E}^3$. Infinitesimal volume measures dV and dv exist in the reference and current regions, respectively. The reference boundary $\partial\mathcal{V}_0$ goes to the surface $\partial\mathcal{V}$ in the current configuration and each have the respective infinitesimal area measures dA and da. External stimuli will be postulated to exist in the form of tractions acting on the body's surface $\partial\mathcal{R}$ and body forces acting through its volume $\mathcal{R}$ in its current configuration. For sub-regions, tractions acting on $\partial\mathcal{V}$ are understood to be due to internal stress acting in $\mathcal{B}$ but may be viewed as being external to $\mathcal{P}$, the sub-part occupying $\mathcal{V}$.

Taking any two points $P_1, P_2 \in \mathcal{E}^3$, one may construct a directed line segment $\overrightarrow{P_1P_2}$, with a sense of direction from P_1 to P_2. A geometric vector space $\mathbb{E}^3$ may be constructed with the usual rules for tip-to-tail vector addition and scalar multiplication. We then have a natural identification between a directed line in $\mathcal{E}^3$ and an element of $\mathbb{E}^3$ as

$$\overrightarrow{P_1P_2} \sim \mathbf{r}_{P_2} - \mathbf{r}_{P_1}, \tag{1.1.1}$$

where $\mathbf{r}_{P_1}$ and $\mathbf{r}_{P_2}$ are position vectors pointing to P_1 and P_2 from an arbitrary common reference point in $\mathcal{E}^3$. The space $\mathcal{E}^3$ may be made into a metric space by defining a distance metric $d(P_1, P_2) \in \mathbb{R}$ which delivers the physical length of the line segment $\overline{P_1P_2}$, where $\mathbb{R}$ is the field of reals. A ruler with any demarcation of units can be used to measure the physical distance.

Suppose a set of geometrically orthogonal line segments $\overline{OP_1}$, $\overline{OP_2}$, and $\overline{OP_3}$ are identified in $\mathcal{E}^3$. A choice of O together with the fixed points P_1, P_2, and P_3 is sufficient to constitute an inertial reference frame to describe a material point's motion. The points P_1, P_2, and P_3 are used to define an orthonormal basis for $\mathbb{E}^3$ as follows:

$$\mathbf{E}_1 = \frac{\mathbf{r}_{P_1} - \mathbf{r}_O}{d(O, P_1)}, \quad \mathbf{E}_2 = \frac{\mathbf{r}_{P_2} - \mathbf{r}_O}{d(O, P_2)}, \quad \mathbf{E}_3 = \frac{\mathbf{r}_{P_3} - \mathbf{r}_O}{d(O, P_3)}. \tag{1.1.2}$$

The points P_1, P_2, and P_3 are assumed to be ordered so that the basis $\{\mathbf{E}_i\}$ is right-handed:

$$\mathbf{E}_1 = \mathbf{E}_2 \times \mathbf{E}_3, \tag{1.1.3}$$

where $\times$ is the usual cross-product of geometric three-vectors.

The vector space $\mathbb{E}^3$ may be made Euclidean by equipping it with the standard inner product (also known as the dot product) $\mathbf{a} \cdot \mathbf{b} = a_i b_i$ and the induced norm $\|\mathbf{a}\| = \sqrt{\mathbf{a} \cdot \mathbf{a}}$ for any two vectors $\mathbf{a} = a_i \mathbf{E}_i \in \mathbb{E}^3$ and $\mathbf{b} = b_i \mathbf{E}_i \in \mathbb{E}^3$. This additional mathematical structure allows us to do geometry on $\mathcal{E}^3$. For example, the length of the segment $\overline{P_1P_2}$ is given by

$$d(P_1, P_2) = \|\mathbf{r}_{P_1} - \mathbf{r}_{P_2}\|, \tag{1.1.4}$$

and the angle between line segments $\overline{OP_1}$ and $\overline{OP_2}$ is given by

$$\angle P_1OP_2 = \cos^{-1}\left(\frac{(\mathbf{r}_{P_1} - \mathbf{r}_O)\cdot(\mathbf{r}_{P_2} - \mathbf{r}_O)}{\|\mathbf{r}_{P_1} - \mathbf{r}_O\|\|\mathbf{r}_{P_2} - \mathbf{r}_O\|}\right). \tag{1.1.5}$$

We choose to fix the reference point $O \in \mathcal{E}^3$ as the physical place from which all other positions are referred. When writing $\mathbf{r}_P$ it is understood that a directed line segment has been constructed that stems from O to P. That is, $\mathbf{r}_O = \mathbf{0}$ serves as the zero element of $\mathbb{E}^3$.

For some point $P \in \mathcal{E}^3$, we may associate a triplet of numbers known as its Cartesian coordinates as the components of $\mathbf{r}_P$ on the basis $\{\mathbf{E}_i\}$:

$$Y^i = \mathbf{r}_P \cdot \mathbf{E}_i \in \mathbb{R}. \tag{1.1.6}$$

The numerical value of Y^i depends on the choice of units for describing physical lengths. A change of units corresponds to a change of coordinates where Y^i and $\mathbf{E}_i$ co-vary and contra-vary accordingly to $\overline{Y}^i$ and $\overline{\mathbf{E}}_i$ to keep $\mathbf{r}_P$ invariant, or tensorial:

$$\mathbf{r}_P = Y^i\mathbf{E}_i = \overline{Y}^i\overline{\mathbf{E}}_i. \tag{1.1.7}$$

The components Y^i additionally serve as a coordinate chart for all of $\mathcal{E}^3$, where the tip of $\mathbf{r}_P$ is mapped into the point $P \in \mathcal{E}^3$ that it coincides with.

Kinematics

A material point X is assigned the reference placement $\mathbf{R}^*$ relative to O which is delivered by the vector-valued function $\boldsymbol{\kappa}_0$:

$$\mathbf{R}^* = \boldsymbol{\kappa}_0(X). \tag{1.1.8}$$

The shape that the body assumes at some time $t \in \mathbb{R}$ is called the current configuration. A time-indexed sequence of current configurations of the body is delivered by the vector-valued function $\boldsymbol{\chi}$ on $\mathcal{B}$ and $\mathbb{R}$, called the motion, which places material points into their current positions:

$$\mathbf{r}^* = \boldsymbol{\chi}(X, t). \tag{1.1.9}$$

It is tacitly assumed that $\mathbf{r}^*$ is relative to O, just as $\mathbf{R}^*$ is. All kinematical information is known in a problem if $\boldsymbol{\chi}$ is able to be determined. Using (1.1.8), we may define a function $\overline{\boldsymbol{\chi}}$ on the subset of $\mathbb{E}^3$ containing all reference placements:

$$\mathbf{r}^* = \overline{\boldsymbol{\chi}}(\mathbf{R}^*, t) = \boldsymbol{\chi}\big(\boldsymbol{\kappa}_0^{-1}(X), t\big). \tag{1.1.10}$$

Invertibility of $\boldsymbol{\chi}$ and $\overline{\boldsymbol{\chi}}$ becomes attainable if they are considered as a collection of time-indexed functions. For example, we may define

$$\mathbf{r}^* = \boldsymbol{\chi}_t(X) = \boldsymbol{\chi}(X, t), \tag{1.1.11}$$

where t is understood to explicitly index a particular function.

Viewing Y^i as Cartesian coordinates for $\mathcal{E}^3$, we find that material points in $\mathcal{R}_0$ are coincident with some values of Y^i. The material points of $\mathcal{B}$ are now identified by a triplet of material coordinates. Therefore, we have the three mappings

$$Y^i = f^i(X). \tag{1.1.12}$$

The coordinates Y^i that coincide with material points in the reference configuration may be considered to follow the material through $\mathcal{E}^3$. The convected coordinates serve as a coordinate patch for $\mathcal{E}^3$ in the region $\mathcal{R}$. Calling the convected coordinates X^i, we have an invertible non-linear change of coordinates on $\mathcal{R}$ for every time step as

$$X^i = g_t^i\big(Y^j\big). \tag{1.1.13}$$

If the body occupies $\mathcal{R}_0$, then $X^i = Y^i$, and g_t^i is the identity map. The current position vector may now be considered as a function of X^i:

$$\mathbf{r}^* = \hat{\boldsymbol{\chi}}\big(X^i, t\big) = \boldsymbol{\chi}\big(g_t^i\big(f^j(X)\big), t\big). \tag{1.1.14}$$

We define the displacement of X from its reference placement as the vector difference

$$\mathbf{u} = \mathbf{r}^* - \mathbf{R}^*. \tag{1.1.15}$$

The velocity of X may be derived as a material time derivative from the position or the displacement:

$$\mathbf{v}^* = \dot{\mathbf{r}}^* = \dot{\mathbf{u}}, \tag{1.1.16}$$

where the superposed dot assumes that X^i are held fixed. The deformation gradient is that linear operator which delivers

$$d\mathbf{r}^* = \mathbf{F}\ d\mathbf{R}^*. \tag{1.1.17}$$

Here, $\mathbf{F}$ is a second order tensor that may be expressed as a sum of tensor products indicated by the symbol $\otimes$. The action of a tensor product on a vector is defined to be $(\mathbf{a}\otimes\mathbf{b})\mathbf{c} = \mathbf{a}(\mathbf{b}\cdot\mathbf{c})$ for any $\mathbf{a},\mathbf{b},\mathbf{c}\in\mathbb{E}^3$. The transpose of a tensor $\mathbf{A}$ is defined as that operator $\mathbf{A}^{\mathrm{T}}$ which satisfies

$$\mathbf{A}\mathbf{a}\cdot\mathbf{b} = \mathbf{a}\cdot\mathbf{A}^{\mathrm{T}}\mathbf{b}, \tag{1.1.18}$$

for any $\mathbf{a},\mathbf{b}\in\mathbb{E}^3$. The trace of a tensor $\mathbf{A}$ is defined as

$$\mathrm{tr}(\mathbf{A}) = \frac{\mathbf{A}\mathbf{a}\cdot(\mathbf{b}\times\mathbf{c}) + \mathbf{a}\cdot(\mathbf{A}\mathbf{b}\times\mathbf{c}) + \mathbf{a}\cdot(\mathbf{b}\times\mathbf{A}\mathbf{c})}{\mathbf{a}\cdot(\mathbf{b}\times\mathbf{c})}, \tag{1.1.19}$$

while the determinant of $\mathbf{A}$ is defined as

$$\det(\mathbf{A}) = \frac{\mathbf{A}\mathbf{a}\cdot(\mathbf{A}\mathbf{b}\times\mathbf{A}\mathbf{c})}{\mathbf{a}\cdot(\mathbf{b}\times\mathbf{c})}, \tag{1.1.20}$$

for any $\mathbf{a}, \mathbf{b}, \mathbf{c} \in \mathbb{E}^3$. A tensor inner product may be defined for any two tensors $\mathbf{A}$ and $\mathbf{B}$ as

$$\mathbf{A} \cdot \mathbf{B} = \mathrm{tr}\big(\mathbf{A}\mathbf{B}^{\mathrm{T}}\big). \tag{1.1.21}$$

An induced norm follows as

$$\|\mathbf{A}\| = \sqrt{\mathbf{A} \cdot \mathbf{A}}. \tag{1.1.22}$$

Note that the symbols $\cdot$ and $\| \, \|$ are used for both second order tensors and geometric vectors, and context is required to distinguish the respective functions.

A small volume element in the reference configuration is given by

$$dV = d\mathbf{R}_1^* \cdot (d\mathbf{R}_2^* \times d\mathbf{R}_3^*), \tag{1.1.23}$$

where $d\mathbf{R}_i^*$ is the small difference between two neighboring reference placements. This element gets carried into dv in the current configuration, where

$$dv = d\mathbf{r}_1^* \cdot (d\mathbf{r}_2^* \times d\mathbf{r}_3^*). \tag{1.1.24}$$

The cofactor of $\mathbf{F}$ is defined as

$$\mathbf{F}^{\mathrm{C}} = \det(\mathbf{F})\mathbf{F}^{-\mathrm{T}}. \tag{1.1.25}$$

Applying (1.1.17) three times, and using the identities $\mathbf{a} \cdot \mathbf{A}\mathbf{b} = \mathbf{A}^{\mathrm{T}}\mathbf{a} \cdot \mathbf{b}$ and $\mathbf{A}\mathbf{a} \times \mathbf{A}\mathbf{b} = \mathbf{A}^{\mathrm{C}}(\mathbf{a} \times \mathbf{b})$, we find

$$dv = J dV, \tag{1.1.26}$$

where the Jacobian is defined as the tensor determinant of $\mathbf{F}$:

$$J = \det(\mathbf{F}). \tag{1.1.27}$$

The displacement gradient is defined as that linear operator which delivers

$$d\mathbf{u} = \mathbf{H} \, d\mathbf{R}^*, \tag{1.1.28}$$

so that

$$\mathbf{H} = \mathbf{F} - \mathbf{I}. \tag{1.1.29}$$

The Lagrange strain is defined in terms of $\mathbf{F}$ and $\mathbf{H}$ as

$$\mathbf{E} = \frac{1}{2}\big(\mathbf{F}^{\mathrm{T}}\mathbf{F} - \mathbf{I}\big) = \frac{1}{2}\big(\mathbf{H} + \mathbf{H}^{\mathrm{T}} + \mathbf{H}^{\mathrm{T}}\mathbf{H}\big), \tag{1.1.30}$$

where $\mathbf{I}$ is the identity tensor: $\mathbf{I}\mathbf{a} = \mathbf{a}$ for any $\mathbf{a} \in \mathbb{E}^3$. To relate the foregoing kinematics to applied loads, we must postulate balance laws for which the processes that $\mathcal{B}$ engages in are assumed to obey.

Balance laws

Every material point $X \in \mathcal{B}$ is assumed to contribute a small amount of inertia to the body through a mass density per unit reference volume measure that is assigned as ρ_0^*. The mass of a given part $\mathcal{P} \subset \mathcal{B}$ which occupies the region $\mathcal{V}_0 \subset \mathcal{R}_0$, may be computed using the postulated mass density via

$$m(\mathcal{P}) = \int_{\mathcal{V}_0} \rho_0^* dV. \tag{1.1.31}$$

We assume no supplies of mass into or out of $\mathcal{P}$, so that the balance of mass becomes a conservation law:

$$0 = \dot{m}. \tag{1.1.32}$$

Since (1.1.32) holds true for all sub-bodies $\mathcal{P} \subseteq \mathcal{B}$, then the localization theorem yields

$$0 = \dot{\rho}_0^*, \tag{1.1.33}$$

As a consequence, ρ_0^* is a conserved quantity for any $X \in \mathcal{B}$ for the course of the motion. Another density ρ^* is found by pushing the integration (1.1.31) forward to the current configuration:

$$m = \int_{\mathcal{V}_0} \rho_0^* dV = \int_{\mathcal{V}} \frac{\rho_0^*}{J} dv, \tag{1.1.34}$$

so that

$$\rho^* = \frac{\rho_0^*}{J} \tag{1.1.35}$$

is a mass density per unit current volume. The linear momentum of any part $\mathcal{P}$ is defined to be

$$\mathbf{G}^* = \int_{\mathcal{V}_0} \rho_0^* \mathbf{v}^* dV, \tag{1.1.36}$$

while the angular momentum about the reference point O is defined as

$$\mathbf{H}_O^* = \int_{\mathcal{V}_0} \rho_0^* \mathbf{r}^* \times \mathbf{v}^* dV. \tag{1.1.37}$$

In contrast to the conservation of mass, we postulate that there exist supplies of linear and angular momentum $\mathbf{F}$ and $\mathbf{M}_O$ which satisfy the balances of linear and angular momentum:

$$\mathbf{F} = \dot{\mathbf{G}}^*, \quad \mathbf{M}_O = \dot{\mathbf{H}}_O^*. \tag{1.1.38}$$

Here, $\mathbf{F}$ is the net external force acting on $\mathcal{P}$ while $\mathbf{M}_O$ is the net external moment about point O acting on $\mathcal{P}$. We assume there exists a traction $\mathbf{t}$ and a body force $\mathbf{b}$ acting on $\mathcal{P}$, where $\mathbf{t}$ is a contact force per unit current area acting on $\partial\mathcal{V}$ and $\mathbf{b}$ is a body force per unit mass acting through $\mathcal{V}$. Generally, $\mathbf{t}$ is from an adjacent body contacting $\mathcal{B}$ while $\mathbf{b}$ is due

to a body at a distance from $\mathcal{B}$. Using the current volume mass density (1.1.35), $\mathbf{t}$ and $\mathbf{b}$ are defined as those vector fields which deliver $\mathbf{F}$ and $\mathbf{M}_O$ according to

$$\mathbf{F} = \int_{\mathcal{V}} \mathbf{b}\rho dv + \int_{\partial\mathcal{V}} \mathbf{t} da, \quad \mathbf{M}_O = \int_{\mathcal{V}} \mathbf{r}^* \times \mathbf{b}\rho dv + \int_{\partial\mathcal{V}} \mathbf{r}^* \times \mathbf{t} da. \tag{1.1.39}$$

Using Cauchy's tetrahedron argument, we may presume that the components $t_i = \mathbf{t} \cdot \mathbf{E}_i$ should be linear in components of the unit normal located at da expressed on the same basis: $N_i = \mathbf{N} \cdot \mathbf{E}_i$. As a consequence, there exists a linear operator $\mathbf{T}$ such that

$$\mathbf{t} = \mathbf{T}\mathbf{N}, \tag{1.1.40}$$

where $\mathbf{T}$ is known as the Cauchy stress. Using the conservation of mass and assuming (1.1.38) to hold for all sub-parts $\mathcal{P} \subseteq \mathcal{B}$, we may apply the divergence theorem and the localization theorem to find the local version of the balance of linear momentum holding for some material point X as

$$\mathrm{div}\mathbf{T} + \rho^* \mathbf{b} = \rho^* \dot{\mathbf{v}}^*. \tag{1.1.41}$$

Here, the divergence of $\mathbf{T}$ may be computed from

$$\mathrm{div}\mathbf{T} = (\mathrm{grad}\mathbf{T})\mathbf{I}, \tag{1.1.42}$$

where $\mathbf{I}$ is the second order identity tensor and $\mathrm{grad}\mathbf{T}$ is defined to be that fourth order tensor which delivers

$$d\mathbf{T} = \mathrm{grad}\mathbf{T}\ d\mathbf{r}^*. \tag{1.1.43}$$

The local version of the angular momentum balance may also be derived. The local balance of angular momentum for a material point X may be found to be equivalent to the symmetry condition

$$\mathbf{T} = \mathbf{T}^{\mathrm{T}}. \tag{1.1.44}$$

Condition (1.1.44) determines three components of the Cauchy stress and may be viewed as a constitutive consequence of the media being non-polar, i.e., that it cannot sustain body or surface torques. The constitutive requirement is implicit in $(1.1.39)_2$, where we assumed that $\mathbf{M}_O$ is comprised only of torques due to moments of tractions and body forces, with no contribution from stress couples.

To derive an engineering stress, we define a force per unit reference area $\mathbf{p}$, the Piola traction, such that it delivers the same amount of incremental force $d\mathbf{f}$ as that delivered across a boundary by $\mathbf{t}$:

$$d\mathbf{f} = \mathbf{t} da = \mathbf{p} dA. \tag{1.1.45}$$

Using Nanson's formula, namely,

$$\mathbf{N} da = \mathbf{F}^{\mathrm{C}} \mathbf{N}_0 dA, \tag{1.1.46}$$

we derive

$$\big(\mathbf{T}\mathbf{F}^{\mathrm{C}}\mathbf{N}_0 - \mathbf{p}\big) dA = \mathbf{0}, \tag{1.1.47}$$

which holds for any non-zero reference area element dA. Applying the localization theorem to an integration of (1.1.47), $\mathbf{p}$ is found to be delivered in the following way:

$$\mathbf{p} = \mathbf{T}\mathbf{F}^{\mathrm{C}}\mathbf{N}_0 = \mathbf{P}\mathbf{N}_0, \tag{1.1.48}$$

where $\mathbf{P} = \mathbf{T}\mathbf{F}^{\mathrm{C}}$ is the first Piola-Kirchhoff stress tensor. Now, the local balance of linear momentum (1.1.41) may be manipulated into a version based on reference configuration quantities:

$$\mathrm{Div}\mathbf{P} + \rho_0^*\mathbf{b} = \rho_0^*\dot{\mathbf{v}}^*, \tag{1.1.49}$$

where

$$\mathrm{Div}\mathbf{P} = (\mathrm{Grad}\mathbf{P})\mathbf{I}, \tag{1.1.50}$$

and $\mathrm{Grad}\mathbf{P}$ is defined to be that linear operator which delivers

$$d\mathbf{P} = \mathrm{Grad}\mathbf{P}\ d\mathbf{R}^*. \tag{1.1.51}$$

The kinetic energy T^* of any sub-body $\mathcal{P}$ may be defined as

$$T^* = \int_{\mathcal{V}_0} \frac{1}{2}\mathbf{v}^* \cdot \mathbf{v}^* \rho_0 dV. \tag{1.1.52}$$

Projecting the local balance of linear momentum (1.1.41) along $\mathbf{v}^*$ and integrating over $\mathcal{V}$, we obtain a power theorem for some part $\mathcal{P}$:

$$\int_{\mathcal{V}_0} \mathbf{p} \cdot \mathbf{v}^* dA + \int_{\mathcal{V}_0} \mathbf{b} \cdot \mathbf{v}^* \rho_0^* dV = \dot{T}^* + \int_{\mathcal{V}_0} \mathbf{P} \cdot \dot{\mathbf{F}} dV. \tag{1.1.53}$$

That is, if the continuum obeys the balance of linear momentum, then the kinetic energy time rate of change and stress power balance the power of the external loads. For a Green-elastic material, we presume the existence of a scalar function, the strain energy, $\rho_0^*\psi^* = \rho_0^*\psi^*(\mathbf{F})$ that is related to the stress power in the following way:

$$\rho_0^*\dot{\psi}^* = \mathbf{P} \cdot \dot{\mathbf{F}}. \tag{1.1.54}$$

We deduce the implication

$$\left(\mathbf{P} - \frac{\partial \rho_0^*\psi^*}{\partial \mathbf{F}}\right) \cdot \dot{\mathbf{F}} = 0, \tag{1.1.55}$$

which, for an internally unconstrained material, must hold true for the motion of any material point X. Here, a second order tensor is defined such that it delivers

$$d(\rho_0^*\psi^*) = \frac{\partial \rho_0^*\psi^*}{\partial \mathbf{F}} \cdot d\mathbf{F}. \tag{1.1.56}$$

We are at liberty to construct a motion in which

$$\dot{\mathbf{F}} = c\left(\mathbf{P} - \frac{\partial \rho_0^*\psi^*}{\partial \mathbf{F}}\right), \tag{1.1.57}$$

where c is a strictly positive scalar of appropriate physical dimension. Using the positivity of the norm, we deduce that

$$\mathbf{P} = \frac{\partial \rho_0^* \psi^*}{\partial \mathbf{F}} \tag{1.1.58}$$

for an unconstrained material. Hence, a prescription for $\rho_0^* \psi^*(\mathbf{F})$ is equivalent to a constitutive equation for $\mathbf{P}$.

For an internally constrained material, $\dot{\mathbf{F}}$ may not be chosen arbitrarily. It must lie in the tangent space at $\mathbf{F}$, $T_{\mathbf{F}}\mathcal{M}$, where $\mathcal{M}$ is the hypersurface on which the internal constraint $\phi^*(\mathbf{F}) = 0$ holds:

$$\mathcal{M} = \{\mathbf{F} : \phi^*(\mathbf{F}) = 0\}. \tag{1.1.59}$$

In this case, the orthogonality condition (1.1.55) implies

$$\mathbf{P} - \frac{\partial \rho_0^* \psi^*}{\partial \mathbf{F}} = \lambda^{\mathrm{I}*} \frac{\partial \phi^*}{\partial \mathbf{F}}, \tag{1.1.60}$$

i.e., the left-hand side of (1.1.60) must lie in the orthogonal complement $T_{\mathbf{F}}^{\perp}\mathcal{M}$. The scalar $\lambda^{\mathrm{I}*}$ is known as a Lagrange multiplier, which must be determined not constitutively, but from satisfaction of the balance laws. We may decompose $\mathbf{P}$ into an active and a reactive piece as follows:

$$\mathbf{P} = \overline{\mathbf{P}} + \hat{\mathbf{P}} = \left.\frac{\partial \rho_0^* \psi^*}{\partial \mathbf{F}}\right|_{\mathcal{M}} + \lambda^{\mathrm{I}*} \frac{\partial \phi^*}{\partial \mathbf{F}}. \tag{1.1.61}$$

By pulling $\mathbf{p}$ back to the reference configuration, we obtain another, practically useless, traction $\mathbf{s}$:

$$\mathbf{s} = \mathbf{F}^{-1}\mathbf{p}. \tag{1.1.62}$$

However, if $\mathbf{s}$ is to be delivered by a stress tensor $\mathbf{S}$ acting on the reference unit normal $\mathbf{N}_0$ to $\partial\mathcal{V}_0$, then we find the mathematically appealing quality that it is symmetric, thanks to the balance of angular momentum:

$$\mathbf{S} = \mathbf{F}^{-1}\mathbf{P} = J\mathbf{F}^{-1}\mathbf{T}\mathbf{F}^{-\mathrm{T}}. \tag{1.1.63}$$

The tensor $\mathbf{S}$ is known as the second Piola-Kirchhoff stress tensor.

For psychological purposes, it is convenient to introduce another basis $\{\mathbf{E}_A\}$, which is identical to $\{\mathbf{E}_i\}$ apart from the notation for indexing. Capitalized indices are to be associated with the reference configuration and will be used to aid our memory of "where" certain tensors are meant to act. For example, a deformation gradient represented as $\mathbf{F} = F_{iA}\mathbf{E}_i \otimes \mathbf{E}_A$ will remind us that $\mathbf{F}$ is meant to act on a geometrical element associated with the reference configuration and it delivers a quantity associated with the current configuration. The components of $\mathbf{P}$ for an internally unconstrained material on the basis $\{\mathbf{E}_i \otimes \mathbf{E}_A\}$ may be computed from (1.1.58) as

$$P_{iA} = \mathbf{P} \cdot \mathbf{E}_i \otimes \mathbf{E}_A = \frac{1}{2}\left(\frac{\partial \rho_0^* \psi^*}{\partial E_{AB}} + \frac{\partial \rho_0^* \psi^*}{\partial E_{BA}}\right) F_{iB}. \tag{1.1.64}$$

Linear elasticity

In linear elasticity, it is assumed that the magnitude of the displacement gradient $\|\mathbf{H}\|$ is small at every material point. We have the following implication from (1.1.30)

$$\mathbf{E} \approx \frac{1}{2}\big(\mathbf{H}^{\mathrm{T}} + \mathbf{H}\big). \tag{1.1.65}$$

We may define a small strain tensor as

$$\boldsymbol{\epsilon} = \frac{1}{2}\big(\mathbf{H}^{\mathrm{T}} + \mathbf{H}\big), \tag{1.1.66}$$

so that $\mathbf{E} \approx \boldsymbol{\epsilon}$ for small $\|\mathbf{H}\|$. For an isotropic material, the strain energy function must depend on the three tensor invariants of $\boldsymbol{\epsilon}$. A quadratic approximation of the strain energy for an isotropic material with no residual stress yields

$$\rho_0^*\psi^* = \frac{\lambda}{2}\mathrm{tr}^2(\boldsymbol{\epsilon}) + \mu\boldsymbol{\epsilon}\cdot\boldsymbol{\epsilon}, \tag{1.1.67}$$

where λ and μ are positive constants known as the Lamé moduli. Prescription (1.1.67) is physically sound in that it obeys the principle of material frame indifference, which implies invariance of $\rho_0^*\psi^*$ when $\mathcal{B}$ is subject to a superposed rigid body motion. By noting the relations

$$\mathbf{P} = (\mathbf{H}+\mathbf{I})\mathbf{S} = \mathbf{T}(\mathbf{H}+\mathbf{I})^*, \tag{1.1.68}$$

we see that if $\|\mathbf{H}\|$ is small, then

$$\mathbf{P} \approx \mathbf{S} \approx \mathbf{T}, \tag{1.1.69}$$

and all stress tensors are approximately equivalent. In the linear theory, $\mathbf{P}$ becomes approximately symmetric. We denote this special case by indicating the stress as $\boldsymbol{\sigma}$. The prescription for stress (1.1.64) becomes

$$\sigma_{iA} \approx \frac{1}{2}\left(\frac{\partial\rho_0^*\psi^*}{\partial\epsilon_{AB}} + \frac{\partial\rho_0^*\psi^*}{\partial\epsilon_{BA}}\right)\delta_{iB} = \frac{1}{2}\left(\frac{\partial\rho_0^*\psi^*}{\partial\epsilon_{Ai}} + \frac{\partial\rho_0^*\psi^*}{\partial\epsilon_{iA}}\right), \tag{1.1.70}$$

and (1.1.67) is written as

$$\begin{aligned}\rho_0^*\psi^* = \frac{\lambda}{2}\mathrm{tr}^2(\boldsymbol{\epsilon}) + \mu\boldsymbol{\epsilon}\cdot\boldsymbol{\epsilon} = \frac{\lambda}{2}(\epsilon_{11}+\epsilon_{22}+\epsilon_{33})^2 \\ +\mu\big(\epsilon_{11}^2+\epsilon_{22}^2+\epsilon_{33}^2+\epsilon_{12}^2+\epsilon_{21}^2+\epsilon_{13}^2+\epsilon_{31}^2+\epsilon_{23}^2+\epsilon_{32}^2\big).\end{aligned} \tag{1.1.71}$$

We compute the constitutive equation for the stress of the linear theory as

$$\boldsymbol{\sigma} = \lambda\mathrm{tr}(\boldsymbol{\epsilon})\mathbf{I} + 2\mu\boldsymbol{\epsilon}. \tag{1.1.72}$$

The foregoing presentation is the knowledge needed to understand the rod theories detailed in the remainder of this dissertation. Formulae similar to (1.1.72) will be developed but for various internal forces associated with the directed rod. There are two methods for obtaining the governing equations of the directed rod: a derivation from three-dimensional continuum mechanics or the direct approach. A discussion of each approach follows.

1.2 Derivations for a rod-like body from three-dimensional continuum mechanics

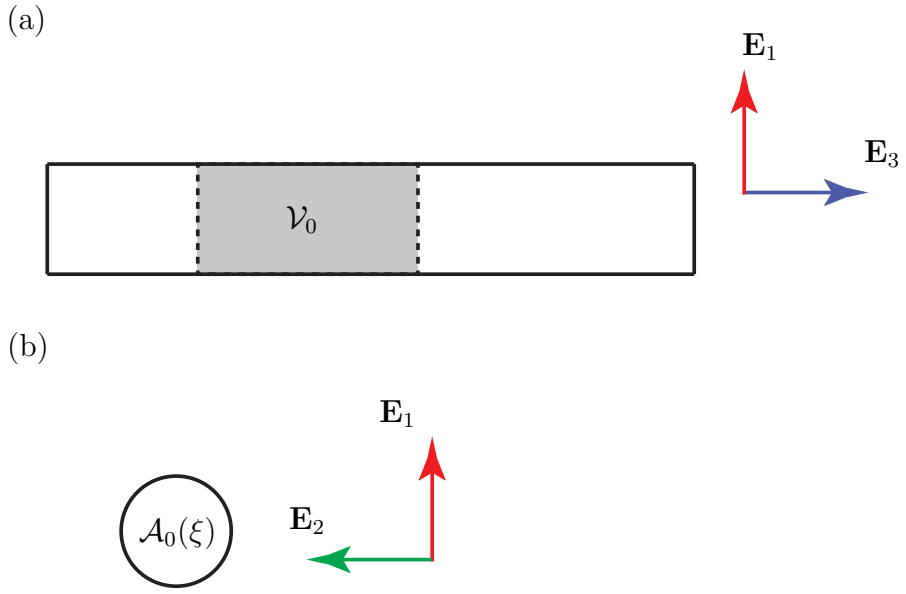

Figure 1.3: *(a) The reference configuration of a solid cylindrical rod-like body with sub-volume $\mathcal{V}_0$ and (b) cross-sectional area $\mathcal{A}_0(\xi)$ at some cross-section located at ξ.*

In this section, we aim to obtain the governing equations for rods using knowledge from three-dimensional continuum mechanics. The developments of this section are simplified versions of the procedures developed by Green and Naghdi [25, 26, 40, 41]. In what follows, Greek indices are assumed to range from 1 to 2. All repeated indices are once again summed per Einstein's convention, unless otherwise stated.

Consider a rod-like body $\mathcal{B}$ whose stress-free reference configuration is displayed in Figure 1.3. We say that a body is "rod-like," or slender, if two of its characteristic length dimensions are smaller compared to another direction, called the longitudinal direction. The body is oriented in its reference configuration so that the straight line $(0, 0, Y^3)$ identifies a curve called the centerline with Y^3 taking on values between 0 and ℓ_0, where ℓ_0 is some physical length determined by the choice of units for Y^i. A new coordinate ξ is introduced to parametrize points on the centerline, where $\xi \in \{Y^3 : 0 \leq Y^3 \leq \ell_0\}$.

Kinematics of a rod-like body

A position vector to the reference centerline relative to O may be constructed as a function of ξ:

$$\mathbf{R} = \mathbf{R}(\xi) = \mathbf{R}^*(0, 0, \xi). \tag{1.2.1}$$

The reference placement of some material point X has the decomposition

$$\mathbf{R}^* = \mathbf{R}^*(Y^\alpha, \xi) = \mathbf{R} + Y^\beta \mathbf{D}_\beta, \tag{1.2.2}$$

where $Y^\beta \mathbf{D}_\beta$ is the position of X relative to $\mathbf{R}$. The vectors $\mathbf{D}_\alpha$ are known as the reference directors and are defined as

$$\mathbf{D}_\alpha = \mathbf{D}_\alpha(\xi) = \left.\frac{\partial \mathbf{R}^*}{\partial Y^\alpha}\right|_{Y^\alpha = 0} = \mathbf{E}_\alpha. \tag{1.2.3}$$

Since we chose Y^α to have a physical length dimension of length, $\mathbf{D}_\alpha$ are unit vectors. A cross-section of the rod-like body is defined as the collection of material points lying in the span of the set $\{\mathbf{D}_\alpha\}$ at some ξ. We may think of ξ as a continuous index for a cross-section. A third director may be introduced as

$$\mathbf{D}_3 = \left.\frac{\partial \mathbf{R}^*}{\partial Y^3}\right|_{Y^\alpha = 0} = \frac{\partial \mathbf{R}}{\partial \xi}. \tag{1.2.4}$$

The third director is generally seen as being auxiliary to $\mathbf{D}_\alpha$ and is introduced to take full advantage of indicial notiation.

The three-dimensional placement of material points into the current configuration (1.1.14) has been constructed to depend on the convected coordinates. Assuming the motion to be smoothly varying in space, we may expand (1.1.14) in a Taylor series about the centerline $X^\alpha = 0$ for any fixed time t and cross-section ξ:

$$\mathbf{r}^*(X^\alpha, \xi, t) = \mathbf{r}^*(0, \xi, t) + \left.\frac{\partial \mathbf{r}^*}{\partial X^\beta}\right|_{X^\alpha = 0} X^\beta + \frac{1}{2} \left.\frac{\partial^2 \mathbf{r}^*}{\partial X^\beta \partial X^\gamma}\right|_{X^\alpha = 0} X^\beta X^\gamma + \cdots. \tag{1.2.5}$$

If the body $\mathcal{B}$ is slender, then the coordinates X^α are small relative to ξ. Therefore, the following approximation for the motion is descriptive for rod-like bodies where the cross-sections are assumed to be small in diameter compared to the overall length:

$$\mathbf{r}^*(X^\alpha, \xi, t) \approx \mathbf{r}^*(0, \xi, t) + \left.\frac{\partial \mathbf{r}^*}{\partial X^\beta}\right|_{X^\alpha = 0} X^\beta. \tag{1.2.6}$$

In the current configuration, we assume the following approximation for the location of three-dimensional material points to hold:

$$\mathbf{r}^* = \mathbf{r}^*(X^\alpha, \xi, t) \approx \mathbf{r} + X^\beta \mathbf{d}_\beta, \tag{1.2.7}$$

where

$$\mathbf{r} = \mathbf{r}(\xi, t) = \mathbf{r}^*(0, \xi, t) \tag{1.2.8}$$

is the placement of the centerline in the current configuration and

$$\mathbf{d}_\alpha = \mathbf{d}_\alpha(\xi, t) = \left.\frac{\partial \mathbf{r}^*}{\partial X^\alpha}\right|_{X^\beta = 0} \tag{1.2.9}$$

are the current configuration directors. The typical problem of determining the motion $\boldsymbol{\chi}$ from continuum mechanics has been reduced to finding the three functions $\mathbf{r}(\xi, t)$ and $\mathbf{d}_\alpha(\xi, t)$. A consequence of approximation (1.2.7) is that planar cross-sections should remain planar and cross-section deformations are homogeneous through the entire section. In addition to $\mathbf{d}_\alpha$, a third current configuration director is derived as:

$$\mathbf{d}_3 = \mathbf{d}_3(\xi, t) = \frac{\partial \mathbf{r}}{\partial \xi}. \tag{1.2.10}$$

Since the coordinates X^i are convected with the material, their material time derivatives are $\dot{X}^i = 0$. We obtain the velocity of a three-dimensional point as the material time derivative

$$\mathbf{v}^* = \dot{\mathbf{r}}^* = \mathbf{v} + X^\beta \mathbf{w}_\beta, \tag{1.2.11}$$

where $\mathbf{v} = \dot{\mathbf{r}}(\xi, t)$ and $\mathbf{w}_\alpha = \dot{\mathbf{d}}_\alpha(\xi, t)$ are the centerline velocity and director velocities at ξ, respectively. The quantity $X^\beta \mathbf{w}_\beta$ may be seen as a relative velocity between any $X \in \mathcal{B}$ and the material point occupying the centerline point of its cross-section. The acceleration is similarly given by

$$\dot{\mathbf{v}}^* = \ddot{\mathbf{r}}^* = \dot{\mathbf{v}} + X^\beta \dot{\mathbf{w}}_\beta, \tag{1.2.12}$$

where $\dot{\mathbf{v}} = \dot{\mathbf{v}}(\xi, t)$ and $\dot{\mathbf{w}}_\alpha = \dot{\mathbf{w}}_\alpha(\xi, t)$ are the centerline acceleration and director accelerations at some ξ, respectively.

Let $s = s(\xi, t)$ denote the arc-length to a material point of the centerline in its current configuration. A centerline stretch μ_3 may then be calculated as

$$\mu_3 = \frac{ds}{d\xi} = \|\mathbf{d}_3\|. \tag{1.2.13}$$

Additionally, we may introduce the cross-section stretches μ_1 and μ_2 as

$$\mu_\alpha = \left\| \left. \frac{\partial \mathbf{r}^*}{\partial X^\alpha} \right|_{X^\beta = 0} \right\| = \|\mathbf{d}_\alpha\|. \tag{1.2.14}$$

The current configuration centerline tangent vector is found as

$$\mathbf{e}_t = \frac{\partial \mathbf{r}}{\partial s} = \mu_3^{-1} \mathbf{d}_3. \tag{1.2.15}$$

It is convenient to introduce the basis $\{\mathbf{e}_i\}$, defined as the unit directions of the current configuration directors:

$$\mathbf{e}_i = \frac{\mathbf{d}_i}{\|\mathbf{d}_i\|}, \quad \text{(no sum)}. \tag{1.2.16}$$

With (1.2.13) and (1.2.16) in view, it should be clear that $\mathbf{e}_3 = \mathbf{e}_t$.

To characterize changes in shape of the rod-like body from its reference configuration, we may introduce the director displacements

$$\boldsymbol{\delta}_i = \boldsymbol{\delta}_i(\xi, t) = \mathbf{d}_i - \mathbf{D}_i. \tag{1.2.17}$$

Using the directors, the displacement of a material point X (1.1.15) becomes

$$\mathbf{u} = \mathbf{u}(X^\alpha, \xi, t) = \mathbf{r} - \mathbf{R} + X^\beta \boldsymbol{\delta}_\beta. \tag{1.2.18}$$

Additionally for the rod-like body, the following deformation measures are noted:

$$\gamma_{ij} = \gamma_{ij}(\xi, t) = \mathbf{d}_i \cdot \mathbf{d}_j - \mathbf{D}_i \cdot \mathbf{D}_j, \quad \kappa_{\alpha i} = \kappa_{\alpha i}(\xi, t) = \mathbf{d}'_\alpha \cdot \mathbf{d}_i - \mathbf{D}'_\alpha \cdot \mathbf{D}_i, \tag{1.2.19}$$

where $(\cdot)' = \frac{\partial(\cdot)}{\partial \xi}$. In the linear theory, small $\|\mathbf{H}\|$ implies small $\|\boldsymbol{\delta}_i\|$, and we have the approximations:

$$\gamma_{ij} \approx \boldsymbol{\delta}_i \cdot \mathbf{E}_j + \boldsymbol{\delta}_j \cdot \mathbf{E}_i, \quad \kappa_{\alpha i} \approx \boldsymbol{\delta}'_\alpha \cdot \mathbf{E}_i. \tag{1.2.20}$$

We may relate the following displacement gradients to director displacements and director displacement gradients:

$$\mathbf{u}_{,\alpha} \approx \boldsymbol{\delta}_\alpha \quad \mathbf{u}_{,3} \approx \mathbf{r}' - \mathbf{E}_3 + X^\beta \boldsymbol{\delta}'_\beta, \tag{1.2.21}$$

and their components

$$u_{i,\alpha} \approx \boldsymbol{\delta}_\alpha \cdot \mathbf{E}_i \quad u_{i,3} \approx \mathbf{r}' \cdot \mathbf{E}_i - \delta_{i3} + X^\beta \boldsymbol{\delta}'_\beta \cdot \mathbf{E}_i. \tag{1.2.22}$$

Here, partial derivatives are with respect to the material coordinates and are denoted with a comma so that $\mathbf{u}_{,\alpha} = \frac{\partial \mathbf{u}}{\partial X^\alpha}$. On the Cartesian basis, we have the linearized Lagrange strain measures

$$\epsilon_{ij} = \boldsymbol{\epsilon} \cdot \mathbf{E}_i \otimes \mathbf{E}_j = \frac{1}{2}(u_{i,j} + u_{j,i}), \tag{1.2.23}$$

The linearized Lagrange strains become

$$\begin{aligned} \epsilon_{\alpha\alpha} = \boldsymbol{\delta}_\alpha \cdot \mathbf{E}_\alpha = \frac{1}{2}\gamma_{\alpha\alpha}, \quad \epsilon_{33} = \mathbf{r}' \cdot \mathbf{E}_3 - 1 + X^\beta \boldsymbol{\delta}'_\beta \cdot \mathbf{E}_3 = \frac{1}{2}\gamma_{33} + X^\beta \kappa_{\beta 3}, \\ \epsilon_{12} = \frac{1}{2}(\boldsymbol{\delta}_2 \cdot \mathbf{E}_1 + \boldsymbol{\delta}_1 \cdot \mathbf{E}_2) = \frac{1}{2}\gamma_{12}, \\ \epsilon_{\alpha 3} = \frac{1}{2}\big(\mathbf{r}' \cdot \mathbf{E}_\alpha + X^\beta \boldsymbol{\delta}'_\beta \cdot \mathbf{E}_\alpha + \boldsymbol{\delta}_\alpha \cdot \mathbf{E}_3\big) = \frac{1}{2}\gamma_{\alpha 3} + \frac{1}{2}X^\beta \kappa_{\beta\alpha}. \end{aligned} \tag{1.2.24}$$

Special sub-volumes

To develop one-dimensional quantities for a rod theory, we select our sub-bodies $\mathcal{P} \subseteq \mathcal{B}$ specially so that $\mathcal{V}_0$ is as displayed in Figure 1.3. The special sub-volume $\mathcal{V}_0$ is bounded by two cross-sections, $\mathcal{A}_0(\xi_1)$ and $\mathcal{A}_0(\xi_2)$, and the lateral surface of the rod which is defined as the union of cross-section boundaries:

$$\mathcal{L}_0(\xi_1, \xi_2) = \bigcup_{\xi_1 \le \xi \le \xi_2} \partial \mathcal{A}_0(\xi). \tag{1.2.25}$$

We may think of $\mathcal{V}_0$ now as being determined by two endpoints, ξ_1 and ξ_2:

$$\mathcal{V}_0(\xi_1, \xi_2) = \mathcal{A}_0(\xi_1) \bigcup \mathcal{L}_0(\xi_1, \xi_2) \bigcup \mathcal{A}_0(\xi_2). \tag{1.2.26}$$

This prescription for $\mathcal{V}_0$ ensures that an external boundary to $\mathcal{B}$ is always included in $\mathcal{V}_0$. That is,

$$\partial\mathcal{V}_0 \bigcap \partial\mathcal{R}_0 \neq \varnothing. \tag{1.2.27}$$

In what follows, the same material that occupies the surfaces $\mathcal{A}_0$ and $\mathcal{L}_0$ occupies $\mathcal{A}$ and $\mathcal{L}$ in the current configuration, respectively.

Kinetic energy, inertias, and momenta

We may substitute approximation (1.2.11) into the definition (1.1.52) for the kinetic energy of a part $\mathcal{P}$ to yield the decomposition:

$$T^* = \frac{1}{2} \int_{\mathcal{V}_0} \left(\mathbf{v} \cdot \mathbf{v} + 2X^\beta \mathbf{w}_\beta \cdot \mathbf{v} + X^\beta X^\gamma \mathbf{w}_\beta \cdot \mathbf{w}_\gamma \right) \rho_0^* dV. \tag{1.2.28}$$

Since the quantities in parentheses of (1.2.28) only depend on ξ and t, we may factor the integral assuming that $\mathcal{V}_0$ was chosen specially to have the form in (1.2.26):

$$T^* = \frac{1}{2} \int_{\xi_1}^{\xi_2} \left(\mathbf{v} \cdot \mathbf{v} \int_{\mathcal{A}_0(\xi)} \rho_0^* dA + 2\mathbf{w}_\beta \cdot \mathbf{v} \int_{\mathcal{A}_0(\xi)} X^\beta \rho_0^* dA + \mathbf{w}_\beta \cdot \mathbf{w}_\gamma \int_{\mathcal{A}_0(\xi)} X^\beta X^\gamma \rho_0^* dA \right) d\xi, \tag{1.2.29}$$

where $d\xi$ is an infinitesimal length measure which characterizes the small width of a small cross-sectional volume that contains a cross-section. Decomposition (1.2.29) is similar to the one due to König in the context of rigid body dynamics, but we do not assume here that $X^\beta \mathbf{w}_\beta$ is perpendicular to $\mathbf{v}$, since the cross-sections are allowed to deform. König's decomposition exploits the orthogonality of the velocity of a material point of a rigid body relative to the center of mass. Regardless, we can make definitions to extract quantities for the one-dimensional theory that are dependent only on ξ and/or t.

The one-dimensional mass density per reference arc-length is defined as:

$$\rho_0 = \rho_0(\xi) = \int_{\mathcal{A}_0(\xi)} \rho_0^* dA. \tag{1.2.30}$$

An interesting consequence of the one-dimensional theory is that it allows for ρ_0^* to tend to infinity if the area of $\mathcal{A}_0$ collapses towards zero. In that event, ρ_0 would remain finite. The one-dimensional reference first inertias, $y_0^{0\alpha} = y_0^{0\alpha}(\xi)$, are defined as

$$\rho_0 y_0^{0\alpha} = \int_{\mathcal{A}_0(\xi)} X^\alpha \rho_0^* dA. \tag{1.2.31}$$

We may think of the vector $y_0^{0\beta}\mathbf{D}_\beta$ as locating the center of mass relative to $(X^1, X^2) = (0, 0)$ for the small cross-sectional volume of width $d\xi$ centered at ξ. Many authors will fix the centerline so that $y_0^{0\alpha} = 0$, as in [47] and [25, (2.9)]. In that case, a decomposition of the kinetic energy identical to König's is recovered. The one-dimensional reference second inertias, $y_0^{\alpha\beta} = y_0^{\alpha\beta}(\xi)$ are defined as

$$\rho_0 y_0^{\alpha\beta} = \int_{\mathcal{A}_0(\xi)} X^\alpha X^\beta \rho_0^* dA. \tag{1.2.32}$$

The mass moment of inertia tensor of $\mathcal{P}$ in its reference configuration about some centerline point $\xi \in [\xi_1, \xi_2]$ is

$$\begin{aligned}\mathbf{J}_0^* &= \int_{\xi_1}^{\xi_2} \left(\int_{\mathcal{A}_0(\xi)} \big(\|\mathbf{R}^* - \mathbf{R}\|^2 \mathbf{I} - (\mathbf{R}^* - \mathbf{R}) \otimes (\mathbf{R}^* - \mathbf{R}) \big) \rho_0^* dA \right) d\xi \\ &= \int_{\xi_1}^{\xi_2} \left((\mathbf{D}_\beta \cdot \mathbf{D}_\gamma)\mathbf{I} \int_{\mathcal{A}_0(\xi)} X^\beta X^\gamma \rho_0^* dA - \mathbf{D}_\beta \otimes \mathbf{D}_\gamma \int_{\mathcal{A}_0(\xi)} X^\beta X^\gamma \rho_0^* dA \right) d\xi \\ &= \int_{\xi_1}^{\xi_2} \Big(\rho_0 y_0^{\beta\gamma} (\mathbf{D}_\beta \cdot \mathbf{D}_\gamma)\mathbf{I} - \rho_0 y_0^{\beta\gamma} \mathbf{D}_\beta \otimes \mathbf{D}_\gamma \Big) d\xi. \end{aligned} \tag{1.2.33}$$

We extract the one-dimensional mass moment of inertia tensor about the centerline for a cross-sectional lamina as

$$\mathbf{J}_0 = \mathbf{J}_0(\xi) = \rho_0 y_0^{\beta\gamma} (\mathbf{D}_\beta \cdot \mathbf{D}_\gamma)\mathbf{I} - \rho_0 y_0^{\beta\gamma} \mathbf{D}_\beta \otimes \mathbf{D}_\gamma. \tag{1.2.34}$$

Hence, $y_0^{\alpha\beta}$ are related to moments and products of inertia of cross-sectional laminae. As in the spectral theorem of linear algebra, it is possible to orient the Cartesian coordinates Y^α so that $y_0^{12} = y_0^{21} = 0$. If the material is homogenous in its mass density, then (1.2.31) and (1.2.32) become

$$\rho_0 y_0^{0\alpha} = \rho_0^* S^\alpha, \quad \rho_0 y_0^{\alpha\beta} = \rho_0^* I^{\alpha\beta}, \tag{1.2.35}$$

where

$$S^\alpha = \int_{\mathcal{A}_0(\xi)} X^\alpha dA, \quad I^{\alpha\beta} = I^{\beta\alpha} = \int_{\mathcal{A}_0(\xi)} X^\alpha X^\beta dA, \tag{1.2.36}$$

are the first and second moments and products of area, respectively, of the reference cross-section $\mathcal{A}_0(\xi)$. Since I^{22} is actually the second moment of area about the X^1 axis, it will be useful to denote

$$S^1 = S_2, \quad S^2 = S_1, \quad I^{11} = I_2, \quad I^{22} = I_1, \quad I^{12} = I_{12}, \tag{1.2.37}$$

where the subscript now identifies which axis the moment of area is taken about.

Using the newly defined one-dimensional inertias, decomposition (1.2.29) becomes

$$T^* = \frac{1}{2}\int_{\xi_1}^{\xi_2} \Big(\rho_0 \mathbf{v}\cdot\mathbf{v} + 2\rho_0 y_0^{0\beta}\mathbf{w}_\beta\cdot\mathbf{v} + \rho_0 y_0^{\beta\gamma}\mathbf{w}_\beta\cdot\mathbf{w}_\gamma\Big)d\xi. \tag{1.2.38}$$

The linear momentum of a cross-sectional lamina per unit reference arc-length is defined as

$$\mathbf{G} = \rho_0\mathbf{v} + \rho_0 y_0^{0\beta}\mathbf{w}_\beta = \int_{\mathcal{A}_0(\xi)} \rho_0^*\mathbf{v}^* dA. \tag{1.2.39}$$

Note that the linear momentum of $\mathcal{P}$ (1.1.36) is related to the one-dimensional linear momentum as

$$\mathbf{G}^* = \int_{\xi_1}^{\xi_2} \mathbf{G}d\xi. \tag{1.2.40}$$

Director momenta are defined as follows:

$$\mathbf{L}^\alpha = \rho_0 y_0^{0\alpha}\mathbf{v} + \rho_0 y_0^{\alpha\beta}\mathbf{w}_\beta = \int_{\mathcal{A}_0(\xi)} X^\alpha \rho_0^*\mathbf{v}^* dA. \tag{1.2.41}$$

Using the one-dimensional momenta, the kinetic energy decomposition (1.2.38) becomes

$$T^* = \frac{1}{2}\int_{\xi_1}^{\xi_2} \big(\mathbf{G}\cdot\mathbf{v} + \mathbf{L}^\beta\cdot\mathbf{w}_\beta\big)d\xi, \tag{1.2.42}$$

so that

$$T = \frac{1}{2}\big(\mathbf{G}\cdot\mathbf{v} + \mathbf{L}^\beta\cdot\mathbf{w}_\beta\big) \tag{1.2.43}$$

may be defined as the kinetic energy per unit reference arc-length for the one-dimensional theory. We may expand and factor the definition for the angular momentum of a part $\mathcal{P}$ (1.1.37) to obtain the decomposition

$$\begin{aligned}\mathbf{H}_O^* &= \int_{\xi_1}^{\xi_2} \Big(\mathbf{r}\times\big(\rho_0\mathbf{v} + \rho_0 y_0^{0\gamma}\mathbf{w}_\gamma\big) + \mathbf{d}_\beta\times\Big(\rho_0 y_0^{0\beta}\mathbf{v} + \rho_0 y_0^{\beta\gamma}\mathbf{w}_\gamma\Big)\Big)d\xi \\ &= \int_{\xi_1}^{\xi_2} \big(\mathbf{r}\times\mathbf{G} + \mathbf{d}_\beta\times\mathbf{L}^\beta\big)d\xi.\end{aligned} \tag{1.2.44}$$

The one-dimensional angular momentum about point O of a cross-sectional lamina is defined as

$$\mathbf{H}_O = \mathbf{H}_O(\xi,t) = \mathbf{r}\times\mathbf{G} + \mathbf{d}_\beta\times\mathbf{L}^\beta. \tag{1.2.45}$$

To relate changes in the one-dimensional quantities developed heretofore to external stimuli, it remains to derive the one-dimensional balance laws.

Balance of mass

For the chosen coordinates, one may establish a relation between volume and area measures as

$$dV = dY^1 dY^2 d\xi = dA d\xi. \tag{1.2.46}$$

An implication of (1.2.7) is that all volume elements dV in a given reference cross-sectional volume deform the same way into their dv counterparts in the current configuration. Therefore, for the current configuration we have

$$dv = (\mathbf{d}_1 \times \mathbf{d}_2) \cdot \mathbf{d}_3 dA d\xi = (\mathbf{e}_1 \times \mathbf{e}_2) \cdot \mathbf{e}_3 da \mu_3 d\xi, \tag{1.2.47}$$

where $da = \mu_1 \mu_2 dA$ is a small (rectangular) cross-sectional area measure for the current configuration. We may now define the one-dimensional current configuration mass density as

$$\rho = \rho(\xi, t) = (\mathbf{e}_1 \times \mathbf{e}_2) \cdot \mathbf{e}_3 \int_{\mathcal{A}(\xi)} \rho^* da. \tag{1.2.48}$$

Recall the conservation of mass for a sub-body $\mathcal{P}$ from (1.1.34) written as

$$\int_{\mathcal{V}_0} \rho_0^* dV = \int_{\mathcal{V}} \rho^* dv. \tag{1.2.49}$$

Factoring the integration along the centerline out of balance law (1.2.49) we find:

$$\int_{\xi_1}^{\xi_2} \left(\int_{\mathcal{A}_0(\xi)} \rho_0^* dA - \mu_3 (\mathbf{e}_1 \times \mathbf{e}_2) \cdot \mathbf{e}_3 \int_{\mathcal{A}(\xi)} \rho^* da \right) d\xi = 0. \tag{1.2.50}$$

With definitions (1.2.30) and (1.2.48) in view, the balance of mass for any sub-body occupying $\mathcal{V}_0(\xi_1, \xi_2)$ becomes

$$\int_{\xi_1}^{\xi_2} (\rho_0 - \mu_3 \rho) d\xi = 0, \tag{1.2.51}$$

which contains quantities that are only a function of ξ and time. Since (1.2.51) is assumed to hold true for all sub-volumes $\mathcal{V}_0(\xi_1, \xi_2)$, then the quantity in the parentheses must be zero by the localization theorem, and we arrive at the local one-dimensional conservation of mass:

$$\rho_0 = \mu_3 \rho. \tag{1.2.52}$$

The local conservation of mass (1.2.52) is not necessarily "point-wise" in the sense that it does not hold for a single material point X, but for a collection of material points comprising a cross-section. An implication of (1.2.52) is that

$$\frac{d}{dt}(\mu_3 \rho) = 0, \tag{1.2.53}$$

so that $\mu_3 \rho$ at some ξ is constant in time.

Balances of inertia

Starting from the point-wise conservation of mass $\rho_0^* = \rho^* J$ from three-dimensional continuum mechanics, which holds true for any X, we are free to write

$$X^\alpha \rho_0^* = X^\alpha \rho^* (\mathbf{d}_1 \times \mathbf{d}_2) \cdot \mathbf{d}_3, \tag{1.2.54}$$

where the Jacobian J has been computed using approximation (1.2.7). An integration over the specially chosen $\mathcal{V}_0$ yields

$$\int_{\xi_1}^{\xi_2} \left(\int_{\mathcal{A}_0(\xi)} X^\alpha \rho_0^* dA - (\mathbf{d}_1 \times \mathbf{d}_2) \cdot \mathbf{d}_3 \int_{\mathcal{A}_0(\xi)} X^\alpha \rho^* dA \right) d\xi = 0. \tag{1.2.55}$$

We may define a current first inertia as

$$y^{0\alpha} = y^{0\alpha}(\xi, t) = (\mathbf{e}_1 \times \mathbf{e}_2) \cdot \mathbf{e}_3 \int_{\mathcal{A}_0(\xi)} X^\alpha \rho^* da, \tag{1.2.56}$$

so that the modified conservation of mass (1.2.55) becomes

$$\int_{\xi_1}^{\xi_2} \left(y_0^{0\alpha} - \mu_3 y^{0\alpha} \right) d\xi = 0. \tag{1.2.57}$$

Since this holds true for any $\mathcal{V}_0$, we arrive at a local conservation of first inertia as

$$y_0^{0\alpha} = \mu_3 y^{0\alpha}. \tag{1.2.58}$$

We therefore have the implication

$$\frac{d}{dt} \left(\mu_3 y^{0\alpha} \right) = 0, \tag{1.2.59}$$

so that the quantity $\mu_3 y^{0\alpha}$ at some ξ is constant in time.

The point-wise conservation (1.2.7) may be further modified as

$$X^\alpha X^\beta \rho_0^* = X^\alpha X^\beta \rho^* (\mathbf{d}_1 \times \mathbf{d}_2) \cdot \mathbf{d}_3. \tag{1.2.60}$$

A similar procedure will result in the definition of the current second inertia as

$$y^{\alpha\beta} = y^{\alpha\beta}(\xi, t) = (\mathbf{e}_1 \times \mathbf{e}_2) \cdot \mathbf{e}_3 \int_{\mathcal{A}_0(\xi)} X^\alpha X^\beta \rho^* da. \tag{1.2.61}$$

Hence, a local conservation of second inertia is recovered as

$$y_0^{\alpha\beta} = \mu_3 y^{\alpha\beta}, \tag{1.2.62}$$

and we have that

$$\frac{d}{dt} \left(\mu_3 y^{\alpha\beta} \right) = 0, \tag{1.2.63}$$

which implies that the quantity $\mu_3 y^{\alpha\beta}$ at some ξ is conserved for all time.

Balance of linear momentum

To get at the one-dimensional balance of linear momentum, we integrate (1.1.49) over the specially chosen $\mathcal{V}_0$ described in (1.2.26) and factor the integral:

$$\int_{\xi_1}^{\xi_2} \int_{\mathcal{A}_0(\xi)} (\mathrm{Div}\mathbf{P} + \rho_0^* \mathbf{b} - \rho_0^* \dot{\mathbf{v}}^*) dA d\xi = \mathbf{0}. \tag{1.2.64}$$

An application of the divergence theorem yields the identity

$$\int_{\xi_1}^{\xi_2} \int_{\mathcal{A}_0(\xi)} \mathrm{Div}\mathbf{P} dA d\xi =$$
$$\int_{\mathcal{A}_0(\xi_1)} \mathbf{P}(-\mathbf{E}_3) dA + \int_{\mathcal{A}_0(\xi_2)} \mathbf{P}\mathbf{E}_3 dA + \int_{\xi_1}^{\xi_2} \oint_{\partial\mathcal{A}_0(\xi)} \mathbf{p} dU d\xi, \tag{1.2.65}$$

where dU is a small length measure on the external boundary. It is understood that $\mathbf{p}$ in (1.2.65) is not delivered by $\mathbf{P}$, but is supplied externally on the boundary $\partial\mathcal{R}$. We define the contact force $\mathbf{n}$ as the net force acting on a cross-section with reference unit normal $\mathbf{N}_0 = \mathbf{E}_3$ from a neighboring cross-section:

$$\mathbf{n} = \mathbf{n}(\xi, t) = \int_{\mathcal{A}_0(\xi)} \mathbf{P}\mathbf{E}_3 dA. \tag{1.2.66}$$

The assigned force is net force per unit reference arc-length acting on a cross-sectional lamina:

$$\rho_0 \mathbf{f} = \rho_0 \mathbf{f}(\xi, t) = \oint_{\partial\mathcal{A}_0(\xi)} \mathbf{p} dU + \int_{\mathcal{A}_0(\xi)} \rho_0^* \mathbf{b} dA. \tag{1.2.67}$$

Since $\mathcal{A}_0(\xi)$ does not change in time, we may write

$$\int_{\mathcal{A}_0(\xi)} \rho_0^* \dot{\mathbf{v}}^* dA = \frac{d}{dt} \int_{\mathcal{A}_0(\xi)} \rho_0^* \mathbf{v}^* dA = \dot{\mathbf{G}}. \tag{1.2.68}$$

Applying the foregoing definitions, the balance of linear momentum for the part $\mathcal{P}$ occupying $\mathcal{V}_0$ becomes

$$\mathbf{n}(\xi_2, t) - \mathbf{n}(\xi_1, t) + \int_{\xi_1}^{\xi_2} \Big(\rho_0 \mathbf{f} - \dot{\mathbf{G}}\Big) d\xi = \mathbf{0}. \tag{1.2.69}$$

Assuming continuity of $\mathbf{n}(\xi, t)$ in ξ, using the fundamental theorem of calculus, and noting that the endpoints of the interval (ξ_1, ξ_2) are fixed in time, expression (1.2.69) may be written as

$$\int_{\xi_1}^{\xi_2} (\mathbf{n}' + \rho_0 \mathbf{f}) d\xi = \frac{d}{dt} \int_{\xi_1}^{\xi_2} \mathbf{G} d\xi. \tag{1.2.70}$$

The domain of integration is now one-dimensional and all integrand quantities are spatially dependent only on ξ, as the dependence on cross-section coordinates has been integrated

away. Since (1.2.70) holds true on all sub-lengths (ξ_1, ξ_2) of the whole length $[0, \ell_0]$, then it must be the case that

$$\mathbf{n}' + \rho_0 \mathbf{f} = \dot{\mathbf{G}}, \tag{1.2.71}$$

which is the local form of the one-dimensional balance of linear momentum. If $\mathbf{n}$ in (1.2.69) is not continuous in ξ, we may use Leibniz rule to establish a jump condition at the singular point $\xi = \gamma$. Assuming a stationary singular point, i.e., $\dot{\gamma} = 0$, we find

$$[\![\mathbf{n}]\!]_\gamma + \mathbf{F}_\gamma = \mathbf{0}, \tag{1.2.72}$$

where

$$[\![\mathbf{n}]\!]_\gamma = \mathbf{n}\big(\gamma^+, t\big) - \mathbf{n}\big(\gamma^-, t\big), \tag{1.2.73}$$

is the jump in $\mathbf{n}$ across the singularity and

$$\mathbf{F}_\gamma = \mathbf{F}_\gamma(t) = \lim_{\chi \to 0} \int_{\gamma - \chi}^{\gamma + \chi} \rho_0 \mathbf{f} d\xi \tag{1.2.74}$$

is a singular force acting in or on the cross-section located at $\xi = \gamma$.

Balances of director momenta

We will now derive the one-dimensional balance of director momentum. The balance of linear momentum (1.1.49) holds for any X. Therefore, we are free to scale it by X^α just as we did when manipulating the mass densities:

$$X^\alpha \mathrm{Div}\mathbf{P} + X^\alpha \rho_0^* \mathbf{b} = X^\alpha \rho_0^* \dot{\mathbf{v}}^*. \tag{1.2.75}$$

Proceeding in the same manner as before and integrating over some sub-volume $\mathcal{V}_0(\xi_1, \xi_2)$, we work out the identity:

$$\begin{aligned} \int_{\mathcal{V}_0} X^\alpha \mathrm{Div}\mathbf{P} dV = &\int_{\mathcal{A}_0(\xi_1)} X^\alpha \mathbf{P}(-\mathbf{E}_3) dA + \int_{\mathcal{A}_0(\xi_2)} X^\alpha \mathbf{P}\mathbf{E}_3 dA \\ &+ \int_{\xi_1}^{\xi_2} \oint_{\partial \mathcal{A}_0(\xi)} X^\alpha \mathbf{p} dU d\xi - \int_{\mathcal{V}_0} \mathbf{P}\mathbf{E}_\alpha dV. \end{aligned} \tag{1.2.76}$$

We define the contact director forces as

$$\mathbf{m}^\alpha = \mathbf{m}^\alpha(\xi, t) = \int_{\mathcal{A}_0(\xi)} X^\alpha \mathbf{P}\mathbf{E}_3 dA, \tag{1.2.77}$$

the intrinsic director forces as

$$\mathbf{k}^\alpha = \mathbf{k}^\alpha(\xi, t) = \int_{\mathcal{A}_0(\xi)} \mathbf{P}\mathbf{E}_\alpha dA, \tag{1.2.78}$$

and the assigned director forces as

$$\rho_0 \mathbf{l}^\alpha = \rho_0 \mathbf{l}^\alpha(\xi, t) = \int_{\mathcal{A}_0(\xi)} X^\alpha \rho_0^* \mathbf{b} dA + \oint_{\partial \mathcal{A}_0(\xi)} X^\alpha \mathbf{p} dU. \tag{1.2.79}$$

Using conservation of mass in noting that $X^\alpha \rho_0^* \dot{\mathbf{v}}^* = \frac{d}{dt}(X^\alpha \rho_0^* \mathbf{v}^*)$, we find

$$\int_{\mathcal{A}_0(\xi)} X^\alpha \rho_0^* \dot{\mathbf{v}}^* dA = \frac{d}{dt} \int_{\mathcal{A}_0(\xi)} X^\alpha \rho_0^* \mathbf{v}^* dA = \dot{\mathbf{L}}^\alpha. \tag{1.2.80}$$

We now arrive at the one-dimensional balance of director momentum:

$$\mathbf{m}^\alpha(\xi_2, t) - \mathbf{m}^\alpha(\xi_1, t) + \int_{\xi_1}^{\xi_2} \Big(\rho_0 \mathbf{l}^\alpha - \mathbf{k}^\alpha - \dot{\mathbf{L}}^\alpha \Big) d\xi = \mathbf{0}. \tag{1.2.81}$$

Assuming continuity of $\mathbf{m}^\alpha$ in ξ, the local version is derived:

$$\mathbf{m}^{\alpha'} - \mathbf{k}^\alpha + \rho_0 \mathbf{l}^\alpha = \dot{\mathbf{L}}^\alpha. \tag{1.2.82}$$

If $\mathbf{m}^\alpha$ in (1.2.81) is not continuous at some $\xi = \gamma$, we may once again apply Leibniz rule to obtain the jump conditions for a stationary singular point γ:

$$[\![\mathbf{m}^\alpha]\!]_\gamma + \mathbf{F}_\gamma^\alpha = \mathbf{0}, \tag{1.2.83}$$

where

$$\mathbf{F}_\gamma^\alpha = \mathbf{F}_\gamma^\alpha(t) = \lim_{\chi \to 0} \int_{\gamma - \chi}^{\gamma + \chi} \rho_0 \mathbf{l}^\alpha d\xi \tag{1.2.84}$$

are singular director forces acting in or on the cross-section at $\xi = \gamma$.

Balance of angular momentum

A one-dimensional balance of angular momentum is also desired. The three-dimensional postulate is recalled as:

$$\int_{\mathcal{V}} \mathbf{r}^* \times \rho^* \mathbf{b} dv + \int_{\partial \mathcal{V}} \mathbf{r}^* \times \mathbf{t} da = \dot{\mathbf{H}}_O^*. \tag{1.2.85}$$

From the definition of the one-dimensional angular momentum (1.2.45), we assume there are no singular sources of mass and inertia to compute

$$\dot{\mathbf{H}}_O^* = \int_{\xi_1}^{\xi_2} \dot{\mathbf{H}}_O d\xi = \int_{\xi_1}^{\xi_2} \Big(\mathbf{r} \times \dot{\mathbf{G}} + \mathbf{d}_\beta \times \dot{\mathbf{L}}^\beta \Big) d\xi. \tag{1.2.86}$$

We remind ourselves from (1.1.45) that the small amount of force transmitted across a current boundary with area element da relates the Cauchy traction to the Piola traction as

$\mathbf{t}da = \mathbf{p}dA$. Applying assumption (1.2.7) and factoring the integral, we find the balance of angular momentum for some specially chosen part $\mathcal{P}$ as:

$$\begin{aligned} &-\mathbf{r}(\xi_1,t)\times\mathbf{n}(\xi_1,t)+\mathbf{r}(\xi_2,t)\times\mathbf{n}(\xi_2,t)\\ &-\mathbf{d}_\beta(\xi_1,t)\times\mathbf{m}^\beta(\xi_1,t)+\mathbf{d}_\beta(\xi_2,t)\times\mathbf{m}^\beta(\xi_2,t)\\ &+\int_{\xi_1}^{\xi_2}\Big(\mathbf{r}\times\rho_0\mathbf{f}+\mathbf{d}_\beta\times\rho_0\mathbf{l}^\beta-\mathbf{r}\times\dot{\mathbf{G}}-\mathbf{d}_\beta\times\dot{\mathbf{L}}^\beta\Big)d\xi=\mathbf{0}. \end{aligned} \tag{1.2.87}$$

Under the usual continuity assumptions, and noting that, barring fracture, $\mathbf{r}$ and $\mathbf{d}_\alpha$ are never expected to jump in ξ, we arrive at the one-dimensional local version:

$$\big(\mathbf{r}\times\mathbf{n}+\mathbf{d}_\beta\times\mathbf{m}^\beta\big)'+\mathbf{r}\times\rho_0\mathbf{f}+\mathbf{d}_\beta\times\rho_0\mathbf{l}^\beta=\mathbf{r}\times\dot{\mathbf{G}}+\mathbf{d}_\beta\times\dot{\mathbf{L}}^\beta. \tag{1.2.88}$$

Note that we may view

$$\mathbf{m}=\mathbf{d}_\beta\times\mathbf{m}^\beta \tag{1.2.89}$$

as a couple acting on the cross-section at ξ due to stress and

$$\mathbf{m}_a=\mathbf{d}_\beta\times\rho_0\mathbf{l}^\beta \tag{1.2.90}$$

as an external couple due to applied loads. Using the balances of linear and director momentum (1.2.71) and (1.2.82), we recover the identity

$$\mathbf{r}'\times\mathbf{n}+\mathbf{d}_\beta\times\mathbf{k}^\beta+\mathbf{d}'_\beta\times\mathbf{m}^\beta=\mathbf{0}, \tag{1.2.91}$$

which is analogous to the symmetry condition on the Cauchy stress (1.1.44) in the three-dimensional theory.

A one-dimensional strain energy

For Green-elastic solids, we would like to develop a one-dimensional strain energy. From $\rho_0^*\psi^* = \rho_0^*\psi^*(\mathbf{F})$, we derive the one-dimensional version as

$$\rho_0\overline{\psi}=\int_{\mathcal{A}_0(\xi)}\rho_0^*\psi^*dA, \tag{1.2.92}$$

where the reason for the overline on $\rho_0\overline{\psi}$ will be discussed shortly. Insertion of (1.2.24) into (1.1.71) yields the resulting $\rho_0\overline{\psi}$ as

$$\begin{aligned}\rho_0\overline{\psi} = \frac{(\lambda+2\mu)A}{8}\left(\gamma_{11}^2+\gamma_{22}^2+\gamma_{33}^2\right)\\ +\frac{\mu A}{2}\left(\frac{(\gamma_{21}+\gamma_{12})^2}{4}+\gamma_{13}^2+\gamma_{23}^2\right)+\frac{\lambda A}{4}(\gamma_{11}\gamma_{22}+\gamma_{11}\gamma_{33}+\gamma_{22}\gamma_{33})\\ +\frac{\mu I^{11}}{2}\left(\kappa_{11}^2+\kappa_{12}^2\right)+\frac{\mu I^{22}}{2}\left(\kappa_{22}^2+\kappa_{21}^2\right)\\ +\frac{(\lambda+2\mu)I^{11}}{2}\kappa_{13}^2+\frac{(\lambda+2\mu)I^{22}}{2}\kappa_{23}^2\\ +\mu I^{12}(\kappa_{11}\kappa_{21}+\kappa_{12}\kappa_{22})+(\lambda+2\mu)I^{12}\kappa_{13}\kappa_{23}\\ +\frac{\lambda S^1}{2}(\gamma_{11}+\gamma_{22}+\gamma_{33})\kappa_{13}+\frac{\lambda S^2}{2}(\gamma_{11}+\gamma_{22}+\gamma_{33})\kappa_{23}\\ +\mu S^1(\gamma_{33}\kappa_{13}+\gamma_{13}\kappa_{11}+\gamma_{23}\kappa_{12})+\mu S^2(\gamma_{33}\kappa_{23}+\gamma_{13}\kappa_{21}+\gamma_{23}\kappa_{22}),\end{aligned} \tag{1.2.93}$$

where $(1.2.36)_{1,2}$ have been used. The centerline may be chosen so that $S^1=0=S^2$ and the coordinates oriented so that $I^{12}=0$. If the material is homogeneous in its mass density, then these choices are equivalent to $y_0^{01}=0=y_0^{02}$ and $y_0^{12}=0$. Now the strain energy for the one-dimensional rod becomes

$$\begin{aligned}2\rho_0\overline{\psi} = \overline{k}_1\gamma_{11}^2+\overline{k}_2\gamma_{22}^2+\overline{k}_3\gamma_{33}^2+\overline{k}_4\frac{(\gamma_{21}+\gamma_{12})^2}{4}+\overline{k}_5\gamma_{13}^2+\overline{k}_6\gamma_{23}^2\\ +\overline{k}_7\gamma_{11}\gamma_{22}+\overline{k}_8\gamma_{11}\gamma_{33}+\overline{k}_9\gamma_{22}\gamma_{33}+\overline{k}_{10}\kappa_{11}^2+\overline{k}_{11}\kappa_{22}^2+\overline{k}_{12}\kappa_{12}^2+\overline{k}_{13}\kappa_{21}^2\\ +\overline{k}_{14}\kappa_{13}^2+\overline{k}_{15}\kappa_{23}^2,\end{aligned} \tag{1.2.94}$$

where the stiffnesses are

$$\begin{aligned}\overline{k}_1=\overline{k}_2=\overline{k}_3=\frac{(\lambda+2\mu)A}{4},\quad \overline{k}_4=\overline{k}_5=\overline{k}_6=\mu A,\quad \overline{k}_7=\overline{k}_8=\overline{k}_9=\frac{\lambda A}{2},\\ \overline{k}_{10}=\overline{k}_{12}=\mu I_2,\quad \overline{k}_{11}=\overline{k}_{13}=\mu I_1,\quad \overline{k}_{14}=(\lambda+2\mu)I_2,\quad \overline{k}_{15}=(\lambda+2\mu)I_1,\end{aligned} \tag{1.2.95}$$

and formulae $(1.2.37)_{3,4}$ have been used. We recall for completeness the relationships between elastic moduli:

$$\lambda=\frac{E\nu}{(1+\nu)(1-2\nu)},\quad \mu=\frac{E}{2(1+\nu)}, \tag{1.2.96}$$

where E and ν are Young's modulus and Poisson's ratio, respectively. It is well known that (1.2.94) fails to produce results that are consistent with exact solutions from three-dimensional elasticity. In [47] it is explained that a more ideal set of stiffness coefficients

which more closely match exact solutions from elasticity is

$$2\rho_0\psi = k_1\gamma_{11}^2 + k_2\gamma_{22}^2 + k_3\gamma_{33}^2 + k_4\frac{(\gamma_{21}+\gamma_{12})^2}{4} + k_5\gamma_{13}^2 + k_6\gamma_{23}^2$$
$$+k_7\gamma_{11}\gamma_{22} + k_8\gamma_{11}\gamma_{33} + k_9\gamma_{22}\gamma_{33} + k_{10}\kappa_{11}^2 + k_{11}\kappa_{22}^2 + k_{12}\kappa_{12}^2 + k_{13}\kappa_{21}^2$$
$$+k_{14}\kappa_{13}^2 + k_{15}\kappa_{23}^2 + k_{16}\kappa_{12}\kappa_{21}, \tag{1.2.97}$$

where

$$k_1 = k_2 = k_3 = \frac{(\lambda+2\mu)A}{4}, \quad k_4 = \mu A, \quad k_5 = k_6 = k\mu A, \quad k_7 = k_8 = k_9 = \frac{\lambda A}{2},$$
$$k_{10} = \mu I_2, \quad k_{11} = \mu I_2, \quad k_{12} = k_{13} = \frac{1}{4}(\mu I_2 + \mu I_1 - \mathscr{D}), \quad k_{14} = EI_2, \quad k_{15} = EI_1,$$
$$k_{16} = \frac{1}{2}(\mu I_2 + \mu I_1 - \mathscr{D}). \tag{1.2.98}$$

Here, k is the shear correction factor [15] and $\mathscr{D}$ is the torsional rigidity. We note that $I_1 + I_2$ may be considered as a polar area moment of inertia.

While one should proceed with caution in applying (1.2.97) to the modeling of isotropic rod-like bodies undergoing small deformations, we have found (1.2.97) to be sufficiently descriptive for use in many problems. For example, (1.2.97) is the basis for a validated model of peristaltic locomotion that is presented in Chapter 2 which is dominated by the Poisson effect. In addition, we have used (1.2.97) as inspiration for the non-linear strain energy postulated for the discrete elastic rod that is presented in Chapter 3. There, we validate the discrete theory against known solutions of Timoshenko beams involving shear deformation and necking problems, which involve cross-sectional strain gradients. If one attempts to model behavior such as bending and warping of cross-sections, (1.2.97) has been found to be in poor agreement with solutions from linear elasticity, as approximation (1.2.7) becomes invalid in those problems.

1.3 The direct approach

In the direct approach, we proceed by presuming the existence of an abstract directed curve. Rather than starting with a rod-like body and adopting approximation (1.2.7), primitive quantities associated with the curve are postulated. To make any practical use of this approach, a mapping from real three-dimensional material to the abstract directed curve will need to be established. For that mapping, (1.2.7) is assumed to be exact. Balance laws for the directed curve are postulated for finite segments, and the localization procedure can be considered to yield point-wise laws, in contrast to the preceding approach from three dimensions. Indicies in this section are to identify quantities associated with the first, second, or third director, rather than being components of objects that are tensorial under a change of convected coordinates.

Kinematics of the abstract curve

Referring to Figure 1.4, the directed curve $\mathcal{B}^{\mathrm{A}}$ comprises the centerline, which is an extensible space curve of material points, and two directors, which are vector fields defined on the centerline. Since we have no access to the convected coordinates X^α, the directors are introduced as a primitive field, rather than as partial derivatives of a three-dimensional placement with respect to material coordinates. The abstract directed curve is assumed to occupy a reference configuration with the parameter ξ assigned physical meaning as the reference centerline arc-length: $\xi \in [0, \ell_0]$. Here, ℓ_0 is the total physical length of the reference centerline, as in the three-dimensional case. A pair of reference directors $\mathbf{D}_\alpha$ are placed at every value of ξ in the reference configuration. A part $\mathcal{P}^{\mathrm{A}}$ of the abstract directed curve is specified by two endpoints ξ_1 and ξ_2: $\mathcal{P}^{\mathrm{A}} = \{\xi, \mathbf{D}_\alpha(\xi) | \xi \in [\xi_1, \xi_2]\}$, where we have used ξ to indicate a centerline material point.

The vector-valued function $\mathbf{R}(\xi)$ delivers the reference placement $\mathbf{R}$ of centerline material points in $\mathcal{E}^3$. Making use of ξ as a Cartesian spatial coordinate for $\mathcal{E}^3$ and aligning a unit vector $\mathbf{E}_3$ along the long axis of the rod-like body, we may write

$$\mathbf{R} = \xi \mathbf{E}_3. \tag{1.3.1}$$

The reference configuration of the abstract curve is assumed to be straight and in its natural state. In contrast to $\boldsymbol{\kappa}_0$ in (1.1.8), the reference configuration is specified by the triplet of vector-valued functions $\{\mathbf{R}(\xi), \mathbf{D}_\alpha(\xi)\}$. We choose to make the identification

$$\mathbf{D}_1 = \mathbf{E}_1, \quad \text{and} \quad \mathbf{D}_2 = \mathbf{E}_2. \tag{1.3.2}$$

The reference configuration region $\mathcal{R}_0$ occupied by the three-dimensional body $\mathcal{B}$ is related to the abstract directed curve as shown in Figure 1.4 by

$$\mathbf{R}^* = \mathbf{R} + X^\beta \mathbf{D}_\beta, \tag{1.3.3}$$

where X^α are the material coordinates for $\mathcal{B}$ that were introduced in the prior sections. The current configuration of the directed curve is given by the vector fields $\mathbf{r} = \mathbf{r}(\xi, t)$ and $\mathbf{d}_\alpha = \mathbf{d}_\alpha(\xi, t)$. It is assumed that $\mathcal{B}$ is placed into the region $\mathcal{R}$ by the relation

$$\mathbf{r}^* = \mathbf{r} + X^\beta \mathbf{d}_\beta. \tag{1.3.4}$$

Relationships (1.3.3) and (1.3.4) are sufficient for constructing images of the three-dimensional body $\mathcal{B}$ given the reference and current configurations of the abstract directed curve. The centerline velocity and director velocities are defined as the material derivatives

$$\mathbf{v} = \dot{\mathbf{r}}, \quad \mathbf{w}_\alpha = \dot{\mathbf{d}}_\alpha. \tag{1.3.5}$$

The solution process amounts to finding $\mathbf{r} = \mathbf{r}(\xi, t)$ and $\mathbf{d}_\alpha = \mathbf{d}_\alpha(\xi, t)$, which are responsive to external influences acting on the curve. These influences will be related to the kinematics via the balance laws for the directed curve.

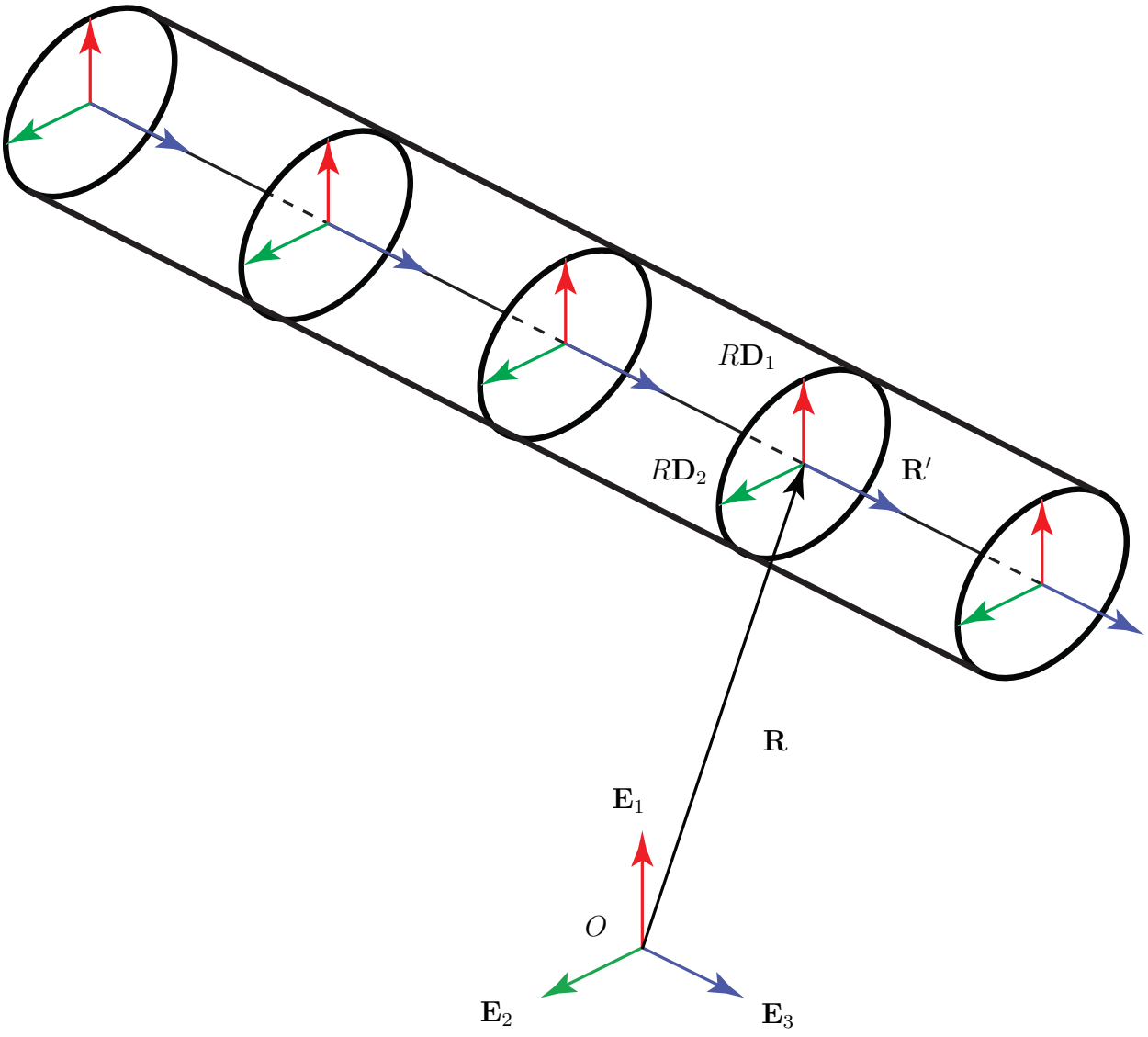

Figure 1.4: *The reference configuration mapping between the abstract directed curve and the real material of the rod-like body.*

We denote the arc-length parameter for the current configuration centerline by s. As before, to take full advantage of indicial notation, the shorthand $\mathbf{D}_3 = \mathbf{R}'$ and $\mathbf{d}_3 = \mathbf{r}'$ is useful. Since any motion where a director $\mathbf{d}_i$ tends to $\mathbf{0}$ or is coincident with another director is unphysical and therefore unanticipated, we are safe to use $\{\mathbf{d}_i\}$ as a basis for $\mathbb{E}^3$. The unit length basis $\{\mathbf{e}_i\}$ is re-introduced as $\mathbf{e}_i = \mathbf{d}_i/\|\mathbf{d}_i\|$. The vector $\mathbf{e}_3 = \mathbf{e}_t$ additionally serves as

the current centerline's unit tangent. The stretches μ_i are found as the length of $\mathbf{d}_i$:

$$\mu_i = \|\mathbf{d}_i\|. \tag{1.3.6}$$

An engineering strain for material line elements along $\mathbf{e}_i$ may be calculated as $\mu_i - 1$. Centerline gradients of field quantities may be computed as directional derivatives along the centerline in the direction of increasing ξ. In terms of the directors, μ'_α may be computed as

$$\mu'_\alpha = \frac{\mathbf{d}_\alpha \cdot \mathbf{d}'_\alpha}{\|\mathbf{d}_\alpha\|}, \quad \text{(no sum)}. \tag{1.3.7}$$

We may refer to μ'_α either as a stretch gradient or a strain gradient. The deformation measures γ_{ij} and $\kappa_{\alpha i}$ are accepted from the previous section.

Balance laws

Several primitive quantities are assumed to exist that belong to the directed curve. These quantities are defined in Table 1.1 and they are not thought to be derivable from quantities associated with three-dimensional continuum mechanics. The following quantities for the

Table 1.1: Primitive quantities associated with the abstract directed curve.

Definition	Primitive
Reference configuration directors	$\mathbf{D}_\alpha(\xi)$
Current configuration directors	$\mathbf{d}_\alpha(\xi, t)$
Reference configuration centerline mass density per unit reference length	$\rho_0(\xi)$
Reference configuration first inertias per unit reference length	$y_0^{0\alpha}(\xi)$
Reference configuration second inertias per unit reference length	$y_0^{\alpha\beta}(\xi)$
Centerline assigned force per unit mass	$\mathbf{f}(\xi, t)$
Director assigned forces per unit mass	$\mathbf{l}^\alpha(\xi, t)$
Contact force	$\mathbf{n}(\xi, t)$
Intrinsic director forces	$\mathbf{k}^\alpha(\xi, t)$
Contact director forces	$\mathbf{m}^\alpha(\xi, t)$
Helmholtz free energy per unit mass	$\psi(\mathbf{d}_i, \mathbf{d}'_\alpha)$

directed curve are defined from the primitive quantities:

$$\begin{aligned}
\mathbf{G} &= \rho_0 \mathbf{v} + \rho_0 y_0^{0\beta} \mathbf{w}_\beta, \\
\mathbf{L}^\alpha &= \rho_0 y_0^{0\alpha} \mathbf{v} + \rho_0 y_0^{\alpha\beta} \mathbf{w}_\beta, \\
\mathbf{H}_O &= \mathbf{r} \times \mathbf{G} + \mathbf{d}_\beta \times \mathbf{L}^\beta, \\
\mathbf{m} &= \mathbf{d}_\beta \times \mathbf{m}^\beta, \\
\mathbf{m}_a &= \mathbf{d}_\beta \times \rho_0 \mathbf{l}^\beta,
\end{aligned} \tag{1.3.8}$$

which are, respectively, the linear momentum, the director momenta, the angular momentum about O, the internal torque, and the applied torque, all per unit reference length of the centerline.

To model the effect of the external loading on the kinematics, it suffices to postulate five balance laws involving the primitive quantities for any part $\mathcal{P}^{\mathrm{A}} \subseteq \mathcal{B}^{\mathrm{A}}$. In order, the balance laws are: six conservations of mass and inertia, a balance of linear momentum, two balances of director momentum, and a balance of angular momentum. They are listed for any part $\mathcal{P}^{\mathrm{A}}$ as

$$\begin{aligned}
\frac{d}{dt}\int_{\xi_1}^{\xi_2} \rho_0 d\xi &= 0, \\
\frac{d}{dt}\int_{\xi_1}^{\xi_2} \rho_0 y_0^{0\alpha} d\xi &= 0, \\
\frac{d}{dt}\int_{\xi_1}^{\xi_2} \rho_0 y_0^{\alpha\beta} d\xi &= 0, \\
\frac{d}{dt}\int_{\xi_1}^{\xi_2} \mathbf{G} d\xi &= [\mathbf{n}]_{\xi_1}^{\xi_2} + \int_{\xi_1}^{\xi_2} \rho_0 \mathbf{f} d\xi, \\
\frac{d}{dt}\int_{\xi_1}^{\xi_2} \mathbf{L}^\alpha d\xi &= [\mathbf{m}^\alpha]_{\xi_1}^{\xi_2} + \int_{\xi_1}^{\xi_2} (\rho_0 \mathbf{l}^\alpha - \mathbf{k}^\alpha) d\xi, \\
\frac{d}{dt}\int_{\xi_1}^{\xi_2} \mathbf{H}_O d\xi &= [\mathbf{r} \times \mathbf{n} + \mathbf{m}]_{\xi_1}^{\xi_2} + \int_{\xi_1}^{\xi_2} (\mathbf{r} \times \rho_0 \mathbf{f} + \mathbf{m}_a) d\xi.
\end{aligned} \tag{1.3.9}$$

The assigned forces $\mathbf{f}$ and $\mathbf{l}^\alpha$ may contain singular pieces at some stationary point γ. The conditions (1.2.74) and (1.2.84) apply in this abstract approach since they are derived from primitive quantities associated with the directed curve. The current configuration inertias may be defined from the conservation laws for mass and inertia as

$$\rho = \rho(\xi, t) = \frac{\rho_0}{\mu_3}, \quad y^{0\alpha} = y^{0\alpha}(\xi, t) = \frac{y_0^{0\alpha}}{\mu_3}, \quad y^{\alpha\beta} = y^{\alpha\beta}(\xi, t) = \frac{y_0^{\alpha\beta}}{\mu_3}. \tag{1.3.10}$$

Using the localization theorem on the balance laws (1.3.9) we recover the local versions from the previous section, namely: (1.2.53), (1.2.59), (1.2.63), (1.2.71), (1.2.82), and (1.2.91).

In the next chapter, peristaltic locomotion is described as a quasistatic process. In such a process, inertial forces are small compared to elastic, constraint, and applied forces, and the rod is assumed to pass through a succession of equilibrium configurations during its motion. We obtain the governing equations for such a case by neglecting the rates of change of linear and director momenta in (1.3.9).

As in the case of Green-elastic materials, we presume the existence of a scalar function $\rho_0\psi$ (cf. (1.1.54)). This function is assumed to satisfy the balance of energy

$$\rho_0\dot{\psi} = \dot{\mathbf{r}}' \cdot \mathbf{n} + \dot{\mathbf{d}}_\beta \cdot \mathbf{k}^\beta + \dot{\mathbf{d}}'_\beta \cdot \mathbf{m}^\beta, \tag{1.3.11}$$

where the right hand side of (1.3.11) is the stress power of the directed curve. For a quasistatic process, the material time derivatives of (1.3.11) are retained as there are non-negligible differences in the strain energy between successive equilibria.

Constitutive relations

Constitutive relations between the internal forces and gradients of the strain energy per unit mass $\rho_0\psi$ must be derived. A representation of the strain energy may be given in terms of the directors and their centerline gradients:

$$\rho_0\psi = \rho_0\hat{\psi}(\mathbf{d}_i, \mathbf{d}'_\alpha). \tag{1.3.12}$$

A notation such as $f = \hat{f}(\mathbf{d}_i, \mathbf{d}'_\alpha)$ means that $\hat{f}$ is a function of $\mathbf{d}_1, \mathbf{d}_2, \mathbf{d}_3, \mathbf{d}'_1$ and $\mathbf{d}'_2$ while one such as $f = \tilde{f}(\mu_i, \mu'_\alpha)$ means that $\tilde{f}$ is a function of μ_1, μ_2, μ_3, μ'_1, and μ'_2. The functional dependence of (1.3.12) on the directors and their gradients is to be constructed in such a way that the strain energy remains invariant under superposed rigid motions so as to obey the principle of material frame indifference. We will make use of a strain energy function of the form $\rho_0\psi = \rho_0\tilde{\psi}(\mu_i, \mu'_\alpha)$, which is automatically properly invariant under superposed rigid motions, no matter the functional form, since μ_i and μ'_α are unaltered under a uniform translation and rotation. To ease the notational burden, we will call the specific strain energy $\rho_0\psi$, a Helmholtz free energy, as w:

$$w = \rho_0\psi = \hat{w}(\mathbf{d}_i, \mathbf{d}'_\alpha) = \tilde{w}(\mu_i, \mu'_\alpha). \tag{1.3.13}$$

By inserting $\hat{w}$ into (1.3.11), an expression which must hold true for all kinematically admissible motions is derived:

$$\left(\mathbf{n} - \frac{\partial\hat{w}}{\partial\mathbf{r}'}\right) \cdot \dot{\mathbf{r}}' + \left(\mathbf{k}^\beta - \frac{\partial\hat{w}}{\partial\mathbf{d}_\beta}\right) \cdot \dot{\mathbf{d}}_\beta + \left(\mathbf{m}^\beta - \frac{\partial\hat{w}}{\partial\mathbf{d}'_\beta}\right) \cdot \dot{\mathbf{d}}'_\beta = 0. \tag{1.3.14}$$

If the medium we are seeking to model is internally unconstrained, then we are at liberty to construct a motion in which

$$\left(\dot{\mathbf{r}}', \dot{\mathbf{d}}_\alpha, \dot{\mathbf{d}}'_\alpha\right) = c\left(\mathbf{n} - \frac{\partial\hat{w}}{\partial\mathbf{r}'}, \mathbf{0}, \mathbf{0}\right), \tag{1.3.15}$$

where c is any strictly positive constant of the appropriate physical dimension. We find a necessary condition following from (1.3.11) as

$$c\left\|\mathbf{n}-\frac{\partial\hat{w}}{\partial\mathbf{r}'}\right\|^2=0, \tag{1.3.16}$$

i.e.,

$$\mathbf{n}-\frac{\partial\hat{w}}{\partial\mathbf{r}'}=\mathbf{0}. \tag{1.3.17}$$

Through an identical set of arguments and noting that $\mathbf{d}'_\alpha$ may be varied independently from $\mathbf{d}_\alpha$ at fixed ξ, the following implications of (1.3.11) are derived:

$$\mathbf{n}=\frac{\partial\hat{w}}{\partial\mathbf{r}'},\quad \mathbf{k}^\alpha=\frac{\partial\hat{w}}{\partial\mathbf{d}_\alpha},\quad \mathbf{m}^\alpha=\frac{\partial\hat{w}}{\partial\mathbf{d}'_\alpha}. \tag{1.3.18}$$

The internal forces for an unconstrained medium are thus constitutively determined by $\hat{w}$. With the help of (1.3.6) and (1.3.7), we calculate the gradients

$$\begin{aligned}\frac{\partial\mu_j}{\partial\mathbf{d}_i}&=\delta^j_i\mathbf{e}_j\quad\text{(no sum)},\\ \frac{\partial\mu'_\beta}{\partial\mathbf{d}_\alpha}&=\delta^\alpha_\beta(\mathbf{I}-\mathbf{e}_\beta\otimes\mathbf{e}_\beta)\frac{\mathbf{d}'_\beta}{\mu_\beta}\quad\text{(no sum)},\\ \frac{\partial\mu'_\beta}{\partial\mathbf{d}'_\alpha}&=\delta^\alpha_\beta\mathbf{e}_\beta\quad\text{(no sum)}.\end{aligned} \tag{1.3.19}$$

Here, $\otimes$ is the tensor product, defined so that $(\mathbf{a}\otimes\mathbf{b})\mathbf{c}=\mathbf{a}(\mathbf{b}\cdot\mathbf{c})$ for any three vectors $\mathbf{a},\mathbf{b},\mathbf{c}\in\mathbb{E}^3$ and $\mathbf{I}$ is the identity tensor: $\mathbf{I}\mathbf{a}=\mathbf{a}$. Using a chain rule, one can establish the relations

$$\begin{aligned}\frac{\partial\hat{w}}{\partial\mathbf{d}_\alpha}&=\frac{\partial\tilde{w}}{\partial\mu_\alpha}\mathbf{e}_\alpha+\frac{\partial\tilde{w}}{\partial\mu'_\alpha}(\mathbf{I}-\mathbf{e}_\alpha\otimes\mathbf{e}_\alpha)\frac{\mathbf{d}'_\alpha}{\mu_\alpha}\quad\text{(no sum)},\\ \frac{\partial\hat{w}}{\partial\mathbf{r}'}&=\frac{\partial\tilde{w}}{\partial\mu_3}\mathbf{e}_3,\quad \frac{\partial\hat{w}}{\partial\mathbf{d}'_\alpha}=\frac{\partial\tilde{w}}{\partial\mu'_\alpha}\mathbf{e}_\alpha\quad\text{(no sum)}.\end{aligned} \tag{1.3.20}$$

The internal forces of (1.3.18) may now be constitutively determined when $\tilde{w}$ is prescribed.

Internal constraints and reactions

To model incompressibility, we admit an internal constraint of the form

$$\phi^{\mathrm{I}}=\phi^{\mathrm{I}}(\mathbf{r}',\mathbf{d}_\alpha,\mathbf{d}'_\alpha)=0, \tag{1.3.21}$$

which yields a restriction on the class of allowable deformations. The deformation of a single cross-section of the rod at ξ is determined by $(\mathbf{r}',\mathbf{d}_\alpha,\mathbf{d}'_\alpha)$ which may be considered as an element of the direct sum

$$\mathbb{V}=\bigoplus_{i=1}^{5}\mathbb{E}^3. \tag{1.3.22}$$

Equation (1.3.21) may now be thought to describe a constraint hypersurface, $\mathcal{M}$, contained in $\mathbb{V}$. Barring any material property changes during the motion, (1.3.21) holds for all time, which implies the orthogonality condition:

$$\dot{\phi} = \frac{\partial \phi^{\mathrm{I}}}{\partial \mathbf{r}'} \cdot \dot{\mathbf{r}}' + \frac{\partial \phi^{\mathrm{I}}}{\partial \mathbf{d}_\beta} \cdot \dot{\mathbf{d}}_\beta + \frac{\partial \phi^{\mathrm{I}}}{\partial \mathbf{d}'_\beta} \cdot \dot{\mathbf{d}}'_\beta = 0. \tag{1.3.23}$$

Thus, a basis vector has been identified for the one-dimensional orthogonal complement to the tangent space of $\mathcal{M}$ at some value of the deformation:

$$\mathrm{Span}\left(\frac{\partial \phi^{\mathrm{I}}}{\partial \mathbf{r}'}, \frac{\partial \phi^{\mathrm{I}}}{\partial \mathbf{d}_\alpha}, \frac{\partial \phi^{\mathrm{I}}}{\partial \mathbf{d}'_\alpha} \right) = T^{\perp}_{(\mathbf{r}', \mathbf{d}_\alpha, \mathbf{d}'_\alpha)} \mathcal{M}. \tag{1.3.24}$$

Reexamining the requirement for kinematic admissibility in (1.3.14), we see that an arbitrarily constructed motion using $\dot{\mathbf{r}}', \dot{\mathbf{d}}_\alpha$, and $\dot{\mathbf{d}}'_\alpha$ could violate the internal constraint. For the internal constraint (1.3.21) to remain true, (1.3.14) holds only in motions for which $\left(\dot{\mathbf{r}}', \dot{\mathbf{d}}_\alpha, \dot{\mathbf{d}}'_\alpha \right)$ is along the tangent space of $\mathcal{M}$. Therefore, an element of the orthogonal complement is found:

$$\left(\mathbf{n} - \frac{\partial \hat{w}}{\partial \mathbf{r}'}, \mathbf{k}^\alpha - \frac{\partial \hat{w}}{\partial \mathbf{d}_\alpha}, \mathbf{m}^\alpha - \frac{\partial \hat{w}}{\partial \mathbf{d}_\alpha} \right) \in T^{\perp}_{(\mathbf{r}', \mathbf{d}_\alpha, \mathbf{d}'_\alpha)} \mathcal{M}. \tag{1.3.25}$$

A Lagrange multiplier λ^{I} now contributes to the contact force, the intrinsic director force, and the contact director force as an unknown scalar along the orthogonal complement:

$$\begin{gathered} \mathbf{n} - \frac{\partial \hat{w}}{\partial \mathbf{r}'}\bigg|_{\mathcal{M}} = \lambda^{\mathrm{I}} \frac{\partial \phi^{\mathrm{I}}}{\partial \mathbf{r}'}, \quad \mathbf{k}^\alpha - \frac{\partial \hat{w}}{\partial \mathbf{d}_\alpha}\bigg|_{\mathcal{M}} = \lambda^{\mathrm{I}} \frac{\partial \phi^{\mathrm{I}}}{\partial \mathbf{d}_\alpha}, \\ \mathbf{m}^\alpha - \frac{\partial \hat{w}}{\partial \mathbf{d}'_\alpha}\bigg|_{\mathcal{M}} = \lambda^{\mathrm{I}} \frac{\partial \phi^{\mathrm{I}}}{\partial \mathbf{d}'_\alpha}. \end{gathered} \tag{1.3.26}$$

The multiplier λ^{I} cannot contribute to changes in strain energy and is therefore to be determined by satisfaction of the balance laws and not by the deformation. Since the internal constraint is assumed to hold throughout the material, $\lambda^{\mathrm{I}} = \lambda^{\mathrm{I}}(\xi)$. In the context of constitutive relations, the part of the internal force attributable to the deformation is termed the active piece while the part containing the Lagrange multiplier is termed the reactive piece.

The strain energy $\hat{w}$ in (1.3.26) is evaluated on $\mathcal{M}$ only after gradients are taken. Alternatively, one may enforce the internal constraint prior to taking gradients. Proceeding this way, a constrained strain energy is defined:

$$\hat{w}_c = \hat{w}|_{\mathcal{M}}, \tag{1.3.27}$$

where $\hat{w}$ is restricted to be evaluated on $\mathcal{M}$. Using $\hat{w}_c$ over $\hat{w}$ results in different associated Lagrange multipliers. We call the multiplier associated with $\hat{w}_c$ as λ^{I}_c, so that

$$\begin{gathered} \mathbf{n} - \frac{\partial \hat{w}_c}{\partial \mathbf{r}'} = \lambda^{\mathrm{I}}_c \frac{\partial \phi^{\mathrm{I}}}{\partial \mathbf{r}'}, \quad \mathbf{k}^\alpha - \frac{\partial \hat{w}_c}{\partial \mathbf{d}_\alpha} = \lambda^{\mathrm{I}}_c \frac{\partial \phi^{\mathrm{I}}}{\partial \mathbf{d}_\alpha}, \\ \mathbf{m}^\alpha - \frac{\partial \hat{w}_c}{\partial \mathbf{d}'_\alpha} = \lambda^{\mathrm{I}}_c \frac{\partial \phi^{\mathrm{I}}}{\partial \mathbf{d}'_\alpha}. \end{gathered} \tag{1.3.28}$$

The resulting equations will yield the same state of deformation. A relationship between λ^{I} and λ_c^{I} may also be established. In general, λ_c^{I} will contain an active piece attributable to the strain energy. We use the constrained strain energy approach in Section 2.4.

External constraints and reactions

Consider an external constraint of the form

$$\phi^{\mathrm{E}} = \phi^{\mathrm{E}}(\mathbf{r}^*) = 0. \tag{1.3.29}$$

This constraint defines a surface, $\mathcal{N}$, in the configuration space $\mathbb{E}^3$ of the placement of a material point with label $\left(X_\gamma^1, X_\gamma^2, \gamma\right)$. If the constraint is to hold for all time, we derive an orthogonality condition on admissible directions for $\dot{\mathbf{r}}^*$:

$$\dot{\phi}^{\mathrm{E}} = \frac{\partial \phi^{\mathrm{E}}}{\partial \mathbf{r}^*} \cdot \dot{\mathbf{r}}^* = 0. \tag{1.3.30}$$

Hence,

$$\frac{\partial \phi^{\mathrm{E}}}{\partial \mathbf{r}^*} \in T_{\mathbf{r}^*}^{\perp}\mathcal{N}, \tag{1.3.31}$$

and the required singular three-dimensional external constraint (or reaction) force, $\mathbf{F}_\gamma^*$, assumed to be powerless given admissible virtual velocities, is unknown in magnitude but not direction as

$$\mathbf{F}_\gamma^* = \lambda^{\mathrm{E}} \frac{\partial \phi^{\mathrm{E}}}{\partial \mathbf{r}^*}. \tag{1.3.32}$$

The assumption $\mathbf{r}^* = \mathbf{r} + X^\beta \mathbf{d}_\beta$, gives us a relation of the form $\mathbf{r}^* = \mathbf{r}^*(\mathbf{r}, \mathbf{d}_\alpha)$. Using a chain rule, we find

$$\dot{\phi}^{\mathrm{E}} = \frac{\partial \phi^{\mathrm{E}}}{\partial \mathbf{r}} \cdot \dot{\mathbf{r}} + \frac{\partial \phi^{\mathrm{E}}}{\partial \mathbf{d}_\beta} \cdot \dot{\mathbf{d}}_\beta = 0, \tag{1.3.33}$$

where $\phi^{\mathrm{E}} = \phi^{\mathrm{E}}(\mathbf{r}, \mathbf{d}_\alpha)$ is another representation of the external constraint. We obtain the singular one-dimensional centerline and director forces:

$$\mathbf{F}_\gamma = \lambda^{\mathrm{E}} \frac{\partial \phi^{\mathrm{E}}}{\partial \mathbf{r}}, \quad \mathbf{F}_\gamma^\alpha = \lambda^{\mathrm{E}} \frac{\partial \phi^{\mathrm{E}}}{\partial \mathbf{d}_\alpha}. \tag{1.3.34}$$

In the case of distributed external constraints where (1.3.30) holds for a range of ξ values, λ^{E} turns into a continuous function of ξ. The constraint forces are then distributed into assigned centerline and director forces as

$$\rho_0 \mathbf{f}_{\mathrm{C}} = \lambda^{\mathrm{E}}(\xi) \frac{\partial \phi^{\mathrm{E}}}{\partial \mathbf{r}}, \quad \rho_0 \mathbf{l}_{\mathrm{C}}^\alpha = \lambda^{\mathrm{E}}(\xi) \frac{\partial \phi^{\mathrm{E}}}{\partial \mathbf{d}_\alpha}, \tag{1.3.35}$$

where λ^{E} now has a different physical dimension to that in (1.3.34). In this circumstance, the exact form of $\lambda^{\mathrm{E}} = \lambda^{\mathrm{E}}(\xi)$ may be statically indeterminate and additional assumptions may be required.

Chapter 2

Worm locomotion

2.1 Introduction

The locomotion strategy of the worm has attracted attention in the growing field of bio-inspired soft robotics. With seemingly minimal structure and control, the worm is capable of using peristalsis both to locomote and burrow tunnels into the earth. The principles of crawling locomotion [12] have many practical uses in, for example, robots for medical endoscopies [59]. One engineering challenge is to develop actuators that achieve the desired locomotion strategies [17]. A recent approach to mimicking muscle contractions has been to use pneumatic artificial muscles (PAMs) [1]. A connection of several PAMs in series may be a good starting point for achieving peristaltic locomotion. Some peristalsis-based soft robots have been successfully designed [9, 37, 38, 61, 62] and analyzed [16, 60].

A worm locomotes by making use of its hydrostatic skeleton. Each segment of the worm contains an incompressible medium called the coelomic fluid. In the broadest terms, the worm advances forward by exploiting the shape-changing properties that come with volume conservation of its skeleton [14, 22, 45]. Pulses of longitudinal and circular muscle contraction are propagated rearward causing regions where the worm fattens and thins. Where the worm longitudinally contracts and fattens, it digs its setae into the soil and establishes an anchor. Other regions of the worm are then either pushed or pulled by an actuation or release of circular muscle contraction. The locomotion strategy of the worm is therefore similar to the stick-slip locomotion seen in some robots [73]. During the locomotion cycle, the connective tissue in the worm's body walls provides a source of elasticity [33] that balances the muscle actuation forces and the internal hydrostatic pressure of the coelomic fluid.

If the engineer of the soft robot wishes to mimic locomotion via peristalsis, they could be aided by a model of the desired locomotion. Some mathematical and numerical descriptions of worm locomotion are available [31, 32, 70]. However, none of the models to date have made use of a continuous director formulation which cleanly facilitates the incompressibility constraint. The goal of this chapter to develop continuous models for compressible and incompressible rod-like bodies engaging in peristaltic locomotion. After development, the

novel model is calibrated and then validated using Quillin's [51, 50] set of experimental measurements for the earthworm *Lumbricus terrestris* (see Figures 2.1 and 2.2). In addition, some data from Kurth and Kier [35] is also used in the benchmarking.

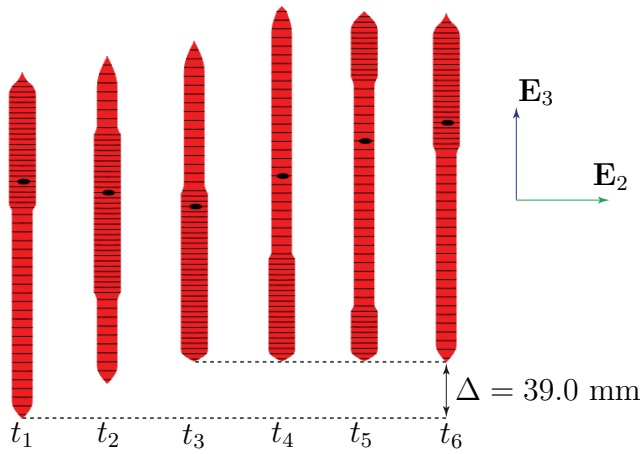

Figure 2.1: *The simulated stride of an earthworm of mass 10* g. *Segment 50 is tracked with a black marking. Samples of the worm's current configuration are taken at* $t_1 = 0$, $t_2 = \frac{t_p}{3}$, $t_3 = \frac{2t_p}{3}$, $t_4 = t_p$, $t_5 = t_p + \frac{t_s}{2}$, *and* $t_6 = t_p + t_s$. *Further details on the parameters of the model can be found in Section 2.8.*

The basis for the model is the director formulation that is central to Green and Naghdi's rod theory [41, 46]. In particular, the worm or soft robot's rod-like (slender) body is mapped into an abstract directed curve that exhibits the key kinematical features of peristaltic locomotion. Lateral and longitudinal stretches, incompressibility constraints, and strain energies are all related to the director fields defined on the abstract curve. The spirit of this chapter is similar to Plaut's article where he describes caterpillar anchoring motion using Euler's elastica [49].

An ansatz

For the deformations in the present chapter, we anticipate that all cross-sections will remain vertical. Our strain energy will be constructed so that there is no resistance to the type of shearing that accompanies such deformations. We hereby adopt the following ansatz for the solution:

$$\mathbf{d}'_\alpha = \mu'_\alpha \mathbf{e}_\alpha = \mu'_\alpha \mathbf{E}_\alpha, \quad \text{(no sum)}. \tag{2.1.1}$$

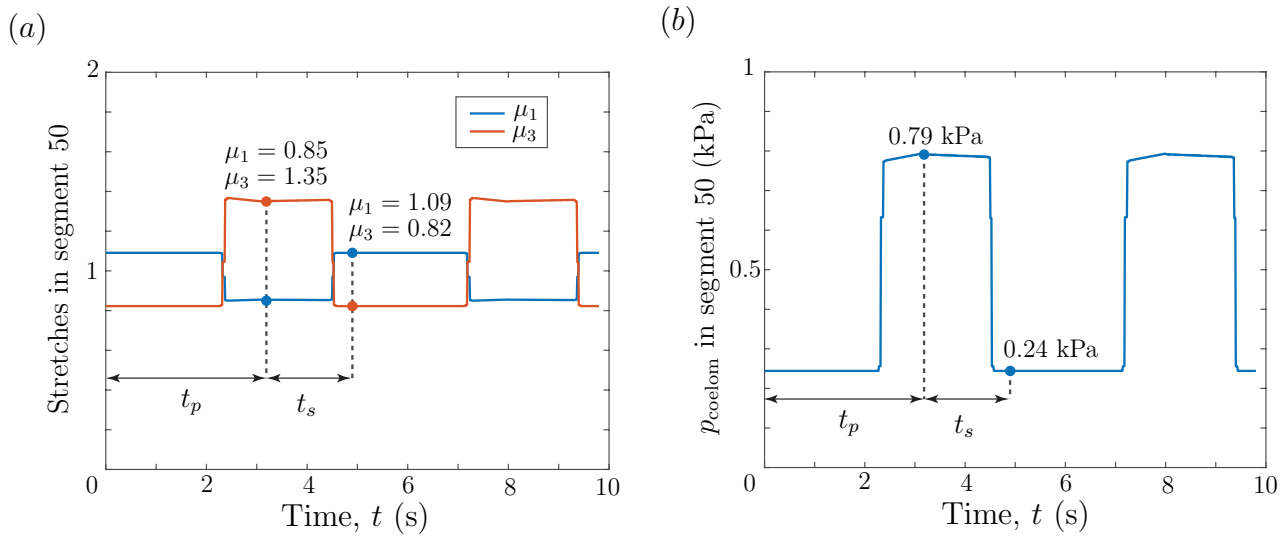

Figure 2.2: *Validation of the biomimetic model of an earthworm of mass 10* g. *Plots of (a) stretches and (b) pressures for segment 50 during multiple strides are displayed. The results presented in this chapter are in general agreement with those measured and predicted by Quillin [51, 50] for the earthworm Lumbricus terrestris. Further details on the parameters of the model can be found in Section 2.8.*

Now, using (1.3.20), we have expressions for the internal forces under the ansatz:

$$\mathbf{n} = \frac{\partial \tilde{w}_c}{\partial \mu_3}\mathbf{e}_3 + \lambda_c^{\mathrm{I}}\frac{\partial \phi^{\mathrm{I}}}{\partial \mathbf{r}'}, \quad \mathbf{k}^\alpha = \frac{\partial \tilde{w}_c}{\partial \mu_\alpha}\mathbf{E}_\alpha + \lambda_c^{\mathrm{I}}\frac{\partial \phi^{\mathrm{I}}}{\partial \mathbf{d}_\alpha},$$
$$\mathbf{m}^\alpha = \frac{\partial \tilde{w}_c}{\partial \mu'_\alpha}\mathbf{E}_\alpha + \lambda_c^{\mathrm{I}}\frac{\partial \phi^{\mathrm{I}}}{\partial \mathbf{d}'_\alpha}. \tag{2.1.2}$$

2.2 Modeling muscle contractions, hydrostatic skeletons, and the ground reaction force

Mechanical models for muscle contraction have been heavily developed [71], with the Hill muscle model being one of the simplest and most elegant models for representing human muscle. The longitudinal and circular muscle contractions of the worm, the elasticity from connective tissues in its body wall, and its hydrostatic skeleton that enables volume conservation is not as well represented in the biomechanical literature. In this section, we address the challenges of modeling constrained multi-directional actuation in the presence of elasticity and how to incorporate these effects into our single continuum model.

Two types of actuators

In this chapter, we consider two types of mechanical actuators: a uni-directional actuator and a tri-directional actuator (Figure 2.3). While a soft robot typically makes use of compliant actuators, such as the compressible PAM, a hybrid soft-hard robot could be designed where a compliant "soft" material encapsulates "hard" actuators. The uni-directional actuator of Figure 2.3(a) is best modeled as a system of three interconnected rigid bodies. Upon longitudinal actuation, pairs of equal but opposite internal forces are generated between the main body and the two sliding arms. If the uni-directional actuator is considered as a single entity, then an overall contraction of the device is effected and the volume of an imaginary cylinder bounding the actuator decreases.

Instead of representing the uni-directional actuator as a multibody rigid system, suppose it is modeled as a single continuum. This approach allows us to simultaneously incorporate the elasticity of a surrounding material. Since the modeling of the forces inside the actuator requires multiple bodies that slide past one another, how do we represent the actuation effects on a single continuum? A pair of external compressive forces of strength P acting on the sliding arms would result in an equivalent contraction as in the real actuator (see the bottom row of Figure 2.3(a)). The difference between the single body and multibody approaches in the rigid system lies only in the internal material forces of the actuator parts: all bodies are in tension during real actuation, while only the sliding arms are in compression during the equivalent external loading.

The tri-directional actuator behaves in a similar manner to the uni-directional actuator. In Figure 2.3(b), we model the main body as a circular disk. Suppose the device is internally constrained so that the volume of the bounding cylinder is conserved. The tri-directional actuator has two modes of actuation: longitudinal and circular. Under the internal constraint, circular contraction causes longitudinal extension. The equivalent effect of two pairs of compressive external forces, all of strength P, may be used to model circular actuation, much like in the case of the uni-directional actuator.

Muscle contractions

Consider again the pair of mechanical actuators from Figure 2.3. We can use these actuators as mechanical analogues to represent the contractile effects of muscles in humans and worms. The musculature of the worm permits two types of contractions: longitudinal muscle contractions that shorten the worm's length and circular muscle contractions that contract its circular cross-sections. Since we consider the worm as a single continuum, the concept of the equivalent loadings in Figure 2.3 is used to model the contractile effects of muscle.

A mechanical analogue for human muscle contraction is the uni-directional actuator displayed in Figure 2.3(a). The sliding action between myosin and actin filaments may be modeled in a continuum by the equivalent forces of strength P. In contrast, the longitudinal and circular contractions of the worm may be modeled as the internally constrained tri-directional actuator of Figure 2.3(b). If one supplies two pairs of external compressive forces

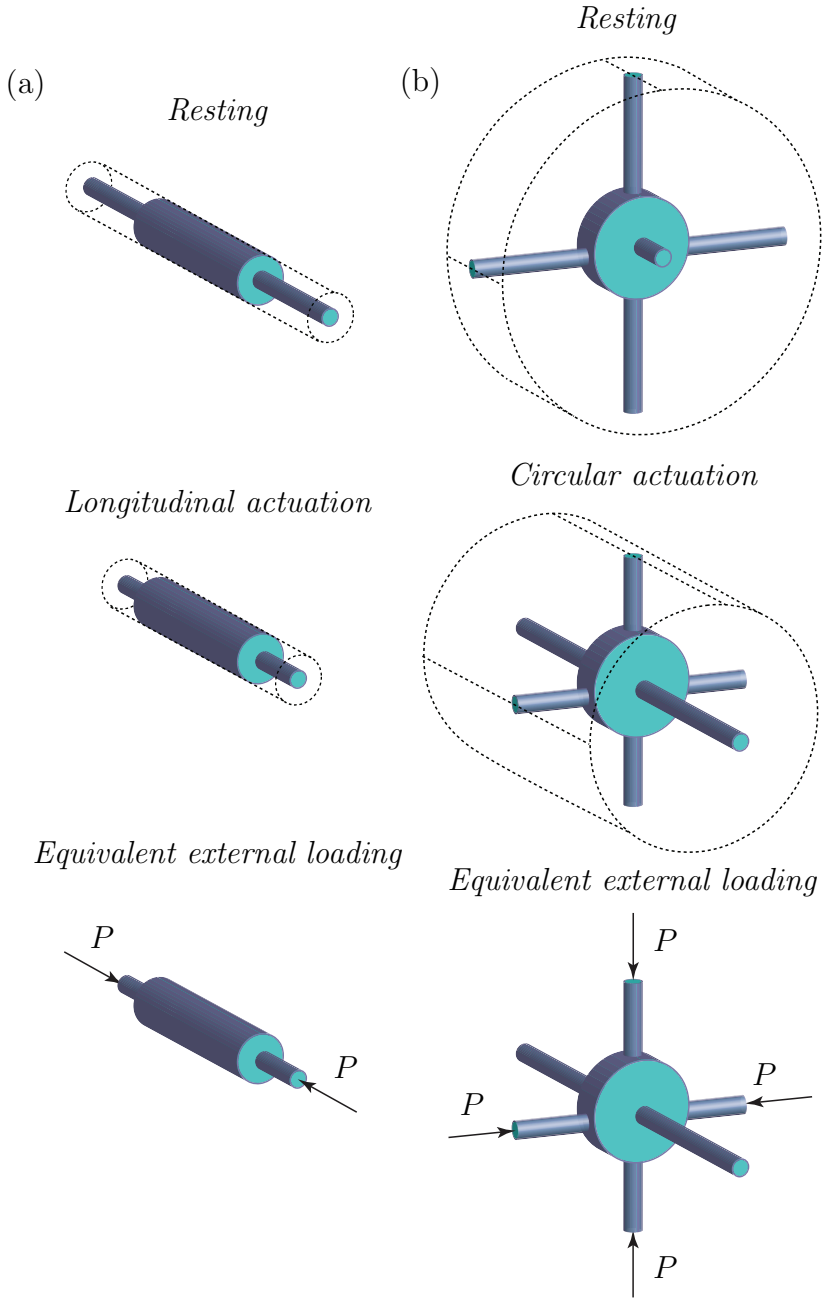

Figure 2.3: *Examples of (a) uni-directional and (b) tri-directional actuators represented as multiple rigid bodies that slide past one another. In its actuated state, the tri-directional actuator is internally constrained to conserve the volume of an imaginary cylinder bounding the sliding arms. Equivalent compressive loads effecting the same actuation are also shown.*

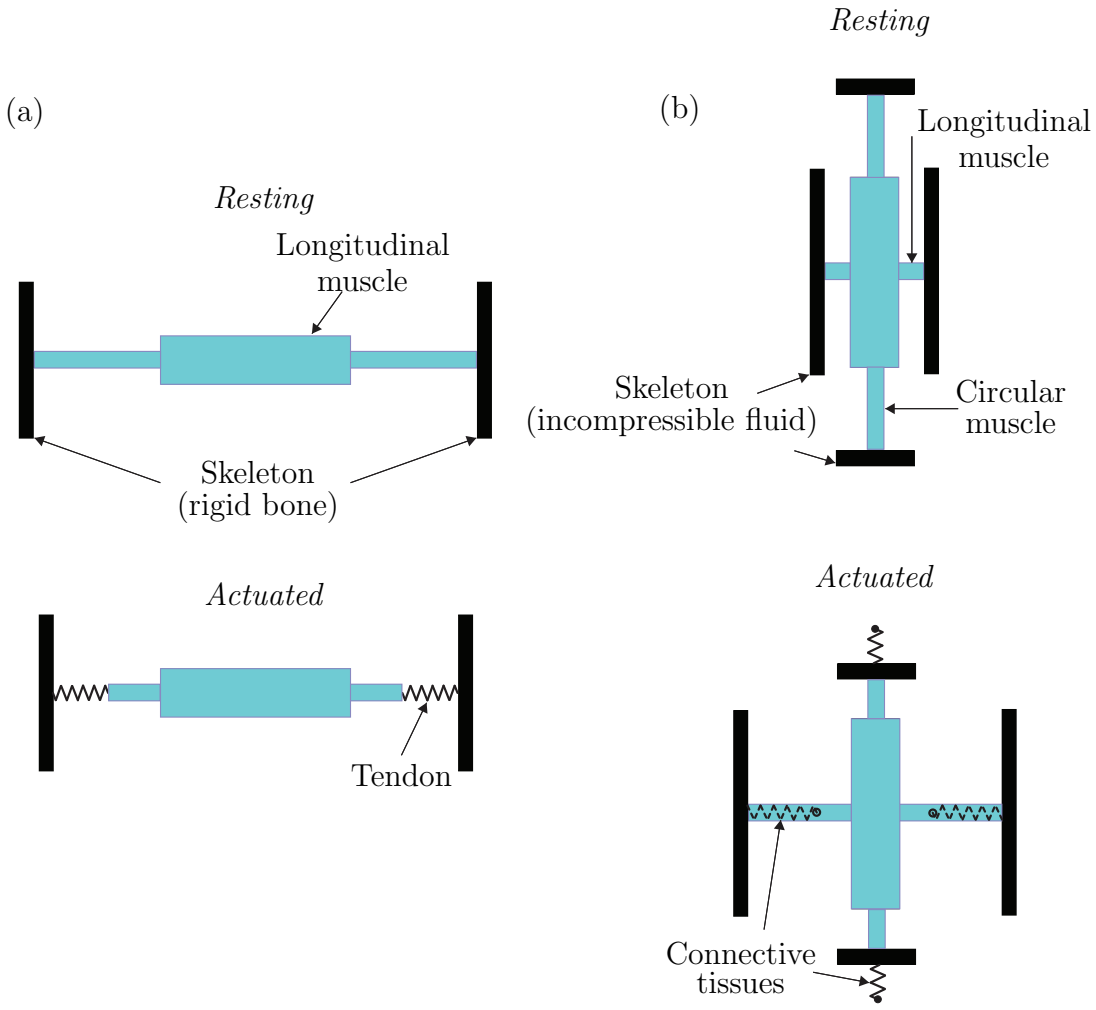

Figure 2.4: *Section views of the mechanical analogues illustrating the difference between (a) human muscle actuation and (b) earthworm muscle actuation. Human muscles engage with an elastic element before pulling on the skeleton. In contrast, worm muscles change the shape of the skeleton, which then engages elastic elements. Black dots indicate inertially fixed points. The elastic element in a human are the tendons while in a worm it is the connective tissue.*

of strength P to model circular muscle contractions, then the unloaded pair of sliding arms extend to maintain the volume of the imaginary bounding cylinder, thereby representing the hydrostatic skeleton.

We believe that the sequence of events during contraction is reversed for human muscles as compared with worm muscles (Figure 2.4). As per the Hill muscle model, a human muscle is attached in series to elastic tendons which are in turn attached to a rigid skeleton. In addition, elastic elements in parallel to the muscle are also present that further increase tension. Upon contraction, the muscle pulls on the tendons, making them tense. The actuating load from the muscle is then transmitted via the tendons to the skeleton which is comprised of rigid bone. When a worm's muscles contract, they first push on the hydrostatic skeleton which is comprised of an incompressible fluid. As the hydrostatic skeleton must maintain its volume, it changes shape until it engages with elasticity from connective tissues in the body wall. The end result is a pressure-loaded hydrostatic skeleton balancing muscle actuation loads and connective tissues in tension. In both humans and worms, the skeleton is ultimately manipulated to produce traction, leading to locomotion.

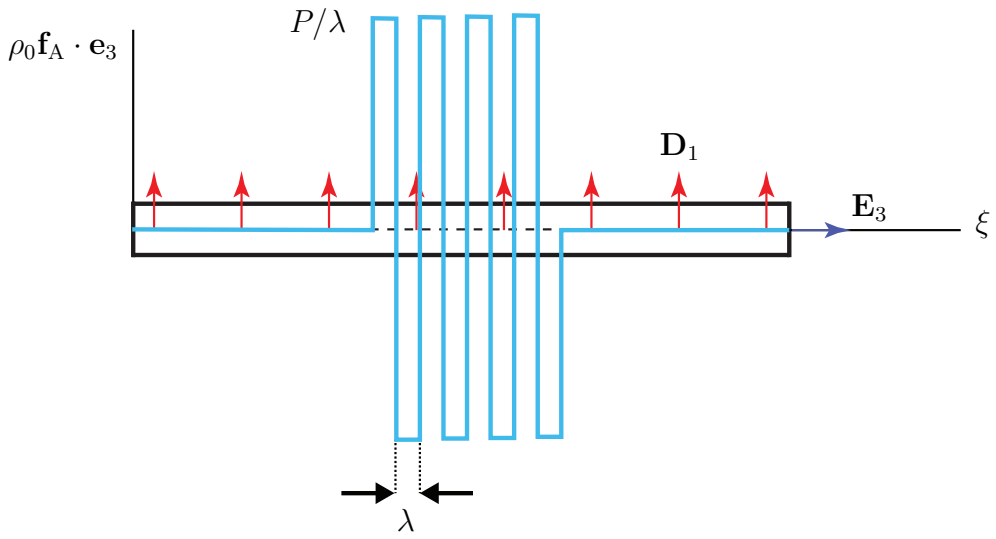

Figure 2.5: *An example of an applied centerline load that would result in a centerline contraction. The function is displayed atop the material domain of the reference configuration, and* $\mathbf{e}_3$ *is the centerline tangent of the current configuration.*

Longitudinal contraction as an assigned force

The assigned forces used to model a worm's muscle contractions are coined active loads.[1] To model the longitudinal contractions, we propose an active centerline load $\rho_0\mathbf{f}_A$ of the

[1]These assigned forces should not be confused with the active piece of the internal forces in the presence of an internal constraint.

form displayed in Figure 2.5. Here, actuation loads of net strength P are represented by distributed forces in windows of reference width λ. When considering real longitudinal muscles in a worm, one realizes that there are many such muscles acting in each chamber of the worm that contract in series. As it would be tedious to model many pairs of discrete loads in series, we will instead construct singularity functions so that the loading is more compatible with continuous equations.

A singularity function known as the doublet is used to model longitudinal contraction. Singularity functions, including the doublet, have found use in modeling point forces, point moments, and distributed couples as distributed forces in Bernoulli-Euler and Timoshenko beams [13, 18, 19]. The doublet that is proposed here is similar in spirit but constructed in a slightly different manner compared to the preceding papers. The active centerline load $\rho_0 \mathbf{f}_\mathrm{A}$ applied at $\xi = \gamma$ is expressed mathematically as

$$\rho_0 \mathbf{f}_\mathrm{A} = D\langle \xi - \gamma \rangle^{-2} \mathbf{e}_3, \tag{2.2.1}$$

where $D > 0$ is the doublet strength of physical dimension force times length, and the function

$$\langle \xi - \gamma \rangle^{-2} = \begin{cases} \infty & \text{at } \xi = \gamma^- \\ 0 & \text{at } \xi = \gamma \\ -\infty & \text{at } \xi = \gamma^+ \\ 0, & \text{otherwise} \end{cases} \tag{2.2.2}$$

is the doublet singularity function, which carries a physical dimension of a length inverse squared. The area under the curve of the doublet over its entire domain is zero, but the area from γ^- to γ is $+1$ while the area from γ to γ^+ is -1. Other definitions of the doublet exist where its integral is defined to yield the Dirac delta singularity function. The doublet here may be obtained as the derivative of a Dirac delta function:

$$\langle \xi - \gamma \rangle^{-2} = \frac{d}{d\xi} \delta(\xi - \gamma), \tag{2.2.3}$$

where

$$\delta(\xi - \gamma) = \begin{cases} \infty & \text{at } \xi = \gamma \\ 0, & \text{otherwise.} \end{cases} \tag{2.2.4}$$

We may consider the doublet defined in (2.2.2) as a pair of opposing Dirac delta functions centered at γ^- and γ^+. The anti-derivative of the doublet defined here is a switch function of unit height that switches on at the singular value of γ.

A discrete sequence of doublets of equal strength acting at $\gamma_1, \ldots, \gamma_n$ may be represented as the series

$$\rho_0 \mathbf{f}_\mathrm{A} = D\mathbf{e}_3 \sum_{i=1}^{n} \langle \xi - \gamma_i \rangle^{-2}. \tag{2.2.5}$$

A continuous distribution of infinitely many equal strength doublets acting in a window (ξ_1, ξ_2) is used to model longitudinal muscle contraction. We let $n \to \infty$ and shrink the

distance between doublets to zero. For any value $\xi \in (\xi_1, \xi_2)$, the balance of linear momentum (1.2.71) may be integrated from ξ^- to ξ to yield

$$\mathbf{n}(\xi) = -\int_{\xi^-}^{\xi} \rho_0 \mathbf{f}_{\mathrm{A}} d\overline{\xi} = -\overline{D}\mathbf{e}_3, \tag{2.2.6}$$

where $\overline{\xi}$ is a dummy variable, $\overline{D}$ has the physical dimension of force, and we have used the fact that $\mathbf{n}(\xi^-) = \mathbf{0}$. Applying this logic iteratively, we find that

$$\mathbf{n}(\xi) = -\overline{D}\mathbf{e}_3 \quad \text{for} \quad \xi_1 < \xi < \xi_2. \tag{2.2.7}$$

That is, $\mathbf{n}$ switches on to a constant magnitude inside the window of longitudinal muscle contraction and becomes continuously nonzero in that window. The magnitude of the longitudinal muscle force is given by $\overline{D}$. In the subsequent sections, we will develop the active and reactive pieces that make up $\mathbf{n}$. For the worm, $\overline{D}$ will balance an elastic piece from the connective tissue and a constraint piece due to the pressurized hydrostatic skeleton.

Circular contraction as assigned director forces

Circular muscle contraction is modeled by a pair of equal strength active director forces. They are derived from three-dimensional considerations (cf. (1.2.79)) assuming a constant magnitude Piola traction $\mathbf{p} = -p\mathbf{e}_r$ acting around a cross-section at $\xi = \gamma$:

$$\rho_0 \mathbf{l}^{\alpha}_{\mathrm{A}} = \oint_{\partial \mathcal{A}_0(\gamma)} -p\mathbf{e}_r X^{\alpha} dU, \tag{2.2.8}$$

where p is a pressure supplying a compressive force per unit reference area of the lateral boundary. If one wants to model the four compressive forces of strength P from the tri-directional actuator of Figure 2.3(b), (1.2.79) may also be used to compute the assigned director force. Noting the geometry defined in Figure 2.6, we compute the second assigned director force due to the pressure loading as

$$\rho_0 \mathbf{l}^2_{\mathrm{A}} = \oint_{\partial \mathcal{A}_0(\gamma)} -p\mathbf{e}_r X^2 R d\phi = -p\pi R^2 \mathbf{e}_2.$$

Since the director load is centrally-directed, it will serve only to change the length of $\mathbf{d}_2$. Carrying out an identical process for $\rho_0 \mathbf{l}^1_{\mathrm{A}}$ reveals the first assigned director force per unit reference length to be

$$\rho_0 \mathbf{l}^1_{\mathrm{A}} = -p\pi R^2 \mathbf{e}_1. \tag{2.2.9}$$

We define the director force strength $\rho_0 l_{\mathrm{A}} = \|\mathbf{l}^1_{\mathrm{A}}\| = \|\mathbf{l}^2_{\mathrm{A}}\| = p\pi R^2$ so that $\rho_0 \mathbf{l}^1_{\mathrm{A}} = -\rho_0 l_{\mathrm{A}} \mathbf{e}_1$ and $\rho_0 \mathbf{l}^2_{\mathrm{A}} = -\rho_0 l_{\mathrm{A}} \mathbf{e}_2$. If the pressure is defined over a window (ξ_1, ξ_2), then the director loads vanish outside of it.

In the locomotion scheme soon to be described, the longitudinal centerline force will be used to anchor the rod while the director forces will be used to advance the rod forwards. We will refer to $\rho_0 \mathbf{f}_{\mathrm{A}}$ as an anchoring load and $\rho_0 \mathbf{l}^1_{\mathrm{A}}$ and $\rho_0 \mathbf{l}^2_{\mathrm{A}}$ as advancing loads.

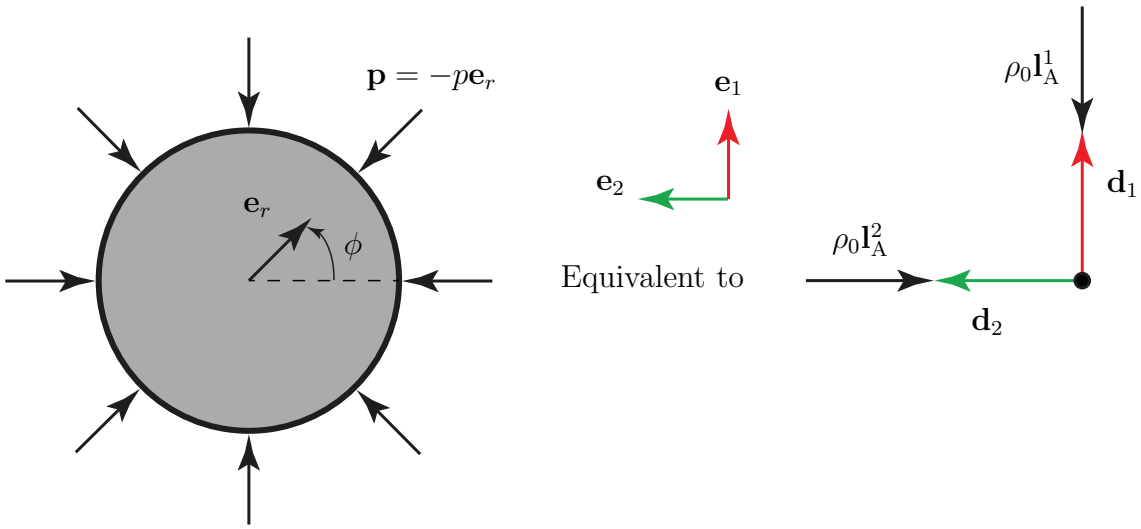

Figure 2.6: *Pressure Piola tractions applied to the lateral boundary of a rod-like body are equivalent to a pair of equal strength, centrally-directed director forces acting on the abstract directed curve.*

Hydrostatic skeletons

A hydrostatic skeleton could be modeled by a global constraint: the total volume of the body must be conserved. This condition may result in infinitely many deformed shapes that satisfy global volume conservation as portrayed in Figure 2 of [14]. Mathematically, global volume conservation may be expressed as

$$\int_0^{\ell_0} [(\mathbf{d}_1 \times \mathbf{d}_2) \cdot \mathbf{r}' - 1] d\xi = \text{constant}. \tag{2.2.10}$$

To render the system determinate, we choose to model the hydrostatic skeleton using a local internal constraint. That is, every cross-sectional volume of width $d\xi$ obeys a conservation of volume. It is known that earthworms possess a segmented hydrostatic skeleton, with muscular septae isolating fluid from adjacent segments [35]. Each chamber therefore acts as its own hydraulic unit, conserving the volume of fluid within it for the course of the motion [45]. On average, it has been shown that most worms have approximately 147 such chambers, regardless of total body length [51]. The internal constraint for local volume conservation is expressed as

$$\phi^{\mathrm{I}} = 0, \tag{2.2.11}$$

where

$$\phi^{\mathrm{I}} = (\mathbf{d}_1 \times \mathbf{d}_2) \cdot \mathbf{r}' - 1. \tag{2.2.12}$$

Notice that local incompressibility implies global incompressibility. In terms of the stretch variables, (2.2.11) becomes

$$\mu_1\mu_2\mu_3 = 1, \tag{2.2.13}$$

which produces a constraint surface in a three-dimensional stretch space. Equation (2.2.13) is nonlinear in the stretch variables. For μ_1, μ_2, and μ_3 close to 1, an approximation of (2.2.13) to first order in the stretches yields

$$\mu_1 + \mu_2 + \mu_3 \approx 3, \tag{2.2.14}$$

where $\mu_1 + \mu_2 + \mu_3 - 3$ may be thought of as a volumetric strain measure for small (linear) deformations. While we may choose to adopt linear constitutive models for the material, we will choose not to drop the nonlinearity of (2.2.13), as it would fundamentally alter the shape of the constraint manifold, thereby allowing for deformations which could violate the incompressibility constraint.

A rod-like body comprised of a nearly incompressible medium is aptly modeled by (2.2.11) and (2.2.12). If $\hat{w}_c(\mathbf{r}', \mathbf{d}_\alpha, \mathbf{d}'_\alpha)$ is the constrained version of the specific strain energy function, then the internal forces in the presence of the local incompressibility constraint become

$$\mathbf{n} = \frac{\partial \hat{w}_c}{\partial \mathbf{r}'} + \lambda_c^{\mathrm{I}} \frac{\mu_1\mu_2}{\mu_3}\mathbf{r}', \qquad \mathbf{k}^1 = \frac{\partial \hat{w}_c}{\partial \mathbf{d}_1} + \lambda_c^{\mathrm{I}} \frac{\mu_2\mu_3}{\mu_1}\mathbf{d}_1, \qquad \mathbf{k}^2 = \frac{\partial \hat{w}_c}{\partial \mathbf{d}_2} + \lambda_c^{\mathrm{I}} \frac{\mu_1\mu_3}{\mu_2}\mathbf{d}_2,$$
$$\mathbf{m}^\alpha = \frac{\partial \hat{w}_c}{\partial \mathbf{d}'_\alpha}. \tag{2.2.15}$$

The ground reaction force

The rod is supported on a ground plane which contains the point $(-R, 0, 0)$ and is spanned by the set $\{\mathbf{E}_2, \mathbf{E}_3\}$ by means of a line of external contact constraints of the form

$$\phi^{\mathrm{E}} = \mathbf{r}^*(-R, 0, \xi) \cdot \mathbf{E}_1 + R = 0. \tag{2.2.16}$$

The resulting external constraint forces are

$$\rho_0 \mathbf{f}_{\mathrm{C}} = \lambda^{\mathrm{E}} \mathbf{E}_1, \qquad \rho_0 \mathbf{l}^1_{\mathrm{C}} = -R\lambda^{\mathrm{E}} \mathbf{E}_1. \tag{2.2.17}$$

A three-dimensional body force in the form of gravity acts to push the rod into the ground plane:

$$\mathbf{b} = -g\mathbf{E}_1. \tag{2.2.18}$$

Using (1.2.67) and (1.2.79), we find that in the presence of only gravity and no ground reaction force, the rod experiences

$$\rho_0 \mathbf{f} = -\rho_0 g \mathbf{E}_1, \qquad \rho_0 \mathbf{l}^1 = \mathbf{0}, \qquad \rho_0 \mathbf{l}^2 = \mathbf{0}. \tag{2.2.19}$$

The exact distribution of λ^{E} in (2.2.17) can only be determined by experimental means. We assume that the ground reaction force at some point ξ supports exactly the weight of the cross-sectional volume of width $d\xi$ above:

$$\lambda^{\mathrm{E}} = \rho g = \frac{\rho_0 g}{\mu_3}. \tag{2.2.20}$$

Depending on how massive the rod is, the ground reaction force serves not only to increase traction, but also to deform circular cross-sections into elliptical cross-sections.

2.3 Governing equations for a compressible rod

While a worm is incompressible, we first admit some compressibility in our constitutive model for potential use in robotic devices. The following constitutive model for an isotropic, internally unconstrained material is assumed:

$$\begin{aligned} 2w = k_{\mathrm{S}}\left[(\mu_1-1)^2+(\mu_2-1)^2+(\mu_3-1)^2\right] + k_{\mathrm{G}}\left[(\mu_1')^2+(\mu_2')^2\right] \\ +2k_{\mathrm{P}}[(\mu_1-1)(\mu_2-1)+(\mu_1-1)(\mu_3-1)+(\mu_2-1)(\mu_3-1)]. \end{aligned} \tag{2.3.1}$$

The proposed strain energy is a quadratic form in $\mu_i - 1$ and μ_α' with off-diagonal stiffness k_{P}, which characterizes, in part, the influence of the Poisson effect. Here, the stiffnesses k_{S} and k_{P} are analogous to the Lamé moduli of three-dimensional linear elasticity. Adopting the ansatz (2.3.2) and using equation (2.1.2), we derive the internal forces as

$$\begin{aligned} \mathbf{k}^1 = (k_{\mathrm{S}}(\mu_1-1)+k_{\mathrm{P}}(\mu_2+\mu_3-2))\mathbf{E}_1, \quad \mathbf{k}^2 = (k_{\mathrm{S}}(\mu_2-1)+k_{\mathrm{P}}(\mu_1+\mu_3-2))\mathbf{E}_2, \\ \mathbf{n} = (k_{\mathrm{S}}(\mu_3-1)+k_{\mathrm{P}}(\mu_1+\mu_2-2))\mathbf{e}_3, \quad \mathbf{m}^\alpha = k_{\mathrm{G}}\mu_\alpha'\mathbf{E}_\alpha, \quad \text{(no sum)}. \end{aligned} \tag{2.3.2}$$

These are the force-stretch relations for a compressible rod. Upon substitution, we are assured that the constitutive relations given in (2.3.2) identically satisfy the balance of angular momentum (1.2.91). No additional information may be gleaned from this balance law and it is henceforth set aside.

We assume that the regions where the anchoring loads $\rho_0\mathbf{f}_{\mathrm{A}}$ act are disjoint from the regions where the advancing loads $\rho_0\mathbf{l}_{\mathrm{A}}^\alpha$ act. The equations for the deformation are therefore piecewise and must be developed independently. The subsequent solutions will be joined together with a special application of boundary conditions.

Governing equations under an anchoring load

Suppose an anchoring load acts in a window of the rod. Assuming that $\mathbf{e}_3' \approx \mathbf{0}$, the governing equations are

$$\begin{aligned} 0 = k_{\mathrm{G}}\mu_1'' - \frac{R\rho_0 g}{\mu_3} - k_{\mathrm{S}}\mu_1 - k_{\mathrm{P}}(\mu_2+\mu_3) + k_{\mathrm{S}} + 2k_{\mathrm{P}}, \\ 0 = k_{\mathrm{G}}\mu_2'' - k_{\mathrm{S}}\mu_2 - k_{\mathrm{P}}(\mu_1+\mu_3) + k_{\mathrm{S}} + 2k_{\mathrm{P}}, \\ -\overline{D} = k_{\mathrm{S}}\mu_3 + k_{\mathrm{P}}(\mu_1+\mu_2) - k_{\mathrm{S}} - 2k_{\mathrm{P}}. \end{aligned} \tag{2.3.3}$$

The following non-dimensional parameters are defined:

$$\tilde{z} = \frac{\xi}{\ell_0}, \qquad \tilde{d} = \frac{\overline{D}}{k_{\mathrm{S}}}, \qquad \tilde{p} = \frac{k_{\mathrm{P}}}{k_{\mathrm{S}}}, \qquad \tilde{g} = \frac{k_{\mathrm{S}}\ell_0^2}{k_{\mathrm{G}}}, \qquad \tilde{m} = \frac{R\rho_0 g\ell_0^2}{k_{\mathrm{G}}}. \tag{2.3.4}$$

Equation $(2.3.3)_3$ is used to solve $\mu_3(\tilde{z})$ as a function of $\mu_1(\tilde{z})$ and $\mu_2(\tilde{z})$:

$$\mu_3 = \overline{\mu}_3(\mu_1, \mu_2) = -\tilde{d} - \tilde{p}(\mu_1 + \mu_2) + 2\tilde{p} + 1. \tag{2.3.5}$$

By substituting (2.3.5) into $(2.3.3)_1$ and $(2.3.3)_2$, the governing equations for $\mu_1(\tilde{z})$ and $\mu_2(\tilde{z})$ take on the non-dimensional forms

$$\begin{aligned}
\frac{d^2\mu_1}{d\tilde{z}^2} &= \frac{\tilde{m}}{\overline{\mu}_3(\mu_1, \mu_2)} + \tilde{g}\mu_1 + \tilde{p}\tilde{g}(\mu_2 + \overline{\mu}_3(\mu_1, \mu_2)) - \tilde{g} - 2\tilde{p}\tilde{g}, \\
\frac{d^2\mu_2}{d\tilde{z}^2} &= \tilde{g}\mu_2 + \tilde{p}\tilde{g}(\mu_1 + \overline{\mu}_3(\mu_1, \mu_2)) - \tilde{g} - 2\tilde{p}\tilde{g}.
\end{aligned} \tag{2.3.6}$$

Governing equations under advancing loads

We now consider a pair of advancing loads acting in a window of the rod. The governing equations become

$$\begin{aligned}
0 &= k_{\mathrm{G}}\mu_1'' - \frac{R\rho_0 g}{\mu_3} - p\pi R^2 - k_{\mathrm{S}}\mu_1 - k_{\mathrm{P}}(\mu_2 + \mu_3) + k_{\mathrm{S}} + 2k_{\mathrm{P}}, \\
0 &= k_{\mathrm{G}}\mu_2'' - p\pi R^2 - k_{\mathrm{S}}\mu_2 - k_{\mathrm{P}}(\mu_1 + \mu_3) + k_{\mathrm{S}} + 2k_{\mathrm{P}}, \\
\mu_3 &= 1 - \frac{k_{\mathrm{P}}}{k_{\mathrm{S}}}(\mu_1 + \mu_2).
\end{aligned} \tag{2.3.7}$$

An additional non-dimensional parameter is defined as

$$\tilde{c} = \frac{p\pi R^2\ell_0^2}{k_{\mathrm{G}}}. \tag{2.3.8}$$

Following the same procedure as in the preceding subsection, the non-dimensional governing equations for $\mu_1(\tilde{z})$, and $\mu_2(\tilde{z})$ become

$$\begin{aligned}
\frac{d^2\mu_1}{d\tilde{z}^2} &= \frac{\tilde{m}}{\hat{\mu}_3(\mu_1, \mu_2)} + \tilde{g}\mu_1 + \tilde{p}\tilde{g}(\mu_2 + \hat{\mu}_3(\mu_1, \mu_2)) + \tilde{c} - \tilde{g} - 2\tilde{p}\tilde{g}, \\
\frac{d^2\mu_2}{d\tilde{z}^2} &= \tilde{g}\mu_2 + \tilde{p}\tilde{g}(\mu_1 + \hat{\mu}_3(\mu_1, \mu_2)) + \tilde{c} - \tilde{g} - 2\tilde{p}\tilde{g},
\end{aligned} \tag{2.3.9}$$

where

$$\mu_3 = \hat{\mu}_3(\mu_1, \mu_2) = 1 - \tilde{p}(\mu_1 + \mu_2). \tag{2.3.10}$$

Boundary conditions and disjoint regions of loading

The rod is assumed to be free from singular loads at its terminal ends. Therefore, (1.2.72) and (1.2.83) yield the conditions

$$[\![\mathbf{n}]\!]_{\xi=0} = \mathbf{0}, \quad [\![\mathbf{m}^\alpha]\!]_{\xi=0} = \mathbf{0}, \quad [\![\mathbf{n}]\!]_{\xi=\ell_0} = \mathbf{0}, \quad [\![\mathbf{m}^\alpha]\!]_{\xi=\ell_0} = \mathbf{0}.$$

Noting the lack of material at 0^- and ℓ_0^+, no internal loads may be supported there, and we find conditions for the internal forces on the non-dimensional domain:

$$\mathbf{n}(\tilde{z}=0) = \mathbf{0}, \quad \mathbf{m}^\alpha(\tilde{z}=0) = \mathbf{0}, \quad \mathbf{n}(\tilde{z}=1) = \mathbf{0}, \quad \mathbf{m}^\alpha(\tilde{z}=1) = \mathbf{0}. \tag{2.3.11}$$

(2.3.12)

Applying $(2.3.2)_4$ to $(2.3.12)_1$ and $(2.3.12)_2$, we find a set of four conditions that complete (2.3.6) and (2.3.9) into boundary value problems:

$$\frac{d\mu_\alpha}{d\tilde{z}}(\tilde{z}=0) = 0, \qquad \frac{d\mu_\alpha}{d\tilde{z}}(\tilde{z}=1) = 0. \tag{2.3.13}$$

Notice from (2.3.5) and (2.3.10) that $(2.3.12)_3$ and $(2.3.12)_4$ are automatically satisfied given (2.3.13).

At any given instant, the rod's domain is broken up into disjoint regions where different loading conditions apply. For generality, suppose there are three regions of loading: anchoring loads in $[0,\gamma)$, advancing loads in (γ,η), and anchoring loads in $(\eta,\ell_0]$. We introduce the non-dimensional parameters

$$\tilde{\gamma} = \frac{\gamma}{\ell_0}, \qquad \tilde{\eta} = \frac{\eta}{\ell_0}, \tag{2.3.14}$$

so that $\tilde{z} = \tilde{\gamma}$, and $\tilde{z} = \tilde{\eta}$ locate the singular points. Since the material is assumed never to fracture,

$$\mu_\alpha\big(\tilde{z} = \tilde{\gamma}^-\big) = \mu_\alpha\big(\tilde{z} = \tilde{\gamma}^+\big), \quad \mu_\alpha\big(\tilde{z} = \tilde{\eta}^-\big) = \mu_\alpha\big(\tilde{z} = \tilde{\eta}^+\big). \tag{2.3.15}$$

To handle the three piecewise boundary value problems, the following dependent variables are defined:

$$y_1 = \mu_1, \quad y_2 = \frac{d\mu_1}{d\tilde{z}}, \quad y_3 = \mu_2, \quad y_4 = \frac{d\mu_2}{d\tilde{z}}, \quad \text{on} \quad 0 \le \tilde{z} \le \tilde{\gamma},$$

$$y_5 = \mu_1, \quad y_6 = \frac{d\mu_1}{d\tilde{z}}, \quad y_7 = \mu_2, \quad y_8 = \frac{d\mu_2}{d\tilde{z}}, \quad \text{on} \quad \tilde{\gamma} \le \tilde{z} \le \tilde{\eta},$$

$$y_9 = \mu_1, \quad y_{10} = \frac{d\mu_1}{d\tilde{z}}, \quad \text{on} \quad \tilde{\eta} \le \tilde{z} \le 1, \quad y_{11} = \mu_2, \quad y_{12} = \frac{d\mu_2}{d\tilde{z}}, \quad \text{on} \quad \tilde{\eta} \le \tilde{z} \le 1.$$

In order to input the problem into a boundary value problem numerical solver, it is necessary to shift the coordinates so that they are on the same domain. We let

$$\tilde{z}_1 = \frac{\tilde{z}}{\tilde{\gamma}}, \qquad \tilde{z}_2 = \frac{\tilde{z}-\tilde{\gamma}}{\tilde{\eta}-\tilde{\gamma}}, \qquad \tilde{z}_3 = \frac{\tilde{z}-\tilde{\eta}}{1-\tilde{\eta}}, \tag{2.3.16}$$

for certain $\tilde{z}$ values so that $0 \leq \tilde{z}_i \leq 1$. Defining a common variable $\tilde{\zeta} = \tilde{z}_i$, the governing equations are successfully redefined to be on the same domain:

$$\begin{aligned}
\frac{dy_1}{d\tilde{\zeta}} &= \tilde{\gamma} y_2, \\
\frac{dy_2}{d\tilde{\zeta}} &= \tilde{\gamma}\left(\frac{\tilde{m}}{\overline{\mu}_3(y_1, y_3)} + \tilde{g} y_1\right) + \tilde{\gamma}(\tilde{p}\tilde{g}(y_3 + \overline{\mu}_3(y_1, y_3)) - \tilde{g} - 2\tilde{p}\tilde{g}), \\
\frac{dy_3}{d\tilde{\zeta}} &= \tilde{\gamma} y_4, \\
\frac{dy_4}{d\tilde{\zeta}} &= \tilde{\gamma}(\tilde{g} y_3 + \tilde{p}\tilde{g}(y_1 + \overline{\mu}_3(y_1, y_3)) - \tilde{g} - 2\tilde{p}\tilde{g}), \\
\frac{dy_5}{d\tilde{\zeta}} &= (\tilde{\eta} - \tilde{\gamma}) y_6, \\
\frac{dy_6}{d\tilde{\zeta}} &= (\tilde{\eta} - \tilde{\gamma})(\tilde{p}\tilde{g}(y_7 + \hat{\mu}_3(y_5, y_7)) + \tilde{c} - \tilde{g} - 2\tilde{p}\tilde{g}), \\
\frac{dy_7}{d\tilde{\zeta}} &= (\tilde{\eta} - \tilde{\gamma}) y_8, \\
\frac{dy_8}{d\tilde{\zeta}} &= (\tilde{\eta} - \tilde{\gamma})(\tilde{g} y_7 + \tilde{p}\tilde{g}(y_5 + \hat{\mu}_3(y_5, y_7))) + (\tilde{\eta} - \tilde{\gamma})(\tilde{c} - \tilde{g} - 2\tilde{p}\tilde{g}), \\
\frac{dy_9}{d\tilde{\zeta}} &= (1 - \tilde{\eta}) y_{10}, \\
\frac{dy_{10}}{d\tilde{\zeta}} &= (1 - \tilde{\eta})\left(\frac{\tilde{m}}{\overline{\mu}_3(y_9, y_{11})} + \tilde{g} y_9\right) + (1 - \tilde{\eta})(\tilde{p}\tilde{g}(y_{11} + \overline{\mu}_3(y_9, y_{11})) - \tilde{g} - 2\tilde{p}\tilde{g}), \\
\frac{dy_{11}}{d\tilde{\zeta}} &= (1 - \tilde{\eta}) y_{12}, \\
\frac{dy_{12}}{d\tilde{\zeta}} &= (1 - \tilde{\eta})(\tilde{g} y_{11} + \tilde{p}\tilde{g}(y_9 + \overline{\mu}_3(y_9, y_{11})) - \tilde{g} - 2\tilde{p}\tilde{g}).
\end{aligned} \tag{2.3.17}$$

Applying (2.3.15) at $\tilde{\gamma}$ and $\tilde{\eta}$ and retaining the conditions of (2.3.13), we find the boundary conditions on the unified domain as

$$\begin{gathered}
y_2(0) = 0, \qquad y_4(0) = 0, \qquad y_{10}(1) = 0, \qquad y_{12}(1) = 0, \\
y_1(1) - y_5(0) = 0, \qquad y_2(1) - y_6(0) = 0, \qquad y_3(1) - y_7(0) = 0, \qquad y_4(1) - y_8(0) = 0, \\
y_5(1) - y_9(0) = 0, \qquad y_6(1) - y_{10}(0) = 0, \qquad y_7(1) - y_{11}(0) = 0, \qquad y_8(1) - y_{12}(0) = 0.
\end{gathered} \tag{2.3.18}$$

A collocation method for numerical integration of boundary value problems can fail to converge in instances where it encounters a singular Jacobian. Thus, at the very least, the following problem parameters should be avoided:

$$\tilde{g} = 0, \qquad \tilde{p} = 1, \qquad \tilde{\gamma} \in \{0, \tilde{\eta}, 1\}, \qquad \tilde{\eta} \in \{0, \tilde{\gamma}, 1\}. \tag{2.3.19}$$

There may be circumstances in which we want equations where there are no singular points or a sole $\tilde{\gamma}$ or $\tilde{\eta}$. In those cases, the governing equations (2.3.17) and boundary conditions (2.3.18) must be modified. The procedure detailed in this section is analogous to those developments: only a redefinition of some variables and reordering of equations is required. In the interests of brevity, these details are omitted.

2.4 Imposition of the local incompressibility constraint

In terms of the stretch variables, the local incompressibility constraint may be expressed as

$$\mu_1\mu_2\mu_3 = 1. \tag{2.4.1}$$

The internal constraint may be cast into the form (1.3.21) using the directors:

$$\sqrt{\mathbf{d}_1\cdot\mathbf{d}_1}\sqrt{\mathbf{d}_2\cdot\mathbf{d}_2}\sqrt{\mathbf{d}_3\cdot\mathbf{d}_3} = 1. \tag{2.4.2}$$

Substituting (2.4.1) into the unconstrained strain energy (2.3.1) and choosing to eliminate μ_3 results in a non-quadratic strain energy function:

$$\begin{aligned} 2w_c = {} & k_{\mathrm{S}}\left[(\mu_1-1)^2+(\mu_2-1)^2+\left(\frac{1}{\mu_1\mu_2}-1\right)^2\right]+k_{\mathrm{G}}\left[(\mu_1')^2+(\mu_2')^2\right] \\ & +2k_{\mathrm{P}}\left[(\mu_1-1)(\mu_2-1)+(\mu_1-1)\left(\frac{1}{\mu_1\mu_2}-1\right)+(\mu_2-1)\left(\frac{1}{\mu_1\mu_2}-1\right)\right], \end{aligned} \tag{2.4.3}$$

where $w_c = \hat{w}_c(\mu_1,\mu_2)$ is the constrained strain energy for an incompressible medium. A quadratic approximation of (2.4.3) close to $\mu_1 = 1 = \mu_2$ and $\mu_1' = 0 = \mu_2'$ yields

$$2w_c \approx 2(k_{\mathrm{S}}-k_{\mathrm{P}})\left[(\mu_1-1)^2+(\mu_2-1)^2+(\mu_1-1)(\mu_2-1)\right]+k_{\mathrm{G}}\left[(\mu_1')^2+(\mu_2')^2\right].$$

Applying (1.3.28) to the quadratic approximation, we derive the following force-stretch relations:

$$\begin{gathered} \mathbf{k}^1 = \left(k_{\mathrm{I}}(2\mu_1+\mu_2-3)+\frac{\lambda_c^{\mathrm{I}}}{\mu_1}\right)\mathbf{E}_1, \quad \mathbf{k}^2 = \left(k_{\mathrm{I}}(2\mu_2+\mu_1-3)+\frac{\lambda_c^{\mathrm{I}}}{\mu_2}\right)\mathbf{E}_2, \\ \mathbf{n} = \lambda_c^{\mathrm{I}}\mu_1\mu_2\mathbf{e}_3, \quad \mathbf{m}^\alpha = k_{\mathrm{G}}\mu_\alpha'\mathbf{E}_\alpha, \quad \text{(no sum)}, \end{gathered} \tag{2.4.4}$$

where

$$k_{\mathrm{I}} = k_{\mathrm{S}} - k_{\mathrm{P}} \tag{2.4.5}$$

is a new stiffness to be discussed in Section 2.6. A relationship between λ_c^{I} and λ^{I} for linear deformations is established as follows:

$$\lambda_c^{\mathrm{I}} = \lambda^{\mathrm{I}} + k_{\mathrm{I}}(2-\mu_1-\mu_2), \tag{2.4.6}$$

where $\mu_3 - 1 \approx 2-\mu_1-\mu_2$ close to $\mu_i = 1$. We observe that λ^{I} is directly related to the constraint pressure while λ_c^{I} contains an additional constitutive piece.

Governing equations under an anchoring load

In deriving the governing equations, we assume once again that $\mathbf{e}_3' \approx \mathbf{0}$ for the resulting deformations. Using the contact force given by (2.2.7), we find a relation for the internal constraint force:

$$\lambda_c^{\mathrm{I}} = -\frac{\overline{D}}{\mu_1\mu_2}. \tag{2.4.7}$$

The balances of director momentum yield the equations for an incompressible rod subject to an anchoring load of strength $\overline{D}$ along its length:

$$\begin{aligned}\mu_1'' &= \frac{R\rho_0 g}{k_{\mathrm{G}}}\mu_1\mu_2 - \frac{\overline{D}}{k_{\mathrm{G}}\mu_1^2\mu_2} + \frac{k_{\mathrm{I}}}{k_{\mathrm{G}}}(2\mu_1+\mu_2-3),\\ \mu_2'' &= -\frac{\overline{D}}{k_{\mathrm{G}}\mu_1\mu_2^2} + \frac{k_{\mathrm{I}}}{k_{\mathrm{G}}}(2\mu_2+\mu_1-3).\end{aligned} \tag{2.4.8}$$

Using the same non-dimensional variables as in $(2.3.4)_1$ and $(2.3.4)_5$ and introducing

$$\tilde{i} = \frac{k_{\mathrm{I}}\ell_0^2}{k_{\mathrm{G}}}, \qquad \tilde{\delta} = \frac{\overline{D}\ell_0^2}{k_{\mathrm{G}}}, \tag{2.4.9}$$

we obtain the non-dimensional form of the governing equations:

$$\begin{aligned}\frac{d^2\mu_1}{d\tilde{z}^2} &= \tilde{m}\mu_1\mu_2 - \frac{\tilde{\delta}}{\mu_1^2\mu_2} + \tilde{i}(2\mu_1+\mu_2-3),\\ \frac{d^2\mu_2}{d\tilde{z}^2} &= -\frac{\tilde{\delta}}{\mu_1\mu_2^2} + \tilde{i}(2\mu_2+\mu_1-3).\end{aligned} \tag{2.4.10}$$

Governing equations under advancing loads

In the case of an advancing load of pressure p applied to the rod, we cannot decouple λ_c^{I} from the equations and the balance of linear momentum is needed:

$$\begin{aligned}\mu_1'' &= \frac{p\pi R^2}{k_{\mathrm{G}}} + \frac{R\rho_0 g}{k_{\mathrm{G}}}\mu_1\mu_2 + \frac{\lambda_c^{\mathrm{I}}}{k_{\mathrm{G}}\mu_1} + \frac{k_{\mathrm{I}}}{k_{\mathrm{G}}}(2\mu_1+\mu_2-3),\\ \mu_2'' &= \frac{p\pi R^2}{k_{\mathrm{G}}} + \frac{\lambda_c^{\mathrm{I}}}{k_{\mathrm{G}}\mu_2} + \frac{k_{\mathrm{I}}}{k_{\mathrm{G}}}(2\mu_2+\mu_1-3),\\ \lambda_c^{\mathrm{I}'} &= -\lambda_c^{\mathrm{I}}\left(\frac{\mu_1'}{\mu_1}+\frac{\mu_2'}{\mu_2}\right).\end{aligned} \tag{2.4.11}$$

By introducing the non-dimensional variable

$$\tilde{\lambda}_c^{\mathrm{I}} = \frac{\lambda_c^{\mathrm{I}}\ell_0^2}{k_{\mathrm{G}}}, \tag{2.4.12}$$

the equations take on a more compact non-dimensional form:

$$\begin{aligned}\frac{d^2\mu_1}{d\tilde{z}^2} &= \tilde{c} + \tilde{m}\mu_1\mu_2 + \frac{\tilde{\lambda}_c^{\mathrm{I}}}{\mu_1} + \tilde{i}(2\mu_1 + \mu_2 - 3),\\ \frac{d^2\mu_2}{d\tilde{z}^2} &= \tilde{c} + \frac{\tilde{\lambda}_c^{\mathrm{I}}}{\mu_2} + \tilde{i}(2\mu_2 + \mu_1 - 3),\\ \frac{d\tilde{\lambda}_c^{\mathrm{I}}}{d\tilde{z}} &= -\tilde{\lambda}_c^{\mathrm{I}}\left(\frac{d\mu_1}{d\tilde{z}}\frac{1}{\mu_1} + \frac{d\mu_2}{d\tilde{z}}\frac{1}{\mu_2}\right).\end{aligned} \tag{2.4.13}$$

Boundary conditions

The procedure for defining variables and breaking up the domain is identical to the procedure discussed in Section 2.3. Added care must be taken in the boundary condition for λ_c^{I}. If there is a singular point γ where γ^- is in a region of anchoring loads and γ^+ is in a region of advancing loads, then we have a jump condition leading to the implication

$$[\![\mathbf{n}]\!]_{\xi=\gamma} = \mathbf{0} \quad \Longrightarrow \quad \tilde{\lambda}_c^{\mathrm{I}}(\gamma^+) = -\frac{\tilde{\delta}}{\mu_1(\gamma^-)\mu_2(\gamma^-)}, \tag{2.4.14}$$

where we have enforced continuity of μ_1 and μ_2 across γ. Similarly, if there is a singular point η, where η^- is in a region of advancing loads and η^+ is in a region of anchoring loads, then we find:

$$[\![\mathbf{n}]\!]_{\xi=\eta} = \mathbf{0} \quad \Longrightarrow \quad \tilde{\lambda}_c^{\mathrm{I}}(\eta^-) = -\frac{\tilde{\delta}}{\mu_1(\eta^+)\mu_2(\eta^+)}. \tag{2.4.15}$$

In the case of a region of anchoring loads followed by advancing loads followed by anchoring loads, as in Section 2.3, the domain is decomposed using the following dependent variables:

$$\begin{aligned} &y_1 = \mu_1, \quad y_2 = \frac{d\mu_1}{d\tilde{z}}, \quad y_3 = \mu_2, \quad y_4 = \frac{d\mu_2}{d\tilde{z}}, \quad \text{on} \quad 0 \le \tilde{z} \le \tilde{\gamma},\\ &y_5 = \mu_1, \quad y_6 = \frac{d\mu_1}{d\tilde{z}}, \quad y_7 = \mu_2, \quad y_8 = \frac{d\mu_2}{d\tilde{z}}, \quad y_9 = \tilde{\lambda}_c^{\mathrm{I}}, \quad \text{on} \quad \tilde{\gamma} \le \tilde{z} \le \tilde{\eta},\\ &y_{10} = \mu_1, \quad y_{11} = \frac{d\mu_1}{d\tilde{z}}, \quad y_{12} = \mu_2, \quad y_{13} = \frac{d\mu_2}{d\tilde{z}}, \quad \text{on} \quad \tilde{\eta} \le \tilde{z} \le 1. \end{aligned} \tag{2.4.16}$$

We once again let

$$\tilde{z}_1 = \frac{\tilde{z}}{\tilde{\gamma}}, \qquad \tilde{z}_2 = \frac{\tilde{z} - \tilde{\gamma}}{\tilde{\eta} - \tilde{\gamma}}, \qquad \tilde{z}_3 = \frac{\tilde{z} - \tilde{\eta}}{1 - \tilde{\eta}}. \tag{2.4.17}$$

Using the common variable $\tilde{\zeta} = \tilde{z}_i$, the governing equations for the incompressible rod become:

$$\begin{aligned}
\frac{dy_1}{d\tilde{\zeta}} &= \tilde{\gamma} y_2, \\
\frac{dy_2}{d\tilde{\zeta}} &= \tilde{\gamma}\left(\tilde{m} y_1 y_3 - \frac{\tilde{\delta}}{y_1^2 y_3} + \tilde{i}(2y_1 + y_3 - 3)\right), \\
\frac{dy_3}{d\tilde{\zeta}} &= \tilde{\gamma} y_4, \\
\frac{dy_4}{d\tilde{\zeta}} &= \tilde{\gamma}\left(-\frac{\tilde{\delta}}{y_1 y_3^2} + \tilde{i}(2y_3 + y_1 - 3)\right), \\
\frac{dy_5}{d\tilde{\zeta}} &= (\tilde{\eta} - \tilde{\gamma}) y_6, \\
\frac{dy_6}{d\tilde{\zeta}} &= (\tilde{\eta} - \tilde{\gamma})\left(\tilde{c} + \tilde{m} y_5 y_7 + \frac{y_9}{y_5} + \tilde{i}(2y_5 + y_7 - 3)\right), \\
\frac{dy_7}{d\tilde{\zeta}} &= (\tilde{\eta} - \tilde{\gamma}) y_8, \\
\frac{dy_8}{d\tilde{\zeta}} &= (\tilde{\eta} - \tilde{\gamma})\left(\tilde{c} + \frac{y_9}{y_7} + \tilde{i}(2y_7 + y_5 - 3)\right), \\
\frac{dy_9}{d\tilde{\zeta}} &= -(\tilde{\eta} - \tilde{\gamma})^2 y_9\left(\frac{y_6}{y_5} + \frac{y_8}{y_7}\right) \\
\frac{dy_{10}}{d\tilde{\zeta}} &= (1 - \tilde{\eta}) y_{11}, \\
\frac{dy_{11}}{d\tilde{\zeta}} &= (1 - \tilde{\eta})\left(\tilde{m} y_{10} y_{12} - \frac{\tilde{\delta}}{y_{10}^2 y_{12}} + \tilde{i}(2y_{10} + y_{12} - 3)\right), \\
\frac{dy_{12}}{d\tilde{\zeta}} &= (1 - \tilde{\eta}) y_{13}, \\
\frac{dy_{13}}{d\tilde{\zeta}} &= (1 - \tilde{\eta})\left(-\frac{\tilde{\delta}}{y_{10} y_{12}^2} + \tilde{i}(2y_{12} + y_{10} - 3)\right).
\end{aligned} \tag{2.4.18}$$

We use (2.4.14) in applying the boundary conditions on the unified domain:

$$\begin{gathered}
y_2(0) = 0, \qquad y_4(0) = 0, \qquad y_{11}(1) = 0, \qquad y_{13}(1) = 0, \\
y_1(1) - y_5(0) = 0, \qquad y_2(1) - y_6(0) = 0, \qquad y_3(1) - y_7(0) = 0, \qquad y_4(1) - y_8(0) = 0, \\
y_5(1) - y_{10}(0) = 0, \qquad y_6(1) - y_{11}(0) = 0, \qquad y_7(1) - y_{12}(0) = 0, \qquad y_8(1) - y_{13}(0) = 0, \\
y_9(0) + \frac{\tilde{\delta}}{y_1(1) y_3(1)} = 0.
\end{gathered} \tag{2.4.19}$$

This completes the development of the boundary value problems for compressible and incompressible rods.

2.5 Kinematical integrating conditions and simulated motion

Now that the boundary value problems have been developed for both the compressible and incompressible rod, it remains to architect a locomotion scheme that allows for $\tilde{\gamma}$ and $\tilde{\eta}$ to migrate along the centerline in order to simulate peristalsis. To that end, a discussion of how to iteratively obtain position vectors and directors in time is needed.

Integrating conditions

Referring to Figure 1.4, the ground plane has unit normal $\mathbf{E}_1$ and passes through the point $(-R, 0, 0)$. We found earlier that the points from the lateral surface of the rod in contact with the ground plane must obey $\mathbf{r}^*(-R, 0, \xi) \cdot \mathbf{E}_1 = -R$. Therefore,

$$(\mathbf{r}^*(-R, 0, \xi) \cdot \mathbf{E}_1)' = 0, \tag{2.5.1}$$

and we have the relation

$$\mathbf{r}' \cdot \mathbf{E}_1 = R\mathbf{d}_1' \cdot \mathbf{E}_1. \tag{2.5.2}$$

Let $x(\xi)$ and $z(\xi)$ be Cartesian coordinates for the current centerline position vector, so that

$$\mathbf{r}(\xi) = x\mathbf{E}_1 + z\mathbf{E}_3. \tag{2.5.3}$$

As $\mathbf{r}'$ does not come out of plane according to the ansatz, suppose that $\mathbf{e}_t = \cos(\theta)\mathbf{E}_3 + \sin(\theta)\mathbf{E}_1$. Now we have two representations for $\mathbf{r}'$:

$$\mathbf{r}' = \mu_3(\cos(\theta)\mathbf{E}_3 + \sin(\theta)\mathbf{E}_1) = x'\mathbf{E}_1 + z'\mathbf{E}_3. \tag{2.5.4}$$

The first order ordinary differential equations for the current centerline position given the strains and strain gradients from integrating (2.3.17) or (2.4.18) are

$$x' = R\mu_1', \;\; z' = \mu_3 \cos(\theta), \;\; \text{where } \theta = \arcsin\left(\frac{R\mu_1'}{\mu_3}\right). \tag{2.5.5}$$

Hence,

$$z' = \sqrt{\mu_3^2 - R^2\mu_1'^2}. \tag{2.5.6}$$

We note that it is expected that $\mu_3 >> R\mu_1'$ for all deformations. Integrating $(2.5.5)_1$ and noting that x should be zero when $\mu_1 = 1$, we find

$$x(\xi) = R(\mu_1(\xi) - 1). \tag{2.5.7}$$

To obtain $z(\xi)$, we assume the existence of a singular fixed, or anchored, point with material coordinates $(-R, 0, \xi_{\mathrm{A}})$. If $z(\xi_{\mathrm{A}})$ is a priori known from another analysis, then $z(\xi)$ is generated via forward and rearward integrations from this point:

$$z(\xi) - z(\xi_{\mathrm{A}}) = \int_{\xi_{\mathrm{A}}}^{\xi} \sqrt{\mu_3^2 - R^2 \mu_1'^2}\, d\bar{\xi}. \tag{2.5.8}$$

Peristalsis

The basis for the locomotion scheme requires the singular points γ and η to migrate rearward through the material. A particular prescription for $\gamma(t)$ and $\eta(t)$ results in a model for peristalsis with pulses of contraction propagating rearward along the rod. The continuous time parameter t is selected so that $t = 0$ indicates the start of the motion. A discrete time index ${}^i t = i t_{\mathrm{step}}$ is introduced, where t_{step} is a time step, so that we can write

$$\gamma\big({}^i t\big) = {}^i\gamma, \quad \eta\big({}^i t\big) = {}^i\eta. \tag{2.5.9}$$

Note that when it comes to the numerical integration, neither γ nor η may actually occupy $\xi = 0, \ell_0$, in accordance with the singular Jacobian conditions of (2.3.19).

The kinematics of the now time-indexed position vector ${}^i\mathbf{r}$ are updated at every ${}^i t$ to advance the rod and simulate the motion. We have the anchoring condition

$${}^i z\big({}^i\xi_{\mathrm{A}}\big) = {}^{i-1} z\big({}^i\xi_{\mathrm{A}}\big). \tag{2.5.10}$$

The update rule becomes

$${}^i z(\xi) = {}^{i-1} z\big({}^i\xi_{\mathrm{A}}\big) + \int_{{}^i\xi_{\mathrm{A}}}^{\xi} \sqrt{{}^i\mu_3{}^2 - R^2\, {}^i\mu_1{}'^2}\, d\bar{\xi}. \tag{2.5.11}$$

The vertical position ${}^i x(\xi)$ is updated according to ${}^i\mu_1(\xi)$ using (2.5.7). It remains to give specific prescriptions for ${}^i\gamma$ and ${}^i\eta$ based on the application at hand.

2.6 Prescriptions for the stiffnesses

The one-dimensional moduli k_{S}, k_{G}, and k_{P} should be physically motivated. We will relate them to Poisson's ratio and other moduli from linear elasticity. To that end, we contemplate two simple experiments - one a simple tension test and the other an application of a uniform hydrostatic load. Our main results are presented in (2.6.7) and (2.6.20).

To interpret the results from the forthcoming thought experiments, it is helpful to consider an inversion of the force-strain relations (2.3.2) for a compressible rod:

$$\begin{bmatrix} \mu_1 - 1 \\ \mu_2 - 1 \\ \mu_3 - 1 \\ \mu_1' \\ \mu_2' \end{bmatrix} = \mathsf{C} \begin{bmatrix} \mathbf{k}^1 \cdot \mathbf{E}_1 \\ \mathbf{k}^2 \cdot \mathbf{E}_2 \\ \mathbf{n} \cdot \mathbf{e}_3 \\ \mathbf{m}^1 \cdot \mathbf{E}_1 \\ \mathbf{m}^2 \cdot \mathbf{E}_2 \end{bmatrix}, \tag{2.6.1}$$

where

$$\mathsf{C} = \frac{1}{k}\begin{bmatrix} k_{\mathrm{P}}+k_{\mathrm{S}} & -k_{\mathrm{P}} & -k_{\mathrm{P}} & 0 & 0 \\ -k_{\mathrm{P}} & k_{\mathrm{P}}+k_{\mathrm{S}} & -k_{\mathrm{P}} & 0 & 0 \\ -k_{\mathrm{P}} & -k_{\mathrm{P}} & k_{\mathrm{P}}+k_{\mathrm{S}} & 0 & 0 \\ 0 & 0 & 0 & k/k_{\mathrm{G}} & 0 \\ 0 & 0 & 0 & 0 & k/k_{\mathrm{G}} \end{bmatrix},$$
$$k = (k_{\mathrm{S}}-k_{\mathrm{P}})(k_{\mathrm{S}}+2k_{\mathrm{P}}). \tag{2.6.2}$$

Simple tension

The first experiment is a simple tension. Suppose a pair of terminal tensile forces of strength F are applied at the endpoints of a free-free compressible rod of reference cross-sectional area $A_0 = \pi R^2$. Then, from the balance laws and jump conditions, $\mathbf{n} = F\mathbf{e}_3 = F\mathbf{E}_3$, $\mathbf{k}^\alpha = \mathbf{0}$, and $\mathbf{m}^\alpha = \mathbf{0}$, i.e., we have assumed no necking behavior since μ_α are free to change at the terminal cross-sections. We may derive from (2.6.1) the stress-strain relation

$$E_{1\mathrm{D}}(\mu_3 - 1) = \frac{F}{A_0}, \tag{2.6.3}$$

where

$$E_{1\mathrm{D}} = \frac{(k_{\mathrm{S}}-k_{\mathrm{P}})(k_{\mathrm{S}}+2k_{\mathrm{P}})}{A_0(k_{\mathrm{P}}+k_{\mathrm{S}})} \tag{2.6.4}$$

is defined to be an elastic modulus derived from the one-dimensional theory. The stiffness $E_{1\mathrm{D}}$ is the ratio of engineering stress to the observed engineering strain in the longitudinal direction. In the same experiment, the rod's cross-sections contract in response to the Poisson effect, and we additionally have the relations

$$\mu_1 - 1 = \mu_2 - 1 = -\frac{k_{\mathrm{P}}}{k}F = -\frac{k_{\mathrm{P}}}{k_{\mathrm{P}}+k_{\mathrm{S}}}(\mu_3 - 1). \tag{2.6.5}$$

We may now define Poisson's ratio as the ratio of lateral to longitudinal strain, as derived from the one-dimensional theory:

$$\nu_{1\mathrm{D}} = \frac{k_{\mathrm{P}}}{k_{\mathrm{P}}+k_{\mathrm{S}}}. \tag{2.6.6}$$

The pair $(E_{1\mathrm{D}}, \nu_{1\mathrm{D}})$ determine the Lamé pair $(k_{\mathrm{S}}, k_{\mathrm{P}})$ as

$$k_{\mathrm{S}} = \frac{1-\nu_{1\mathrm{D}}}{(1+\nu_{1\mathrm{D}})(1-2\nu_{1\mathrm{D}})}E_{1\mathrm{D}}A_0, \quad k_{\mathrm{P}} = \frac{\nu_{1\mathrm{D}}}{(1+\nu_{1\mathrm{D}})(1-2\nu_{1\mathrm{D}})}E_{1\mathrm{D}}A_0. \tag{2.6.7}$$

A hydrostatic pressure

We next consider an experiment where the rod is exposed to a uniform, or hydrostatic, pressure p. In that case, $\mathbf{k}^1 = -pA_0\mathbf{E}_1$, $\mathbf{k}^2 = -pA_0\mathbf{E}_2$, and $\mathbf{n} = -pA_0\mathbf{E}_3 = -pA_0\mathbf{e}_3$. From

the strain-force relations (2.6.1), we find that the isotropic material is subject to a pure dilatation:

$$\mu_1 - 1 = \mu_2 - 1 = \mu_3 - 1 = -\frac{k_S - k_P}{k} p A_0. \tag{2.6.8}$$

Therefore, we have the summation of strains as:

$$\mu_1 + \mu_2 + \mu_3 - 3 = -\frac{k_S - k_P}{k} p A_0. \tag{2.6.9}$$

The deformation is homogeneous for uniform material properties. If V is the global post-deformation volume, and V_0 is the global reference configuration volume, then we have

$$\frac{V}{V_0} = \mu_1 \mu_2 \mu_3, \tag{2.6.10}$$

which, for deformations close to $\mu_1 \equiv \mu_2 \equiv \mu_3 \equiv 1$, we may approximate to first order in the stretches as

$$\frac{V}{V_0} \approx 1 + \mu_1 + \mu_2 + \mu_3 - 3. \tag{2.6.11}$$

Consequently, the volumetric strain is approximately

$$\frac{\Delta V}{V_0} \approx \mu_1 + \mu_2 + \mu_3 - 3, \tag{2.6.12}$$

where

$$\Delta V = V - V_0 \tag{2.6.13}$$

is the global volume difference. Expression (2.6.9) now becomes

$$\kappa_{1D} \frac{\Delta V}{V_0} = -p, \tag{2.6.14}$$

where

$$\kappa_{1D} = \frac{k_S + 2k_P}{A_0} \tag{2.6.15}$$

is a bulk modulus derived from the one-dimensional theory. Given the pair (E_{1D}, κ_{1D}), we may combine (2.6.7) and (2.6.15) to find ν_{1D} as

$$\nu_{1D} = \frac{1 - E_{1D}/\kappa_{1D}}{2}. \tag{2.6.16}$$

Hence, for the incompressible case where $\kappa_{1D} >> E_{1D}$, we have $\nu_{1D} = 0.5$ and, using L'Hôpital's rule on the difference between $(2.6.7)_1$ and $(2.6.7)_2$,

$$k_I = k_S - k_P = \frac{2}{3} E_{1D} A_0. \tag{2.6.17}$$

To gain insight into k_{G} for compressible and incompressible materials, we look towards results from the direct approach.

Suppose a three-dimensional body is comprised of isotropic linearly elastic material. Following [47], we can approximate the classical three-dimensional strain energy from linear elasticity for such materials comprising a rod-like body as

$$\begin{aligned} 2w = {} & k_1\Big[\big(\mu_1^2-1\big)^2+\big(\mu_2^2-1\big)^2+\big(\mu_3^2-1\big)^2\Big]+k_2\Big[\big(\mu_1'\mu_1\big)^2+\big(\mu_2'\mu_2\big)^2\Big] \\ & +2k_3\big[\big(\mu_1^2-1\big)\big(\mu_2^2-1\big)+\big(\mu_1^2-1\big)\big(\mu_3^2-1\big)+\big(\mu_2^2-1\big)\big(\mu_3^2-1\big)\big], \end{aligned} \tag{2.6.18}$$

where

$$k_1=\frac{E_{3\mathrm{D}}\pi R^2(1-\nu_{3\mathrm{D}})}{4(1+\nu_{3\mathrm{D}})(1-2\nu_{3\mathrm{D}})},\quad k_2=\frac{E_{3\mathrm{D}}\pi R^4}{8(1+\nu_{3\mathrm{D}})},\quad k_3=\frac{\nu_{3\mathrm{D}}}{1-\nu_{3\mathrm{D}}}k_1.$$

Here, $E_{3\mathrm{D}}$ and $\nu_{3\mathrm{D}}$ are, respectively, Young's modulus and Poisson's ratio from the three-dimensional theory. If we approximate (2.6.18) to quadratic order near $\mu_1=\mu_2=\mu_3=1$ and $\mu_1'=\mu_2'=0$, we find:

$$\begin{aligned} 2w \approx {} & 4k_1\big[(\mu_1-1)^2+(\mu_2-1)^2+(\mu_3-1)^2\big]+k_2\Big[\big(\mu_1'\big)^2+\big(\mu_2'\big)^2\Big] \\ & +2k_3[4(\mu_1-1)(\mu_2-1)+4(\mu_1-1)(\mu_3-1)+4(\mu_2-1)(\mu_3-1)]. \end{aligned} \tag{2.6.19}$$

We are therefore justified in assigning

$$k_{\mathrm{S}}=\frac{E_{3\mathrm{D}}\pi R^2(1-\nu_{3\mathrm{D}})}{(1+\nu_{3\mathrm{D}})(1-2\nu_{3\mathrm{D}})},\qquad k_{\mathrm{G}}=\frac{E_{3\mathrm{D}}\pi R^4}{8(1+\nu_{3\mathrm{D}})},\qquad k_{\mathrm{P}}=\frac{\nu_{3\mathrm{D}}}{1-\nu_{3\mathrm{D}}}k_{\mathrm{S}}. \tag{2.6.20}$$

Note that $(2.6.20)_1$ and $(2.6.20)_3$ reconcile with the stiffnesses developed in (2.6.7). We conclude that $E_{1\mathrm{D}}=E_{3\mathrm{D}}=E$ and $\nu_{1\mathrm{D}}=\nu_{3\mathrm{D}}=\nu$. The one-dimensional bulk modulus is therefore also equivalent to its three-dimensional counterpart, and so we may redefine $\kappa_{1\mathrm{D}}=\kappa$. Using E and ν, which may be determined from an experiment, we assign

$$k_{\mathrm{G}}=\frac{E\pi R^4}{8(1+\nu)} \tag{2.6.21}$$

for compressible materials and

$$k_{\mathrm{G}}=\frac{E\pi R^4}{12} \tag{2.6.22}$$

for incompressible materials. Consequently, any one of the pairs (E,ν), (E,κ), or (κ,ν) along with A_0 define a compressible material while E along with A_0 define an incompressible material for the one-dimensional theory.

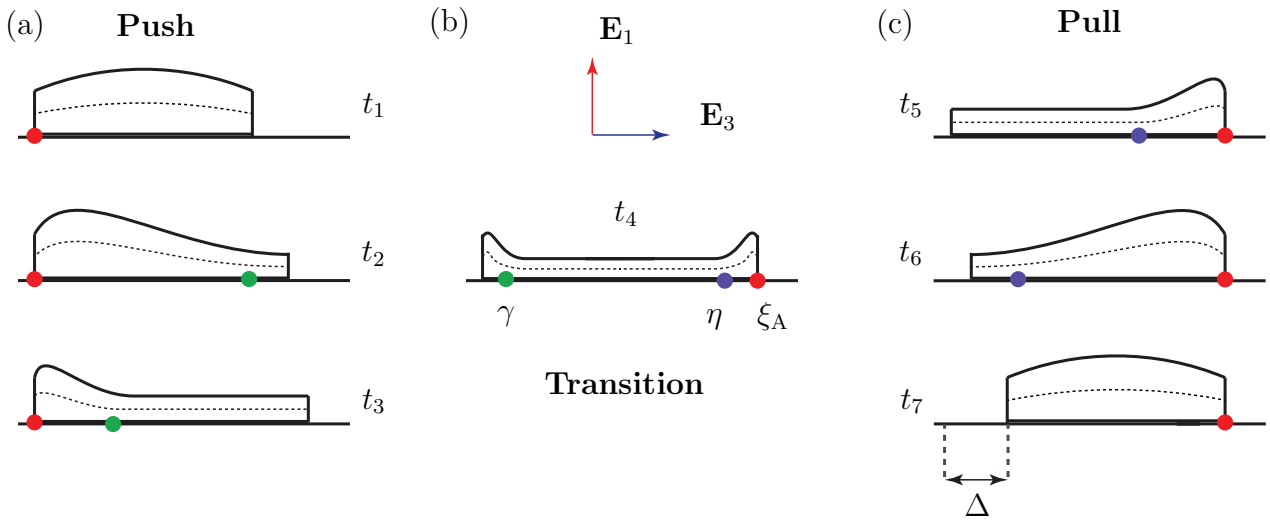

Figure 2.7: *A single cycle of a theoretical push-pull locomotion scheme effected by a particular prescription for $\gamma(t)$ (green) and $\eta(t)$ (blue). The strategy is to (a) push using a rear anchor point (red), (b) transition to a forward anchor point, and then (c) pull using a forward anchor point. The time indices are ordered such that $t_1 < t_2 < t_3 < \cdots$.*

2.7 A peristalsis-driven soft robot

To drive a soft robot using peristalsis, we choose to architect a *push-pull* locomotion scheme, with the anchor point being either $\xi_A = 0$ during pushing or $\xi_A = \ell_0$ during pulling (Figure 2.7). In this case, the equations developed in Section 2.3 are useful. A prescription for $\gamma(t)$ and $\eta(t)$ is desired. Let t_{pause} indicate a pause time between cycles. We assume that the rod is fully longitudinally contracted for $0 \leq t < t_{\text{pause}}$. At $t = t_{\text{pause}}^+$, γ begins to migrate rearward from ℓ_0 at a propagation speed v:

$$\gamma(t) = \ell_0 - v(t - t_{\text{pause}}), \quad t_{\text{pause}} < t \leq t_{\text{pause}} + \frac{\ell_0}{v}. \tag{2.7.1}$$

The rod begins to push itself forward using circular contractions and a rear anchor. At some point, the rod transitions to a forward anchor point. Let T indicate the percentage of the rod that γ has left to migrate through before an η is initiated at ℓ_0. If, for example, $T = 0.25$, then η appears at ℓ_0 when γ reaches $\ell_0/4$, which is the scenario displayed in Figure 2.7. We take the propagation speed for $\eta(t)$ to be the same as that for $\gamma(t)$. Hence, we have

$$\begin{aligned} \eta(t) &= \ell_0 - v\left(t - t_{\text{pause}} - \frac{\ell_0}{v}(1 - T)\right), \\ t_{\text{pause}} + \frac{\ell_0}{v}(1 - T) &< t \leq t_{\text{pause}} + \frac{\ell_0}{v}(2 - T). \end{aligned} \tag{2.7.2}$$

When γ reaches $\xi = 0$, it vanishes and the rod becomes subject only to an η. In this period, the rod is pulling itself forward using a forward anchoring point by sending a rearward pulse of longitudinal contractions. When the time $t = t_{\text{pause}} + \frac{\ell_0}{v}(2 - T)$ is reached, another pause elapses, and the cycle continues. The rod achieves a net forward displacement every cycle. Discrete values of ${}^i\tilde{\gamma}$ and ${}^i\tilde{\eta}$ for the push-pull prescription are displayed in Figure 2.8. Care must be taken so that neither ${}^i\tilde{\gamma} = 0, \ell_0$ nor ${}^i\tilde{\eta} = 0, \ell_0$.

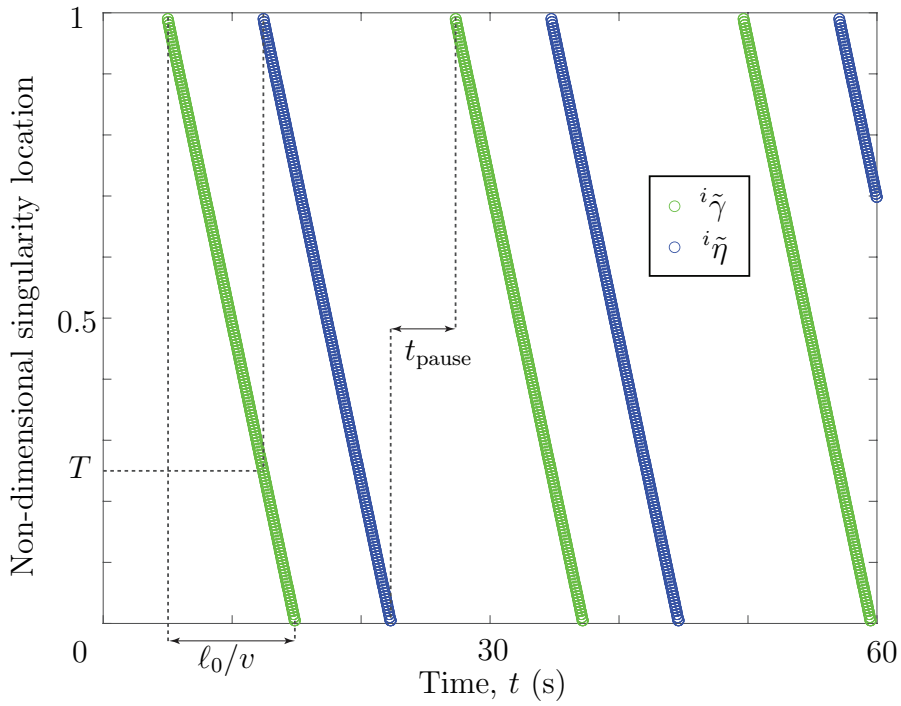

Figure 2.8: *Push-pull prescriptions for ${}^i\tilde{\gamma}$ and ${}^i\tilde{\eta}$ according to (2.7.1) and (2.7.2). We do not allow the discrete values of γ and η to get too close to 0 or ℓ_0. Results are displayed for a rod of reference length $\ell_0 = 10$ in $= 25.4$ cm and propagation speed $v = 2.54$ cm/s. The time parameters are $t_{step} = 0.01$ s, $t_{pause} = 5$ s, and $T = 0.25$ s.*

Realistic parameters must be prescribed to demonstrate that the theory is useful in practice. The variables remaining to be prescribed are: (1) an inertial parameter ρ_0^*, (2) geometric parameters R and ℓ_0, (3) compressible material properties E and ν, and (4) kinetic parameters $\overline{D}$ and p. With soft polymers in mind for a soft robot (see [36] for a relevant perspective), we select for a simulation, in SI units,

$$\rho_0^* = 1 \text{ g} \cdot \text{cm}^{-3}, \qquad R = 2.54 \text{ cm}, \qquad \ell_0 = 25.4 \text{ cm}, \qquad E = 10 \text{ kPa},$$
$$\nu = 0.3, \qquad \overline{D} = 1 \text{ N}, \qquad p = 1 \text{ psi} = 6.89 \text{ kPa}. \tag{2.7.3}$$

The propulsive kinematics is prescribed to be those graphed in Figure 2.8. For the case of modeling a pneumatic artificial muscle (PAM), one might choose $\overline{D} = 0$, and p could be neg-

ative. If a hydraulic artificial muscle is desired to be modeled, then the governing equations of Section 2.4 for incompressible media may prove to be more applicable. Simulation results for the compressible soft robot described in this section are displayed in Figure 2.9.

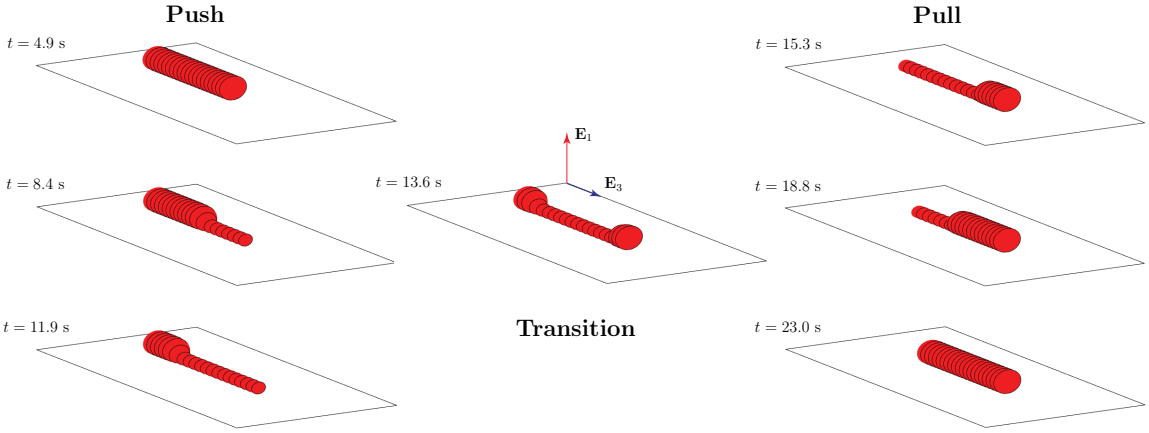

Figure 2.9: *A potential soft robot engaging in push-pull locomotion with the parameters of (2.7.3) and locomotion scheme as in Figures 2.7 and 2.8.*

2.8 Biomimetic modeling of an earthworm

The locomotory gait of the earthworm *Lumbricus terrestris* was studied in [50]. The worm is described to advance by first protruding its anterior end in a push phase with the posterior end serving as an anchoring "foot." Next, a stance phase is initiated where the anterior end serves as the foot for anchoring and the posterior end is dragged forwards in a pull phase. Following Figure 2.10, we define t_p as the protrusion time and t_s as the stance time. A prescription for $\tilde{\gamma}$ and $\tilde{\eta}$ in time is designed (Figure 2.11) based on the gait cycle displayed in Figure 2.10 along with knowledge of the protrusion and stance times. We choose $\tilde{\eta}$ to decrease from 0.5 to 0 over half the protrusion time, while $\tilde{\gamma}$ decreases from 1 to 0.75 over the first half of the protrusion time and then speeds up to decrease from 0.75 to 0 over the second half. When $\tilde{\gamma}$ reaches 0.5, the worm enters its stance phase and another wave of circular contraction begins to pass rearward via the initiation of an $\tilde{\eta}$ traversing at a uniform material speed. The resulting net displacement accomplished by the worm in a given cycle is its stride length.

Quillin's model [50] allows for a continuum of anchoring points. Our model includes some strain gradient elasticity, meaning that actions at one location of the worm may effect strains in another: sections of the worm that are contracting longitudinally versus circularly may not be fully insulated from one another. Since we are choosing a singular point for anchoring, "backslipping" may be accounted for in our model. For the stance phase, the anchoring point is chosen as the anterior end. In the beginning part of the protrusion phase,

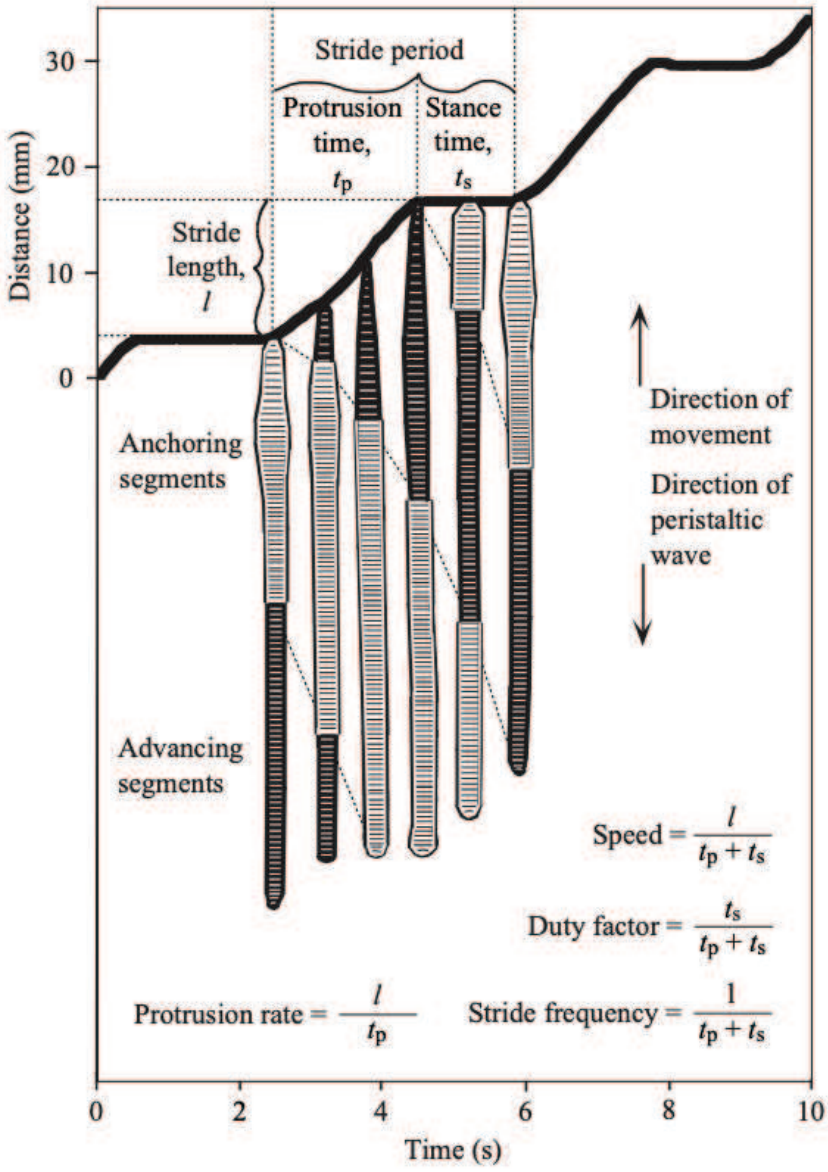

Figure 2.10: *The peristaltic crawling of an earthworm Lumbricus terrestris and its relevant kinematic variables [50]. Reproduced with written permission from the author.*

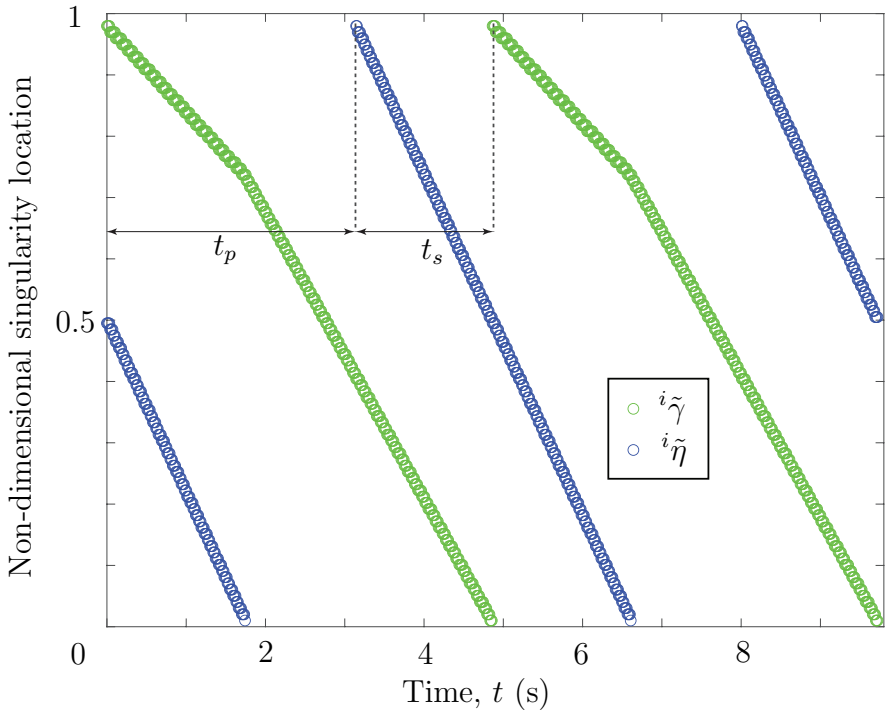

Figure 2.11: *Protrusion-stance prescriptions for* $^i\tilde{\gamma}$ *and* $^i\tilde{\eta}$ *intending to mimic the locomotion scheme of Figure 2.10. Protrusion and stance times for a worm of 10* g *are found to be* $t_p = 3.15$ s *and* $t_s = 1.75$ s*, respectively.*

the anchoring point is chosen to be the average of γ and η, while in the latter part of the phase, it is chosen to be the rear. The prescribed anchoring behavior as displayed in Figure 2.12 reconciles with that displayed in Figure 2.10.

An average adult worm of mass 10 g [35] is chosen to be modeled. Empirical scaling relationships for input to the model are collected in Table 2.1. The relationships in Table 2.1, from top to bottom, are: stance time-body mass, protrusion time-body mass, resting length-body mass, and resting diameter-body mass, where the diameter of the 30th segment from the anterior end was measured in [35]. For the worm of mass 10 g, geometric and kinematical parameters are calculated and have been inserted into Table 2.1.

Some efforts have been made to quantify the amount of tension produced by longitudinal and circular muscle contractions of a dissected strip of muscle from an earthworm, *Pheretima communissima* [29, 66, 67]. These authors concede that their results are only qualitative, as their dissected strips contained both circular and longitudinal muscle. Nonetheless, their estimates can yield an order of magnitude estimate for the anchoring and advancing loads. From [66], peak longitudinal and circular muscle tensions from phasic contractions of 10 mm by 1 mm dissected strips of muscle were measured as

$$T_{\text{circ,peak}} = 0.3 \text{ gf}, \quad \text{and} \quad T_{\text{long,peak}} = 0.186 \text{ gf}, \tag{2.8.1}$$

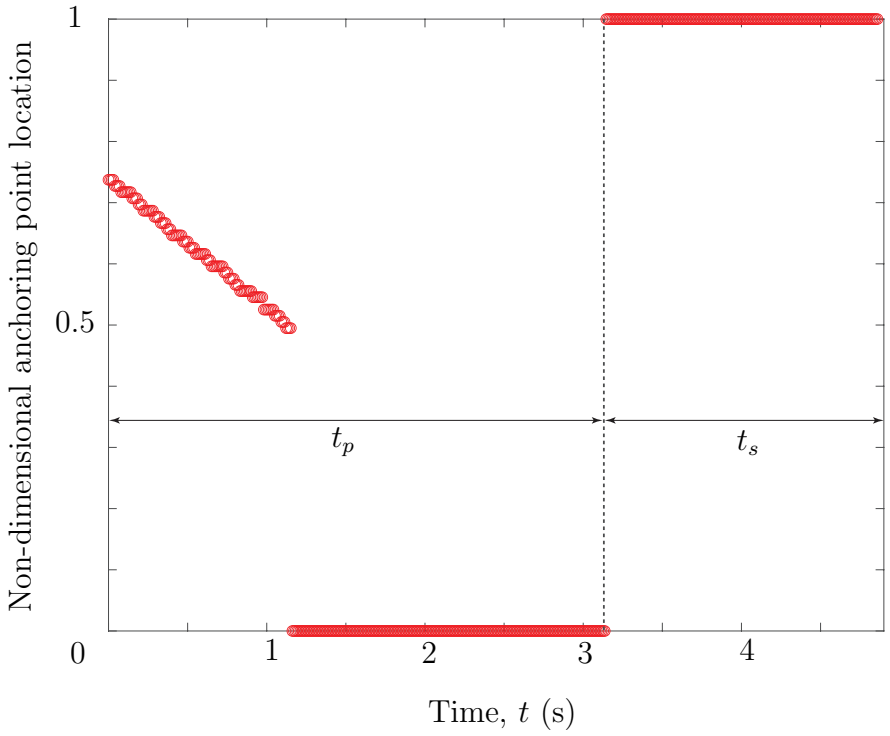

Figure 2.12: *Non-dimensional location of the anchoring point, designed to mimic the locomotion scheme of Figure 2.10.*

where the units of tension are gram-force. A worm of diameter 7.6 mm has a circumference of 23.88 mm. For a 10 mm by 1 mm dissected strip of circular muscle cut azimuthally, an equivalent peak advancing pressure is derived as

$$p_{\text{peak}} = 5.7 \text{ kPa}. \tag{2.8.2}$$

If a ring of longitudinally cut muscle fibers are arranged circularly, then the net result is 23.88 linear actuators (recall Figure 2.3(a)) acting in parallel. The total amount of peak longitudinal force generated in the worm is therefore derived as

$$\overline{D}_{\text{peak}} = 43.6 \text{ mN}. \tag{2.8.3}$$

We will assume that for the locomotory gait of the 10 g worm, only a certain percentage of its peak load is used. This percentage is calibrated to match the anticipated kinematics and coelomic pressure.

The elastic parameter E of the worm comes from connective tissue fibers that are arranged helically in the body wall [33, 51, 63]. The passive tension of muscle was also measured in [29, 67], but it is difficult to discern the resting length of the tissue that was stretched. In a simple force-stretch experiment involving a worm, we would be required to separate the

Table 2.1: Empirical scaling relationships collected from the literature on earthworm (*Lumbricus terrestris*) kinematics and geometry. Results are listed for an adult worm of mass 10 g.

Empirical Relationship	Output for $m = 10$ g	Source
$t_s = 1.6m^{0.04}$	1.75 s	Quillin [50]
$t_p = 2.5m^{0.1}$	3.15 s	Quillin [50]
$\ell_0 = 10^2 m^{0.397}$	250 mm	Kurth & Kier [35]
$2R = 10^{0.6} m^{0.278}$	7.6 mm	Kurth & Kier [35]

stress from the elastic tension from the compressive hydrostatic pressure. A procedure could be devised where the coelomic fluid in each segment is drained prior to a tensile test. Given the lack of empirical data in the literature and the inherent difficulty of extracting E from a simple force-stretch test, we chose to calibrate the stiffness to match expected kinematic results for a 10 g worm from [50].

Anticipated outcomes

Quillin [50] found a stride length-body mass scaling relationship as

$$\Delta = 15m^{0.4}, \tag{2.8.4}$$

where Δ is the stride length in units of mm. For an adult worm of 10 g, relationship (2.8.4) yields a stride length of $\Delta = 38.6$ mm. According to our theory, the stride length may be calculated as

$$\Delta = (\mathbf{r}(\ell_0, t_p + t_s) - \mathbf{r}(\ell_0, 0)) \cdot \mathbf{E}_3. \tag{2.8.5}$$

In addition, Quillin [50] found the extremal cross-section and longitudinal strains during contraction to be approximately constant irrespective of body mass. For segment 50 of an

earthworm, Quillin measured a cycle-averaged longitudinal strain of 0.60 and a circumferential strain of -0.25, where the strains are between longitudinal and circular lengths of segments. These observed strains yield a ratio of stretches as

$$\frac{\mu_1|_{\text{circ}}}{\mu_1|_{\text{long}}} = 0.75, \qquad \frac{\mu_3|_{\text{circ}}}{\mu_3|_{\text{long}}} = 1.60, \tag{2.8.6}$$

where $(\mu_1|_{\text{circ}}, \mu_3|_{\text{circ}})$ and $(\mu_1|_{\text{long}}, \mu_3|_{\text{long}})$ are evaluated at times of maximum circular and longitudinal contraction, respectively. Segment 50 was found to be a distance of approximately $\frac{2}{5}\ell_0$ from the anterior end of the worm in its reference configuration based on a diagram in [51].

We assume the reactive piece of the Piola traction acting anywhere on the cross-section is related to the coelomic pressure as

$$\hat{\mathbf{P}}\mathbf{E}_3 = -p_{\text{coelom}}\mathbf{E}_3, \tag{2.8.7}$$

where $\hat{\mathbf{P}}$ is the reactive part of the Piola stress. Taking p_{coelom} to be uniform, assuming $\mathbf{e}_3$ to be near to $\mathbf{E}_3$, and applying (1.2.66) and $(2.4.4)_1$, we derive:

$$p_{\text{coelom}} = \frac{-\lambda^{\text{I}}\mu_1\mu_2}{\pi R^2}, \tag{2.8.8}$$

where we recall from (2.4.5) the relation between the Lagrange multipliers:

$$\lambda^{\text{I}} = \lambda^{\text{I}}_c - k_{\text{I}}(2 - \mu_1 - \mu_2). \tag{2.8.9}$$

Quillin [51] measured a rest pressure of approximately 0.1 kPa. Our estimates do not account for a resting pressure, other than the minimal (10 Pa) amount of pressure that is developed under the deformation of the worm's own weight. During peristalsis, Quillin reported pressures of about 0.3 kPa for longitudinal muscle contraction and 0.8 kPa for circular muscle contraction.

Results

To match the expected outcomes, we calibrated the elastic modulus to be $E = 2$ kPa, which is on the order of the stiffness for the soft tissue comprising the human spleen [3]. Additionally, we chose the magnitude of the longitudinal and circular contractile loads to be $\overline{D} = 0.6\overline{D}_{\text{peak}}$ and $p = 0.238p_{\text{peak}}$, respectively. For these parameters, our simulation results for the biomimetic modeling of a worm are displayed in Figures 2.1 and 2.2.

We found the stretches in segment 50 to be $\mu_1 = 0.85$ and $\mu_3 = 1.35$ during circular contraction and $\mu_1 = 1.09$ and $\mu_3 = 0.82$ during longitudinal contraction. To compare with the result in (2.8.6), we compute

$$\frac{\mu_1|_{\text{circ}}}{\mu_1|_{\text{long}}} = 0.78, \quad \text{and} \quad \frac{\mu_3|_{\text{circ}}}{\mu_3|_{\text{long}}} = 1.65, \tag{2.8.10}$$

yielding a percent error of 4% and 3%, respectively.

The theoretical coelomic pressure was found to swing between a low of 0.24 kPa when segment 50 was subject to longitudinal contraction and a high of 0.79 kPa when segment 50 was subject to circular contraction. These values are in general agreement with the peaks and troughs reported in [51]. Lastly, the stride length was found to be 39 mm. Compared to the stride length of 38.6 mm predicted by scaling relationship (2.8.4), a percent error of 1% is computed. We conclude that the directed rod model developed in this chapter appears to be suitable for biomimetic modeling of an earthworm.

2.9 Conclusion

Boundary value problems for the static deformation of a directed rod that is permitted to stretch in three directions have been developed. Two linearly elastic isotropic material models were assumed with incompressibility being imposed as an internal constraint. The elastic parameters have been related to empirical quantities that one can measure in an experiment involving small deformations. Actuation effects, whether from robotic actuators or muscle contraction, have been modeled as external compressive loads. The actuator loads are treated mathematically using a doublet function for an assigned centerline force and a uniform pressure for a pair of assigned director forces. Designs of push-pull and protrusion-stance locomotion schemes were suggested along with suitable predictions for a singular anchoring point. The theory has been demonstrated for use in the modeling of soft robotic devices and the biomimetic modeling of an earthworm.

Biomimetic modeling of the worm could be improved if better data on the muscle forces sustained during a locomotory gait cycle and the elastic properties due to connective tissues in the body wall were collected. Regardless, we have demonstrated that the theory predicts acceptable results after a reasonable calibration of the parameters.

Chapter 3

A discretized model for planar motions of a rod

3.1 Introduction

Modern computational models that aim to recreate and predict motions of slender continua are continually being refined to improve their physical validity and computational efficiency. The first algorithms to model these motions were established decades ago with the advent of the finite element method. Simple cases of the finite element method involving one-dimensional elements have been applied to model slender bodies such as bars, Bernoulli-Euler beams, and Timoshenko beams. In order to improve speed and accuracy, many other novel discretizations have recently been developed [11, 39, 72], including the absolute nodal coordinate formulation (ANCF) which employs a set of gradient vectors to accommodate large deformation problems [20, 48, 64]. One of the latest contributions to the field is known as Discrete Elastic Rods (DER) ([4, 6, 5, 30]). This theory can be considered as a discrete formulation of Kirchhoff's rod theory. DER is well suited for simulating three-dimensional motions of rods that can stretch, bend, and twist. The formulation has found widespread adoption in the computer graphics community. Whether or not DER will gain a similar acceptance with engineers interested in the accurate structural response of beams and columns or the dynamic response of deforming soft robots remains to be seen. A planar version of this theory has recently been championed by Goldberg et al. [21] for application to locomoting soft robots.

In this chapter, we develop a novel discrete model for a rod undergoing planar motions. The model is based on Green and Naghdi's rod theory [25, 26, 42] as described in the first chapter. Their rod theory is sufficiently general to capture stretching, bending, torsion, and cross-sectional deformations. Thus, can view it as a generalization of Kirchhoff's rod theory, the basis for DER. Referring to Figure 3.1, we consider a rod theory to make use of a trio of material curves. One of these curves is the centerline, while the other two will soon be termed directorlines. In this chapter's discrete planar theory, we model the rod using a pair

of material curves. We will use results from Green and Naghdi's theory as inspiration for the discrete planar rod's postulated strain energy function and balance laws (3.3.36).

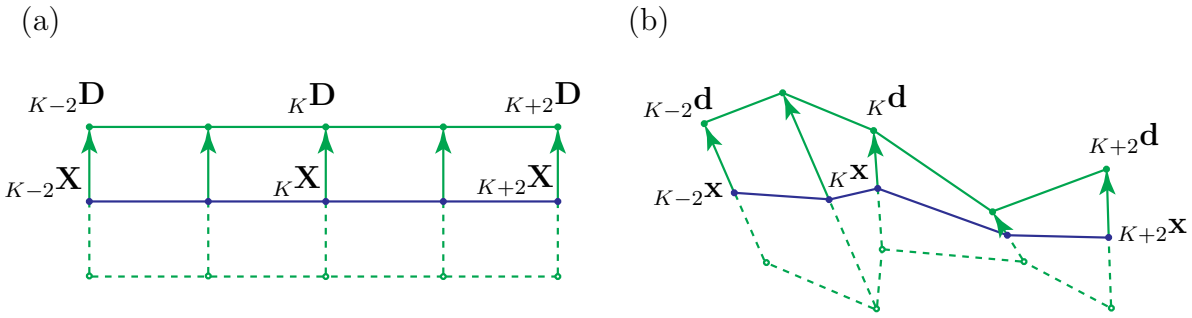

Figure 3.1: *(a) A part of the reference configuration of the discrete directed curve which is comprised of finitely many centerline vertices* $_K\mathbf{X}$ *and directors* $_K\mathbf{D}$ *attached at every centerline vertex. (b) An arbitrary current configuration of the part of the rod in (a). The solid lines indicate the centerline and directorline. The dashed lines help to show how the material of the rod-like body is related to the abstract directed curve. In the case shown, the centerline is chosen as the line of area centers, and the bottom boundary of the rod-like body is gotten by a reflection of the directors across the centerline.*

Our work deviates from that of DER in that it uses a different nonlinear elastic energy postulate and incorporates additional deformation modes such as shearing, cross-sectional stretch, and the Poisson effect. Some readers may find our formulation to be similar to the efforts of Brand and Rubin [10] and Rubin [56, 57, 54, 55]. These researchers have developed a numerical theory of a directed continua. Our work, though inspired by the same theory, differs from that of Rubin's in several ways. For one, the geometry established for our strain measures and the postulated constitutive relations are different. Additionally, our formulation focuses more on the minimal mathematical structure associated with using only the centerline position vectors and directors rather than executing a rigorous discretization of the higher-order tensors that are inherent to the continuous one-dimensional and three-dimensional theories.

The objective for this work is to develop a discretization that is simple, computationally efficient, and physically accurate. It is our hope that, alongside mechanicians, the computer graphics community may find this work useful in their own simulations of slender continua. We also aim to make the theory amenable to the modeling of situations that may involve external actuators, constraints, and contact, as is standard in the modeling of soft robotics. In essence, our formulation is similar in form to the Discrete Element Method (DEM) in that a continuous rod is modeled as a system of particles with assigned inertias interacting with one another as they exchange kinetic and elastic potential energies (cf. [39, 72]).

We begin by introducing the method for discretizing a continuous rod consisting of real material into a system of abstract particles. We proceed by defining the limited mathematical structure used in the theory: a set of centerline position vectors and relative position vectors

in each cross-section. The desired strains are then devoloped using the geometry of the directors and centerline edge vectors. These strains are used in a strain energy function that is insensitive to superposed rigid body motions. Following the main postulates of the chapter, we derive the internal elastic forces acting on each particle. Finally, a validation of the discrete theory is performed by comparing the numerical solutions against analytical solutions of static deformations of general beams.

3.2 Necessary elements from the continuous theory

Relevant ideas from the continuous theory of the first chapter are reiterated here in order to reveal the underlying assumptions of the discrete theory. Recall that a "rod-like body" is a three-dimensional continuum which satisfies a criterion based on length scales. Figure 3.2 shows a rod-like body with physical length scales L and D. L is measured along the dominant length of the rod in its "longitudinal" direction. The length D is the largest physical dimension that may be found in a direction transverse to that along which L is measured. If the ratio $\frac{D}{L} << 1$, then the body is considered rod-like and is well-suited to being modeled accurately by a directed curve.

As described in the direct approach of Chapter 1, the centerline of the directed curve is imagined as being constituted of a new abstract material that is assigned material and inertial properties. Then, the centerline is intrinsically a material curve that is allowed to stretch, but it is not necessarily a material curve belonging to the rod-like body. The centerline does not need to coincide with the line of area centers nor the line of mass centers of the rod-like body, although the resulting equations tend to decouple and gain tractability if one of these choices is made. A typical analysis involves determining the motion or equilibrium configuration of a directed curve given boundary conditions and possibly initial conditions. The behavior of the real material is then ascertained with a knowledge of how it is distributed relative to the abstract directed curve in the reference configuration.

The main advantage of a rod theory is in its limited mathematical structure compared to that found in three-dimensional continuum mechanics. Relative to the fixed point O, the vector function $\mathbf{R}(\xi)$, $\xi \in [0, \ell_0]$, places abstract centerline material points in Euclidean three-space, thereby tracing out a smooth space curve, $\mathcal{C}$. The two reference director fields are delivered by the function $\mathbf{D}_\alpha(\xi)$, $\alpha \in \{1, 2\}$, which trace out smooth space curves $\mathcal{D}_\alpha$ that are placed relative to $\mathcal{C}$. These two curves are termed "directorlines." The directorlines themselves are also thought of as being comprised of a new abstract elastic material that is permitted only to stretch and compress.

As in prior chapters, the following equality is assumed to hold for material points in the reference configuration:

$$\mathbf{R}^*(X^\alpha, \xi) = \mathbf{R}(\xi) + X^\alpha \mathbf{D}_\alpha(\xi), \tag{3.2.1}$$

The assumed equality in Expression (3.2.1) implies a few restrictions on the chosen coordinates $\{\xi, X^1, X^2\}$. Since $\mathbf{R}^*$ is linear in X^α, the cross-section coordinates in their most

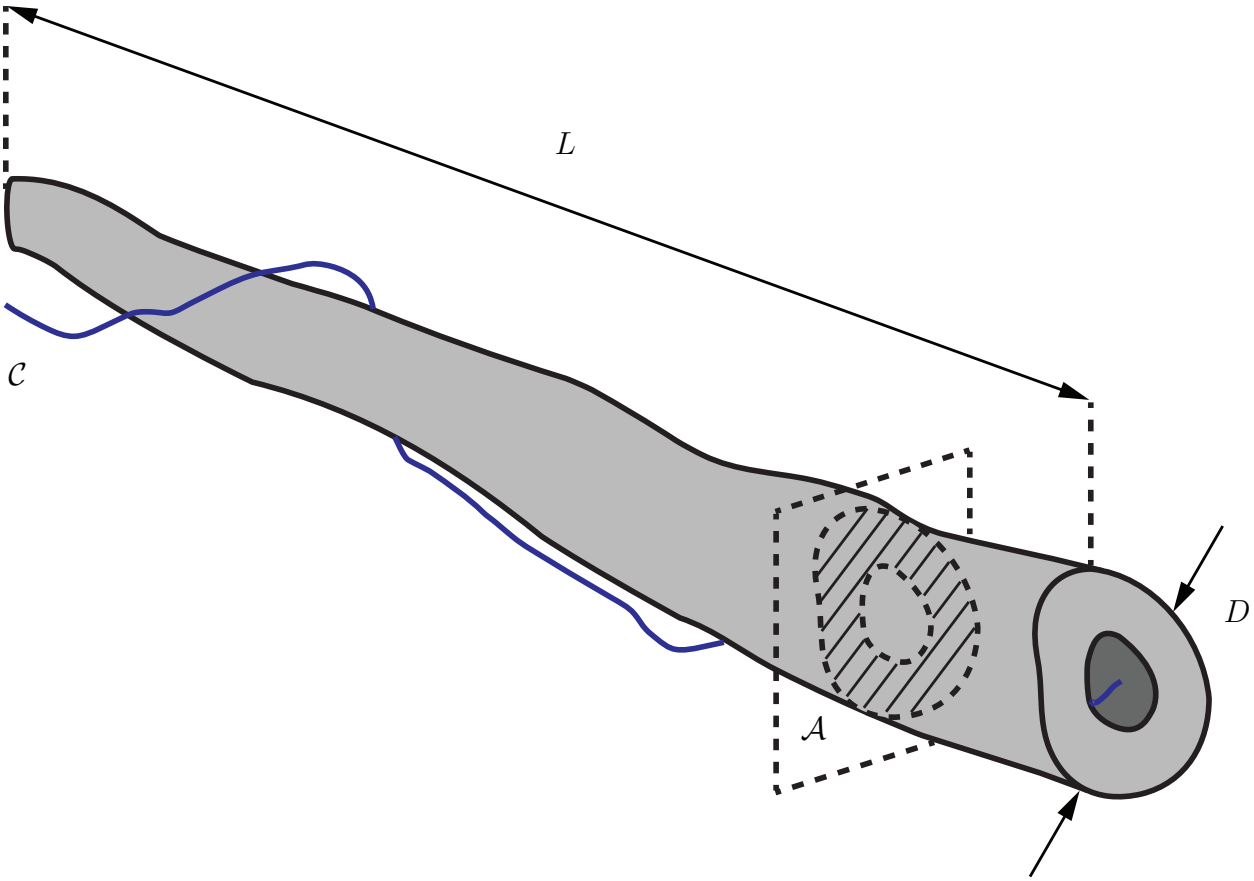

Figure 3.2: *A rod-like body in its natural state is one which satisfies $L >> D$. A sufficiently close centerline is shown along with a possible cross-section of the rod-like body which is shown as the hashed area.*

general form are oblique Cartesian coordinates (Figure 3.3). Additionally, the cross-sections must be planar since $\text{Span}(\mathbf{D}_\alpha) = \mathbb{E}^2$, where $\mathbb{E}^2$ is a two-dimensional plane of vectors.

The cross-section coordinates X^α may have arbitrary (but smoothly varying) numerical values. In the scenario that we choose to change the values of X^α, the vectors $\mathbf{D}_\alpha$ scale accordingly so that $X^\alpha \mathbf{D}_\alpha$ remains an invariant position vector. It cannot be immediately deduced which of these quantities is responsible for carrying the required physical dimension of length. In contrast to previous chapters, it is convenient to choose a dimensionless X^α so that the point $(X^1, X^2) = (1, 1)$ is close to the boundary of the rod-like body, as portrayed by the method shown in Figure 3.3. With this choice, the vectors $\mathbf{D}_\alpha$ have a physical dimension of length. We characterize the width W and height H of a cross-section $\mathcal{A}$ in its reference configuration using the directions of $\mathbf{D}_\alpha$. These physical dimensions are obtained by orthogonally projecting the cross-section onto lines spanned by $\mathbf{D}_\alpha$, and measuring the length of the projected cross-section image (see Figure 3.3).

As in prior chapters, a first-order Taylor expansion of the current position to a material point yields the approximation for placement material points into the current configuration:

$$\mathbf{r}^*(X^\alpha, \xi) \approx \mathbf{r}(\xi) + X^\alpha \mathbf{d}_\alpha(\xi). \tag{3.2.2}$$

Approximation (3.2.2) is acceptable only if $\|\mathbf{d}_\alpha\|$ are small compared to the overall length L, so that higher-order terms in the Taylor expansion may be neglected. Thus, the centerline is not a completely arbitrary smooth space curve. It must be at least sufficiently near to the material of the rod-like body in its reference configuration for the first-order Taylor expansion to be valid. As previously discussed, if the cross-sections remain plane throughout the motion, and deformations in the cross-section plane are homogeneous, then (3.2.2) is exact.

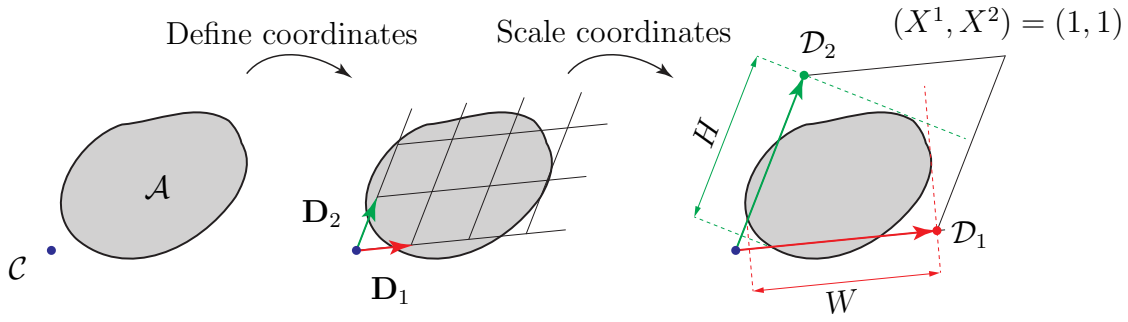

Figure 3.3: *Once an arbitrary but sufficiently close centerline has been chosen, a ξ-coordinate surface intersected with the rod-like body defines a cross-section. The cross-section coordinates may be chosen as oblique Cartesian and are scaled such that the reference directors point to the lateral surface of the rod-like body.*

The arbitrary nature of the centerline and cross-sections may present difficulties in interpreting quantities such as intrinsic curvature, intrinsic shear, and other "intrinsic" strains. We observe that these quantities may be mathematically induced: they depend on the choice of coordinates, of which there are limitless possibilities. Note that we have ruled out a priori the possibility of an intrinsic centerline stretch by assigning ξ to be an arc length coordinate. By ensuring that we always subtract away the "intrinsic" quantities in our strain measures, the strain energy function is guaranteed to be sensitive to the relative displacements of material points towards, away, or along one another. Take, for example, the function that delivers the strain energy per unit reference arc length $\rho_0\psi$ associated with Euler's inextensible elastica:

$$\rho_0\psi = \frac{EI}{2}(\kappa - \kappa_0)^2, \tag{3.2.3}$$

where ρ_0 is a linear mass density per unit reference arc length, ψ is the specific strain energy per unit mass, EI is the bending stiffness, κ is the current curvature of the centerline, and κ_0 is the so-called intrinsic curvature of the centerline in the reference configuration. The strain

that is used in the strain energy function must be a relative *difference* between real changes in curvature of the centerline due to motion of material points and the mathematically induced quantities due to a choice of coordinates. While κ_0 may be mathematically induced, $\kappa - \kappa_0$ is a physical quantity that increments in the circumstance of nonzero displacement gradients.

The strain energy postulate (3.2.3) is a minimum when the rod is in its reference state, which exposes yet another underlying assumption. The reference state of the three-dimensional continuum must coincide with one of the rod-like body's natural states, while the reference state of the directed curve is arbitrary up to the foregoing restrictions. A natural state of the continuum is a static configuration that it assumes when it is subject to a traction-free boundary. In the discrete theory, we will assume the reference configuration is coincident with one of the rod-like body's natural states.

We will assume for the rest of this chapter that the motion of the rod-like body is planar. Let $\mathbf{E}_2$ point in a direction opposite to that in which gravity acts. Suppose a set of planes with unit normal $\mathbf{E}_1$ intersect the three-dimensional body in its reference configuration. The material points in the intersection are assumed to remain confined to their respective plane for all time, i.e., the body undergoes parallel-plane motion and displacements out of the plane are unable to be modeled. Any equilibrium of the directed curve will leave the body in a state of plane strain. We choose to identify the material planes oriented by unit normal $\mathbf{E}_1$ as X^1 coordinate surfaces. The coordinate X^2 is chosen to have coordinate curves that run vertically in each cross-section with values positively varying along $\mathbf{E}_2$. The X^1 coordinate surface containing the centerline is the surface of interest for the model. We assume the motion of all adjacent X^1 coordinate surfaces to be identical to that which contains the centerline. The director $\mathbf{d}_2$ lies in the centerline plane of motion for all time. With these choices for the curvilinear coordinates, $\mathbf{d}_1$ becomes a fixed vector normal to the plane of motion, i.e., $\mathbf{d}_1 = W\mathbf{E}_1$ for all time. In what follows, we drop the postscripts on X^2 and $\mathbf{d}_2$ as we will be concerned with the through-the-thickness behavior only in this direction and the related motion of $\mathbf{d}_2$.

3.3 The geometry of motion

Kinematic quantities for the discrete directed curve

We begin by dividing the centerline of the continuous directed curve into $N-1$ equally sized parts. The boundary of each part defines two centerline vertices, so that there are N centerline vertices in all. By connecting the centerline vertices with straight lines hereafter referred to as "edges," we obtain the discrete reference centerline. We denote the total length of the discrete reference centerline by $\mathcal{L}$. The cross-sections are taken to be the intersection of the ${}_K\xi$ coordinate surfaces with the material of the rod-like body, where

$$ {}_K\xi = \frac{K\ell_0}{N-1}, \qquad (K = 0, \ldots, N-1). \tag{3.3.1}$$

Within each cross-section lies a director in the centerline's plane of motion that points to the boundary of the rod-like body. We let the tips of these vectors locate the director vertices. By connecting the director vertices with straight lines in the reference configuration, we obtain the discrete reference directorline, an approximation of the material boundary. Figure 3.1(a) shows a discrete directed curve in its reference configuration. We obtain an approximate image of the rod-like body with knowledge of how its continuous distribution of material relates geometrically to the centerline and the directorline in the reference configuration. While the directorline has already been chosen as a material line approximately on the boundary of the rod-like body in this theory, we are still at liberty to choose a centerline and directorline that are convenient for the particular problem being modeled.

We let ${}_K\mathbf{X}$ indicate the reference position vector of the Kth centerline vertex relative to some fixed point O while ${}_K\mathbf{D}$ indicates the reference position vector of the Kth director vertex relative to the Kth centerline vertex. Quantities assigned to vertices are ornamented with a lower prescript while quantities that belong to an edge are ornamented with an upper prescript. To facilitate an implementation of this theory in a programming language such as C++, indices are ordered from 0 up to $N-1$. The 0th and $(N-1)$th centerline vertices are referred to as the boundary centerline vertices, while the $K = 1, \ldots, N-2$ vertices are called interior centerline vertices. Note that, in view of the rod-like body we are trying to model, all director vertices may be considered boundary vertices for our choice of directorline.

As the rod undergoes a motion, the Kth centerline vertex is located in $\mathbb{E}^3$ by the vector ${}_K\mathbf{x}$ at the current time, t. Likewise, the Kth directorline vertex is positioned relative to ${}_K\mathbf{x}$ by the vector ${}_K\mathbf{d}$ in the current configuration. The centerline displacement is therefore given by

$$ {}_K\mathbf{u} = {}_K\mathbf{x} - {}_K\mathbf{X}, \qquad (K = 0, \ldots, N-1), \tag{3.3.2} $$

while the relative directorline displacement is

$$ {}_K\boldsymbol{\delta} = {}_K\mathbf{d} - {}_K\mathbf{D}, \qquad (K = 0, \ldots, N-1). \tag{3.3.3} $$

Using the centerline position vectors, we can construct the centerline edge vectors in the reference and current configurations:

$$ {}^K\mathbf{E} = {}_{K+1}\mathbf{X} - {}_K\mathbf{X}, \qquad {}^K\mathbf{e} = {}_{K+1}\mathbf{x} - {}_K\mathbf{x}, \qquad (K = 0, \ldots, N-2). \tag{3.3.4} $$

Discrete reference and current edge unit tangent vectors may then be defined through a scaling:

$$ {}^K\mathbf{T} = \frac{{}^K\mathbf{E}}{\left\|{}^K\mathbf{E}\right\|}, \qquad {}^K\mathbf{t} = \frac{{}^K\mathbf{e}}{\left\|{}^K\mathbf{e}\right\|}, \qquad (K = 0, \ldots, N-2). \tag{3.3.5} $$

We can similarly define reference and current unit vectors in the Kth cross-section:

$$ {}_K\hat{\mathbf{D}} = \frac{{}_K\mathbf{D}}{\left\|{}_K\mathbf{D}\right\|}, \qquad {}_K\hat{\mathbf{d}} = \frac{{}_K\mathbf{d}}{\left\|{}_K\mathbf{d}\right\|}, \qquad (K = 0, \ldots, N-1). \tag{3.3.6} $$

For the continuous directed curve, the tangent vector at a point on the centerline is obtained using an arc length derivative in which the change in position vector can be probed directly

behind and ahead of the point of interest. The discrete edge tangent vectors of (3.3.5) reflect a one-sided approximation to the centerline vertex tangent. A more accurate centerline vertex tangent can be developed which uses information from the vertices directly behind and ahead of the vertex of interest and is only defined at the interior vertices:

$$ {}_K\mathbf{T} = \frac{{}^{K+1}\mathbf{X} - {}^{K-1}\mathbf{X}}{\left\|{}^{K-1}\mathbf{E} + {}^{K}\mathbf{E}\right\|}, \qquad {}_K\mathbf{t} = \frac{{}^{K+1}\mathbf{x} - {}^{K-1}\mathbf{x}}{\left\|{}^{K-1}\mathbf{e} + {}^{K}\mathbf{e}\right\|}, \qquad (K = 1, \ldots, N-2). \tag{3.3.7} $$

At the two boundary centerline vertices, we may set the vertex tangent equal to the edge tangent, which reflects the use of one-sided limits:

$$ {}_0\mathbf{T} = {}^{0}\mathbf{T}, \qquad {}_0\mathbf{t} = {}^{0}\mathbf{t}, \tag{3.3.8} $$

and

$$ {}_{N-1}\mathbf{T} = {}^{N-2}\mathbf{T}, \qquad {}_{N-1}\mathbf{t} = {}^{N-2}\mathbf{t}. \tag{3.3.9} $$

To integrate quantities distributed along the rod such as the strain energy density, we need to introduce a discrete integration measure in the reference configuration. Here, we choose to use the Voronoi length, which is the average of the reference edge lengths surrounding an interior centerline vertex:

$$ {}_KL = \frac{1}{2}\left(\left\|{}^{K-1}\mathbf{E}\right\| + \left\|{}^{K}\mathbf{E}\right\|\right), \qquad (K = 1, \ldots, N-2). \tag{3.3.10} $$

At the boundary nodes, we define the reference Voronoi lengths as

$$ {}_0L = \frac{1}{2}\left\|{}^{0}\mathbf{E}\right\|, \qquad \text{and} \qquad {}_{N-1}L = \frac{1}{2}\left\|{}^{N-2}\mathbf{E}\right\|. \tag{3.3.11} $$

It is helpful to notice that

$$ \sum_{K=0}^{N-2}\left\|{}^{K}\mathbf{E}\right\| = \mathcal{L} = \sum_{K=0}^{N-1} {}_KL. \tag{3.3.12} $$

Similar discrete integration measures exist at each node (vertex) in the current configuration:

$$ {}_K\ell = \frac{1}{2}\left(\left\|{}^{K-1}\mathbf{e}\right\| + \left\|{}^{K}\mathbf{e}\right\|\right), \qquad (K = 1, \ldots, N-2), \tag{3.3.13} $$

with

$$ {}_0\ell = \frac{1}{2}\left\|{}^{0}\mathbf{e}\right\|, \qquad \text{and} \qquad {}_{N-1}\ell = \frac{1}{2}\left\|{}^{N-2}\mathbf{e}\right\|. \tag{3.3.14} $$

With the aim of quantifying a discrete curvature, a reference and current turning angle at each interior centerline vertex is defined using the edge tangents:

$$ |{}_K\Phi| = \arccos\left({}^{K-1}\mathbf{T} \cdot {}^{K}\mathbf{T}\right), \qquad |{}_K\varphi| = \arccos\left({}^{K-1}\mathbf{t} \cdot {}^{K}\mathbf{t}\right), \qquad (K = 1, \ldots, N-2). \tag{3.3.15} $$

We may employ the following approximations to the turning angle at the boundary vertices:

$$|_0\Phi| = \arccos({}_0\mathbf{T} \cdot {}_1\mathbf{T}), \qquad |_0\varphi| = \arccos({}_0\mathbf{t} \cdot {}_1\mathbf{t}), \tag{3.3.16}$$

and

$$|_{N-1}\Phi| = \arccos\big({}_{N-2}\mathbf{T} \cdot {}_{N-1}\mathbf{T}\big), \qquad |_{N-1}\varphi| = \arccos\big({}_{N-2}\mathbf{t} \cdot {}_{N-1}\mathbf{t}\big). \tag{3.3.17}$$

Whether the rod is curving upwards or downwards is indeterminate with definitions (3.3.15)-(3.3.17). To compute this, we assign to the turning angle the sign of the following scalar triple product:

$$\frac{{}_K\varphi}{|{}_K\varphi|} = \operatorname{sgn}\big(-\mathbf{E}_1 \cdot \big({}^{K-1}\mathbf{t} \times {}^K\mathbf{t}\big)\big), \tag{3.3.18}$$

where $\mathbf{E}_1$ is the unit vector normal to the plane of motion. A positive value of ${}_K\varphi$ then corresponds to an upward curving rod, where we remind the reader that $\mathbf{E}_2$ was defined to point "up." An analogous procedure may be carried out in the reference configuration.

Stretches and strains

We now use the preceding geometrical developments to construct strain measures which are natural to the discrete theory. It is imperative that the measures to be introduced are insensitive to rigid motions that are superposed on the rod. We will aim to satisfy this physical requirement by construction, which will simultaneously satisfy the principles known as "observer invariance" and "material frame indifference." We first introduce the stretch (or "stretch ratio") ${}^K\mu$ associated with the Kth centerline edge as

$${}^K\mu = \frac{\big\|{}^K\mathbf{e}\big\|}{\big\|{}^K\mathbf{E}\big\|}, \qquad (K = 0, \ldots, N-2). \tag{3.3.19}$$

The stretch ${}_K\mu$ associated with the Kth centerline vertex is calculated using a ratio of the Voronoi lengths:

$${}_K\mu = \frac{{}_K\ell}{{}_KL}, \qquad (K = 0, \ldots, N-1). \tag{3.3.20}$$

Vertex and edge centerline stretching strains may be identified as ${}_K\mu - 1$ and ${}^K\mu - 1$, respectively, which are discrete versions of engineering normal strain along the centerline. One may also define a discrete version of the Green-Lagrange strain along the centerline as $\frac{1}{2}({}_K\mu^2 - 1)$, if so desired. We choose not to confer symbols to these quantities and will later prefer to postulate our strain energy directly in terms of stretches. The stretch associated with the Kth cross-section is

$${}_K\lambda = \frac{\|{}_K\mathbf{d}\|}{\|{}_K\mathbf{D}\|}, \qquad (K = 0, \ldots, N-1), \tag{3.3.21}$$

where ${}_K\lambda - 1$ is an engineering normal strain in the cross-section. Note that we have no freedom to define a mathematical intrinsic stretch along the centerline or in the cross-section

as we have assigned physical meaning to ξ and $\|{}_K\mathbf{D}\|$, thereby constraining their numerical values. We also make a note that the cross-section stretch defined in (3.3.21) is distinctly different from the "normal cross-sectional stretch" defined by Rubin and Naghdi in [43, 53]. We prefer to conceive of the stretch ${}_K\lambda$ as being associated with the material of a single cross-section that we follow rather than for the instantaneous collection of material points along the principal normal of the centerline, which vary in the presence of nonzero tangential shear deformation.

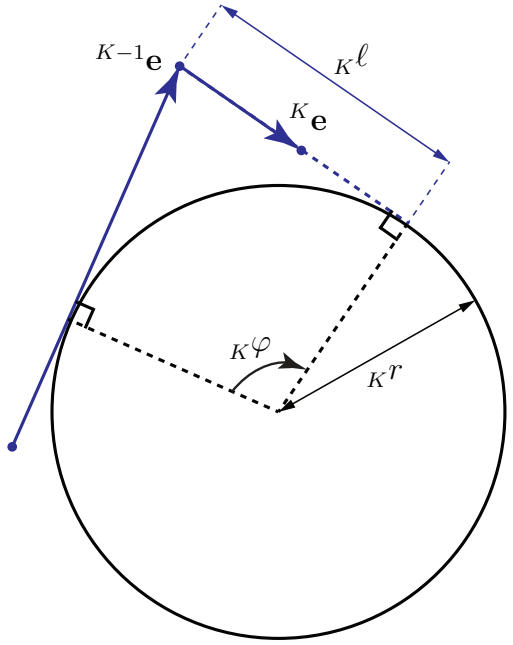

Figure 3.4: *The use of the Voronoi length in defining the discrete osculating circle. The turning angle ${}_K\varphi$ in this graphic is negative. This construction is adapted from Bobenko [8].*

Following Bergou et al.'s formulation of DER [4, 6, 5], we use a concept from discrete differential geometry [8] to define a discrete centerline curvature. Using the Voronoi length and the turning angle, we define a discrete osculating circle at every centerline vertex (Figure 3.4). The center of this circle is at the intersection of two lines perpendicular to each edge at one Voronoi length away from the centerline vertex. Trigonometry is used to show that the reference and current radii of curvature are

$$ {}_KR = \frac{{}_KL}{2}\cot\left(\frac{{}_K\Phi}{2}\right), \quad {}_Kr = \frac{{}_K\ell}{2}\cot\left(\frac{{}_K\varphi}{2}\right), \qquad (K = 0, \ldots, N-1). \tag{3.3.22} $$

The curvature at any centerline vertex is then defined as:

$$ {}_KK = \frac{2}{{}_KL}\tan\left(\frac{{}_K\Phi}{2}\right), \quad {}_K\kappa = \frac{2}{{}_K\ell}\tan\left(\frac{{}_K\varphi}{2}\right), \qquad (K = 0, \ldots, N-1). \tag{3.3.23} $$

Observe that both curvatures are signed. Curvatures of this type are also a central kinematic quantity in Bergou et al.'s [4, 6, 5] theory of a discrete elastic rod.

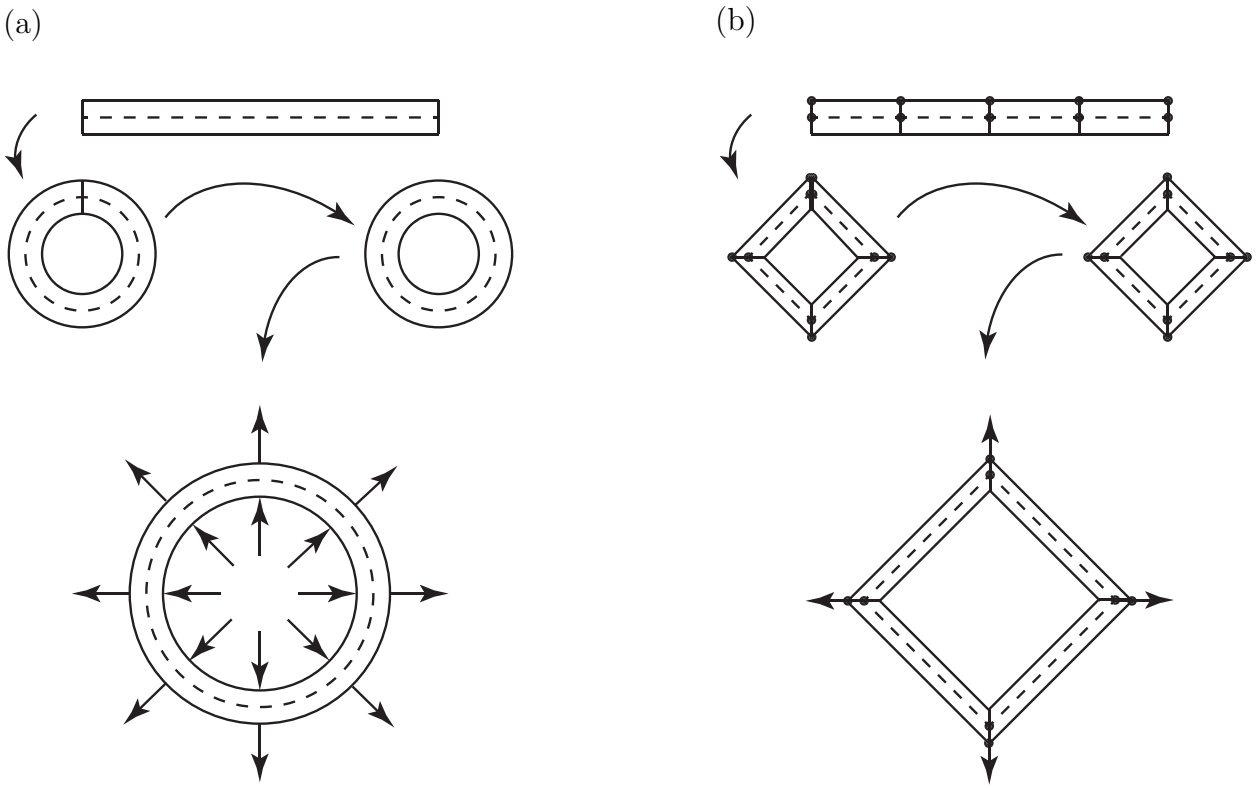

Figure 3.5: *(a) Pure bending followed by uniform stretch for a continuous rod. (b) Bending followed by uniform stretch in the discrete model.*

The definition of a curvature to measure bending is non-trivial when the rod is extensible. To elaborate, we refer the reader to Figure 3.5(a) and recall a scenario discussed by Antman [2, Chapter 4] to illustrate his definition of curvature. In Figure 3.5(a), we see a continuous rod which is bent into a circle and then inflated uniformly by an applied pressure. In Figure 3.5(b), we repeat an analogous experiment with the discrete rod. Once the rod is inflated, the curvature ${}_K\kappa$ in the current configuration decreases since the Voronoi lengths at each vertex increase as a result of the stretching of the rod. On the other hand, a reference-based curvature given by ${}_K\mu\,{}_K\kappa$ is unaffected by the inflation. It can be shown that, so long as the thickness of the rod is much smaller in comparison to the radius of curvature of bending, that the bending moment should be unaffected by the inflation. Therefore, we opt to use ${}_K\mu\,{}_K\kappa$ as the bending strain measure. This choice is in accordance with that used by the authors in [44] who studied an extensible elastica.[1]

[1]That is, the bending moment was given by the constititutive relation $EI\frac{\partial\theta}{\partial\xi}$ where ξ is the arc length

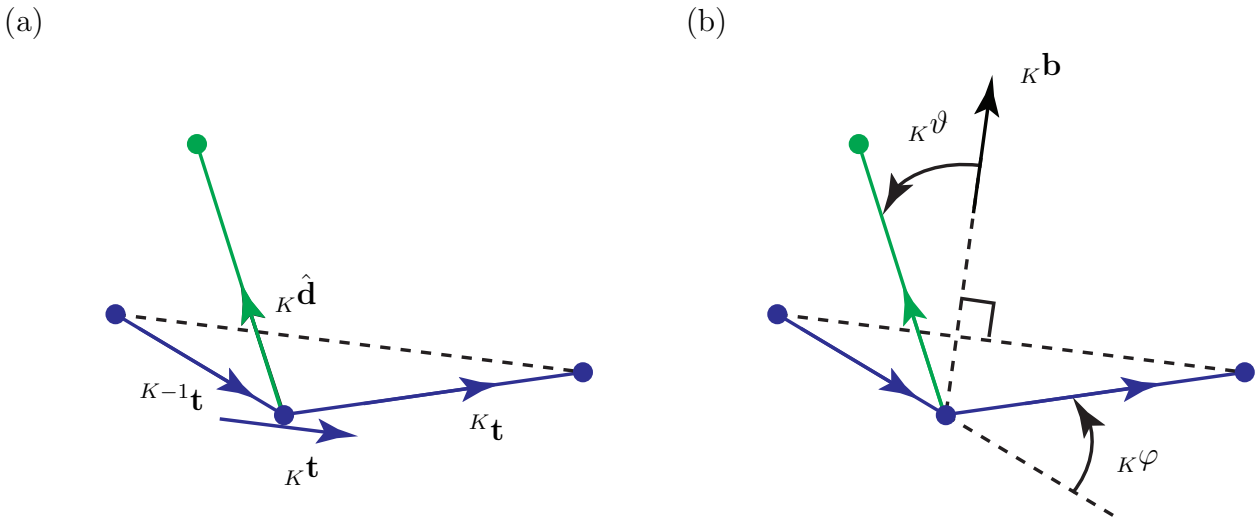

Figure 3.6: *(a) The edge tangents,* ${}^{K-1}\mathbf{t}$ *and* ${}^{K}\mathbf{t}$*, vertex tangent,* ${}_K\mathbf{t}$*, and director unit vector,* ${}_K\hat{\mathbf{d}}$*. (b) The shear and turning angles,* ${}_K\vartheta$ *and* ${}_K\varphi$*, and a discrete Bishop frame vector* ${}_K\mathbf{b}$*.*

The shear strain is the change in angle from the reference to the current configuration between two infinitesimal material line elements of the centerline and the cross-section. Referring to Figure 3.6, we define the discrete shearing angles as follows:

$$|{}_K\Theta| = \arccos\Big({}_K\hat{\mathbf{D}} \cdot {}_K\mathbf{B}\Big), \quad |{}_K\vartheta| = \arccos\Big({}_K\hat{\mathbf{d}} \cdot {}_K\mathbf{b}\Big), \quad (K = 0, \ldots, N-1), \tag{3.3.24}$$

where ${}_K\vartheta$ is for the current configuration and ${}_K\Theta$, the "intrinsic shear angle," is mathematically induced and pertains to the reference configuration. In the definitions of the shear angles, we have made use of the discrete reference and current Bishop frame vectors, ${}_K\mathbf{B}$ and ${}_K\mathbf{b}$, which are defined as

$${}_K\mathbf{B} = {}_K\mathbf{T} \times \mathbf{E}_1, \quad \text{and} \quad {}_K\mathbf{b} = {}_K\mathbf{t} \times \mathbf{E}_1, \quad (K = 0, \ldots, N-1). \tag{3.3.25}$$

We note that the Bishop vector is well-defined *where* the centerline has a point of inflection and does not suffer a discontinuity *when* the centerline has a change in the sense of curvature, in contrast to the Serret-Frenet triad (cf. [7, 28]). The sign of the current shearing angle is given by

$$\frac{{}_K\vartheta}{|{}_K\vartheta|} = \operatorname{sgn}\Big(-\mathbf{E}_1 \cdot \Big({}_K\mathbf{b} \times {}_K\hat{\mathbf{d}}\Big)\Big), \tag{3.3.26}$$

so that a negative shearing angle corresponds to an acute angle between ${}_K\hat{\mathbf{d}}$ and ${}_K\mathbf{t}$. An analogous interpretation holds for the reference shearing angle.

parameter of the extensible rod in a reference configuration and θ is the angle subtended by the tangent vector to the rod's centerline with a fixed direction. The curvature of the rod in the present configuration is $\kappa = \frac{\partial\theta}{\partial s} = \mu^{-1}\frac{\partial\theta}{\partial\xi}$ where $\mu = \frac{\partial s}{\partial\xi}$ is the stretch of the rod.

The shear strain is the difference ${}_K\vartheta - {}_K\Theta$, a quantity that increments during shear deformation regardless of the angle of ${}_K\mathbf{D}$, which we are still free to choose. However, the classic definition of shear strain involves two material line elements that are perpendicular to one another in the reference configuration. Because of the apparent lack of utility in having the freedom to identify an intrinsic shear angle, we insist hereafter that ${}_K\mathbf{D}$ be chosen such that ${}_K\hat{\mathbf{D}} = {}_K\mathbf{B}$. Now the cross-sections are orthogonal to the centerline in the reference configuration, and we can exploit the attractive nonlinear properties of the function $\tan({}_K\vartheta)$ as a shear strain measure in our constitutive function.

Inertias, momenta, and the kinetic energy

A set of (coordinate-dependent) inertias may be derived by inspecting the kinetic energy per reference length associated with the Kth cross-section:

$$\begin{aligned} 2\,{}_KT &= \int_{{}_K\mathcal{A}} \left({}_K\dot{\mathbf{x}} + X\,{}_K\dot{\mathbf{d}}\right) \cdot \left({}_K\dot{\mathbf{x}} + X\,{}_K\dot{\mathbf{d}}\right) \rho_0^* dA \\ &= {}_K\dot{\mathbf{x}} \cdot \left({}_K\dot{\mathbf{x}} \int_{{}_K\mathcal{A}} \rho_0^* dA + {}_K\dot{\mathbf{d}} \int_{{}_K\mathcal{A}} X \rho_0^* dA \right) \\ &\quad + {}_K\dot{\mathbf{d}} \cdot \left({}_K\dot{\mathbf{x}} \int_{{}_K\mathcal{A}} X \rho_0^* dA + {}_K\dot{\mathbf{d}} \int_{{}_K\mathcal{A}} XX \rho_0^* dA \right). \end{aligned} \tag{3.3.27}$$

The inertias are identified as

$$\begin{aligned} {}_K\rho_0 &= \int_{{}_K\mathcal{A}} \rho_0^* dA, \\ {}_K\rho_0\,{}_KY^{02} &= \int_{{}_K\mathcal{A}} X \rho_0^* dA, \\ {}_K\rho_0\,{}_KY^{22} &= \int_{{}_K\mathcal{A}} XX \rho_0^* dA. \end{aligned} \tag{3.3.28}$$

Here, ρ_0^* is the density of the rod-like body in its reference configuration, while dA is an infinitesimal area measure for the cross-section ${}_K\mathcal{A}$. The quantities ${}_KY^{02}$ and ${}_KY^{22}$ are called the first inertia and the second inertia, respectively. They have no physical dimension since we assigned the length dimension to the vector ${}_K\mathbf{d}$. The reader is invited to compare the discrete inertias introduced in (3.3.28) with their continuous counterparts in (1.2.30), (1.2.31), and (1.2.32). In many works, it is common to make a choice of coordinates which defines the centerline as the curve for which ${}_KY^{02} = 0$ identically so that the centerline motion is decoupled from directorline motion. We refrain from making this restriction here with the goal of accommodating contact problems, where it is desired to choose the centerline as a material line of contact. With our newly defined inertias, we may express the kinetic energy of the Kth cross-section as

$$2\,{}_KT = {}_K\dot{\mathbf{x}} \cdot {}_K\mathbf{G} + {}_K\dot{\mathbf{d}} \cdot {}_K\mathbf{L}, \tag{3.3.29}$$

where

$$ {}_K\mathbf{G} = {}_K\rho_0\, {}_K\dot{\mathbf{x}} + {}_K\rho_0\, {}_KY^{02}\, {}_K\dot{\mathbf{d}}, \tag{3.3.30} $$

and

$$ {}_K\mathbf{L} = {}_K\rho_0\, {}_KY^{02}\, {}_K\dot{\mathbf{x}} + {}_K\rho_0\, {}_KY^{22}\, {}_K\dot{\mathbf{d}}, \tag{3.3.31} $$

are the linear momentum and director momentum of cross-section K, respectively. Note that ${}_K\mathbf{G}$ is the linear momentum of the cross-section and therefore a physical invariant, while ${}_K\mathbf{L}$ is a momentum that depends on the choice of coordinates. The angular momentum of a cross-section of the rod is given by

$$ {}_K\mathbf{H}_O = {}_K\mathbf{x} \times {}_K\mathbf{G} + {}_K\mathbf{d} \times {}_K\mathbf{L}, \tag{3.3.32} $$

an invariant quantity. The total angular momentum $\mathbf{H}_O$ relative to a fixed point O and the kinetic energy T of the rod are assumed to be given by the approximations

$$ \mathbf{H}_O = \sum_{K=0}^{N-1} {}_K\mathbf{H}_O\, {}_KL, \quad \text{and} \quad T = \sum_{K=0}^{N-1} {}_KT\, {}_KL. \tag{3.3.33} $$

The balance laws

We recall that the rod was divided into parts that contained the edge vectors according to (3.3.1). The averaged balance laws that will be postulated are for parts that are instead centered on the discrete cross-sections. If $\mathbf{G}$ stands for the linear momentum per unit reference length of the continuous directed curve, then we approximate the time rate of change of linear momentum of a cross-section centered part as

$$ \frac{d}{dt} \int_{{}_K\xi - \ell_0/2/(N-1)}^{{}_K\xi + \ell_0/2/(N-1)} \mathbf{G} d\xi \approx {}_K\dot{\mathbf{G}}\, {}_KL, \quad (K = 0, \ldots, N-1). \tag{3.3.34} $$

In a similar vein, if $\mathbf{L}$ indicates the director momentum per unit reference length of the continuous directed curve, then the time rate of change of director momentum of a cross-section centered part is approximated as

$$ \frac{d}{dt} \int_{{}_K\xi - \ell_0/2/(N-1)}^{{}_K\xi + \ell_0/2/(N-1)} \mathbf{L} d\xi \approx {}_K\dot{\mathbf{L}}\, {}_KL, \quad (K = 0, \ldots, N-1). \tag{3.3.35} $$

We now postulate partwise balances of mass, inertia, linear momentum, director momentum, and energy for the discrete directed curve:

$$\begin{gathered}
{}_K\dot{\rho}_0\,{}_KL = 0,\\
\dot{\overline{{}_K\rho_0\,{}_KY^{02}}}\,{}_KL = 0,\\
\dot{\overline{{}_K\rho_0\,{}_KY^{22}}}\,{}_KL = 0,\\
{}_K\dot{\mathbf{G}}\,{}_KL = {}_K\mathbf{F},\\
{}_K\dot{\mathbf{L}}\,{}_KL = {}_K\mathbf{P},\\
\left({}_K\dot{T} + {}_K\dot{\Pi}_{\mathrm{e}}\right){}_KL = {}_K\mathbf{F}_{\mathrm{ext}}\cdot{}_K\dot{\mathbf{x}} + {}_K\mathbf{P}_{\mathrm{ext}}\cdot{}_K\dot{\mathbf{d}},\\
(K = 0,\dots,N-1).
\end{gathered} \tag{3.3.36}$$

Here, ${}_K\Pi_{\mathrm{e}}\,{}_KL$ is the strain energy content of the Kth part while the meaning of the forces ${}_K\mathbf{F}$, ${}_K\mathbf{P}$, ${}_K\mathbf{F}_{\mathrm{ext}}$, and ${}_K\mathbf{P}_{\mathrm{ext}}$ will soon be expounded. These balance laws can be considered as the discrete counterparts to the balance laws for the directed rod theory that was developed by Green and Naghdi [25, 26, 42]. Equation $(3.3.36)_1$ is used to solve the mass density per unit current length at the Kth centerline vertex, ${}_K\rho$, as

$${}_K\rho_0\,{}_KL = \text{constant} = {}_K\rho\,{}_K\ell, \quad (K = 0,\dots,N-1), \tag{3.3.37}$$

where ${}_K\ell$ is known once the set of vectors $\{{}_K\mathbf{x}\}$ is known. It follows from the conservation of mass that we also have the conservation of first and second inertias:

$${}_K\rho_0\,{}_KY^{02}\,{}_KL = \text{constant} \quad (K = 0,\dots,N-1), \tag{3.3.38}$$

and

$${}_K\rho_0\,{}_KY^{22}\,{}_KL = \text{constant} \quad (K = 0,\dots,N-1). \tag{3.3.39}$$

Note that the equations of motion $(3.3.36)_4$ and $(3.3.36)_5$ are coupled if ${}_KY^{02} \neq 0$. These two equations are to be simultaneously integrated to solve for the quantities ${}_K\mathbf{x}$ and ${}_K\mathbf{d}$.

We call ${}_K\mathbf{F}$ and ${}_K\mathbf{P}$ the discrete centerline vertex force and the discrete directorline vertex force, respectively. These quantities represent the net effects of external body forces that act in each part, externally applied lateral tractions that act on each part, internal forces that act in each part, and an exchange of internal forces due to contact with neighboring parts, which itself may be thought of as an external load acting on the boundary vertices of each part. We admit a decomposition of the forces as follows:

$${}_K\mathbf{F} = {}_K\mathbf{F}_{\mathrm{ext}} + {}_K\mathbf{F}_{\mathrm{int}}, \quad {}_K\mathbf{P} = {}_K\mathbf{P}_{\mathrm{ext}} + {}_K\mathbf{P}_{\mathrm{int}}. \tag{3.3.40}$$

Here, ${}_K\mathbf{F}_{\mathrm{ext}}$ and ${}_K\mathbf{P}_{\mathrm{ext}}$ are prescribed forces due to body forces and laterally applied tractions, while ${}_K\mathbf{F}_{\mathrm{int}}$ and ${}_K\mathbf{P}_{\mathrm{int}}$ are the constitutively determined internal forces (including contact forces) due to straining. It remains to develop expressions for ${}_K\mathbf{F}_{\mathrm{int}}$ and ${}_K\mathbf{P}_{\mathrm{int}}$ in terms of a strain energy function in the forthcoming section.

A bending moment ${}_K\mathbf{M}$ applied to the Kth cross-section of the rod can be represented as a couple of equal but opposite forces acting at the lateral ends of the cross-section. The moment is modeled as an applied director force according to the following relation:

$$ {}_K\mathbf{P}_{\text{ext}} = \frac{{}_K\mathbf{M}}{{}_K\lambda H} \times {}_K\hat{\mathbf{d}}. \tag{3.3.41} $$

Four coordinates determine the position, rotation, and stretch of the Kth cross-section. In other words, we use four degrees of freedom to capture the deformation of the discrete cross-sections in this model. These coordinates are listed in an array as follows:

$$ {}_K\mathsf{q} = \left[{}_K\mathbf{x}\cdot\mathbf{E}_3, {}_K\mathbf{x}\cdot\mathbf{E}_2, {}_K\mathbf{d}\cdot\mathbf{E}_3, {}_K\mathbf{d}\cdot\mathbf{E}_2\right]^T, \tag{3.3.42} $$

where $[\cdot]^T$ indicates the transpose of the array. A mass matrix associated with the Kth cross-section can be constructed:

$$ {}_K\mathsf{M} = {}_K\rho_0\,{}_KL \begin{bmatrix} 1 & 0 & {}_KY^{02} & 0 \\ 0 & 1 & 0 & {}_KY^{02} \\ {}_KY^{02} & 0 & {}_KY^{22} & 0 \\ 0 & {}_KY^{02} & 0 & {}_KY^{22} \end{bmatrix}. \tag{3.3.43} $$

Now the kinetic energy of the Kth cross-section may be expressed as the quadratic form

$$ 2\,{}_KT = {}_K\dot{\mathsf{q}}^T\,{}_K\mathsf{M}\,{}_K\dot{\mathsf{q}}. \tag{3.3.44} $$

Finally, we define a forcing vector for the Kth cross-section by

$$ {}_K\mathsf{F} = \left[{}_K\mathbf{F}\cdot\mathbf{E}_3, {}_K\mathbf{F}\cdot\mathbf{E}_2, {}_K\mathbf{P}\cdot\mathbf{E}_3, {}_K\mathbf{P}\cdot\mathbf{E}_2\right]^T. \tag{3.3.45} $$

Using the conservations of mass and inertia, the equations of motion $(3.3.36)_4$ and $(3.3.36)_5$ are expressed in their Cartesian component form:

$$ {}_K\mathsf{M}\,{}_K\ddot{\mathsf{q}} = {}_K\mathsf{F}, \quad (K = 0, \ldots, N-1). \tag{3.3.46} $$

It will be the case, however, that ${}_K\mathsf{F}$ is not only a function of ${}_K\dot{\mathsf{q}}$, ${}_K\mathsf{q}$, and t, but will also depend on the behavior of ${}_{K-1}\mathbf{x}$, ${}_{K-1}\mathbf{d}$, ${}_{K+1}\mathbf{x}$, ${}_{K+1}\mathbf{d}$ and possibly their time derivatives if dissipation is present in the form of damping. Working towards the goal of rendering the equations of motion amenable to a numerical integration, we assemble a global mass matrix:

$$ \mathsf{M} = \text{diag}\big({}_0\mathsf{M}, \cdots, {}_K\mathsf{M}, \cdots, {}_{N-1}\mathsf{M}\big), \tag{3.3.47} $$

where diag() takes the cross-section mass matrices and centers them along the diagonal of M. Thus, M, a $4N \times 4N$ array, will be a banded matrix. Similarly, we construct a global forcing vector:

$$ \mathsf{F} = \left[{}_0\mathsf{F}^T, \ldots, {}_K\mathsf{F}^T, \ldots, {}_{N-1}\mathsf{F}^T\right]^T. \tag{3.3.48} $$

A global array of coordinates is also constructed:

$$\mathsf{q} = \left[{}_0\mathsf{q}^T, \ldots, {}_K\mathsf{q}^T, \ldots, {}_{N-1}\mathsf{q}^T \right]^T. \tag{3.3.49}$$

The $4N$ equations of motion governing the behavior of the entire rod can now be presented as

$$\mathsf{M}\ddot{\mathsf{q}} = \mathsf{F}. \tag{3.3.50}$$

This canonical form is suitable for a numerical integration by a method of one's choosing. To close the system of equations, we must now turn our attention towards finding expressions for the internal forces in the rod due to straining by postulating an appropriate strain energy function.

3.4 The constitutive equations

Constitutive relations

To establish the relationship between the internal forces and the strain energy function, we begin by assuming that a function $\Pi_{\mathrm{e}} = \hat{\Pi}_{\mathrm{e}}({}_K\mathbf{x}, {}_K\mathbf{d})$ exists such that

$$\Pi_{\mathrm{e}} = \sum_{J=0}^{N-1} {}_J\Pi_{\mathrm{e}}\, {}_JL, \tag{3.4.1}$$

which was implicitly accepted in our adoption of the balance of energy $(3.3.36)_6$. Using a simultaneous application of the balance laws $(3.3.36)_{1-6}$, one can then show the following power balance:

$$\dot{\Pi}_{\mathrm{e}} = -\sum_{J=0}^{N-1} \left({}_J\mathbf{F}_{\mathrm{int}} \cdot {}_J\dot{\mathbf{x}} + {}_J\mathbf{P}_{\mathrm{int}} \cdot {}_J\dot{\mathbf{d}} \right), \tag{3.4.2}$$

where Π_{e} is the strain (elastic potential) energy content of the entire rod and the right hand-side of (3.4.2) reflects the total stress power of the internal forces. Given the assumed functional dependence of Π_{e} on all the position vectors, we calculate

$$\dot{\Pi}_{\mathrm{e}} = \sum_{J=0}^{N-1} \left(\frac{\partial \hat{\Pi}_{\mathrm{e}}}{\partial {}_J\mathbf{x}} \cdot {}_J\dot{\mathbf{x}} + \frac{\partial \hat{\Pi}_{\mathrm{e}}}{\partial {}_J\mathbf{d}} \cdot {}_J\dot{\mathbf{d}} \right), \tag{3.4.3}$$

from which it follows that

$$\sum_{J=0}^{N-1} \left[\left({}_J\mathbf{F}_{\mathrm{int}} + \frac{\partial \hat{\Pi}_{\mathrm{e}}}{\partial {}_J\mathbf{x}} \right) \cdot {}_J\dot{\mathbf{x}} + \left({}_J\mathbf{P}_{\mathrm{int}} + \frac{\partial \hat{\Pi}_{\mathrm{e}}}{\partial {}_J\mathbf{d}} \right) \cdot {}_J\dot{\mathbf{d}} \right] = 0, \tag{3.4.4}$$

which must hold for all possible motions. Assuming that ${}_K\mathbf{F}_{\text{int}}$ and ${}_K\mathbf{P}_{\text{int}}$ are independent of ${}_K\dot{\mathbf{x}}$ and ${}_K\dot{\mathbf{d}}$, we make a deduction from Equation (3.4.4) by constructing motions which have

$$ {}_K\dot{\mathbf{x}} = c^2\left({}_K\mathbf{F}_{\text{int}} + \frac{\partial\hat{\Pi}_{\text{e}}}{\partial_K\mathbf{x}}\right) \quad \text{with} \quad {}_J\dot{\mathbf{x}} = \mathbf{0},\ J \neq K, \quad \text{and with} \quad {}_J\dot{\mathbf{d}} = \mathbf{0}, \tag{3.4.5} $$

and then constructing another set of motions that have

$$ {}_J\dot{\mathbf{x}} = \mathbf{0} \quad \text{with} \quad {}_K\dot{\mathbf{d}} = d^2\left({}_K\mathbf{P}_{\text{int}} + \frac{\partial\hat{\Pi}_{\text{e}}}{\partial_K\mathbf{d}}\right) \quad \text{and with} \quad {}_J\dot{\mathbf{d}} = \mathbf{0},\ J \neq K, \tag{3.4.6} $$

where c and d are arbitrary nonzero scalars that have the appropriate physical dimension. The implications that follow lead to a necessary condition relating the internal forces to the strain energy:

$$ {}_K\mathbf{F}_{\text{int}} = -\frac{\partial\hat{\Pi}_{\text{e}}}{\partial_K\mathbf{x}} \quad \text{and} \quad {}_K\mathbf{P}_{\text{int}} = -\frac{\partial\hat{\Pi}_{\text{e}}}{\partial_K\mathbf{d}}, \quad (K = 0, \ldots, N-1). \tag{3.4.7} $$

These are the sought-after constitutive relations for the material. It may appear suspicious at this point to permit a strain energy that has a functional dependence on position vectors. When we postulate our strain energy we will adopt the principle that the strain energy is invariant under superposed rigid body motions of the discrete rod. This principle can be used to show that the strain energy can depend only on the *magnitudes of differences* of the position vectors rather than ${}_K\mathbf{x}$ alone.

Lumped geometric and material properties

Before we postulate a strain energy function, we introduce some lumped geometric and material properties that will be of use in the stiffness coefficients. If $A(\xi)$ is the area of each cross-section at ξ of the continuous directed curve, then the discrete area ${}_KA$ associated with the Kth cross-section is

$$ {}_KA = \frac{\int_{{}_K\xi-\ell_0/2/(N-1)}^{{}_K\xi+\ell_0/2/(N-1)} A\,d\xi}{{}_KL}, \quad (K = 1, \ldots, N-2). \tag{3.4.8} $$

We also introduce a discrete edge area ${}^KA$ as an average over the Kth edge:

$$ {}^KA = \frac{\int_{{}_K\xi}^{{}_{K+1}\xi} A\,d\xi}{\left\|{}^K\mathbf{E}\right\|}, \quad (K = 0, \ldots, N-2). \tag{3.4.9} $$

The discrete areas ${}_0A$ and ${}_{N-1}A$ at the boundary vertices are assigned as follows:

$$ {}_0A = \frac{{}^0A}{2}, \quad {}_{N-1}A = \frac{{}^{N-2}A}{2}. \tag{3.4.10} $$

Other geometric and material quantities from the continuous theory that need to be discretized are the second moment of area about the centerline in the reference configuration about the $\mathbf{E}_1$ axis, $I(\xi)$, Young's modulus, $E(\xi)$, the shear modulus, $G(\xi)$, and Poisson's ratio, $\nu(\xi)$. The procedure for discretization is exactly the same as for the obtaining the discrete areas, and we simply list the resulting discrete quantities in the table that follows.

Table 3.1: Lumped material and geometric properties used in the discrete theory.

	Vertex Quantities	Edge Quantities
Geometric Properties	${}_K A \quad {}_K I$	${}^K A \quad {}^K I$
Material Properties	${}_K E \quad {}_K G \quad {}_K \nu$	${}^K E \quad {}^K G \quad {}^K \nu$

The strain energy

In the one-dimensional theory of a directed curve, significant efforts have been made to derive a suitable one-dimensional strain energy function from a three-dimensional strain energy function [23, 24, 25, 47, 58]. Unfortunately, the underlying assumption of homogenous deformations implicit in approximation (3.2.2) does not realistically capture a majority of motions for the rod-like body. Take, for example, the flexure of a cuboid that occurs in the application of terminal end moments. The one-dimensional theory fails to capture through-the-thickness variations and interesting effects such as anticlastic curvature that is discussed in the works of [27, 65, 68]. Acknowledging that there will be some error inherent in *every* postulated strain energy that is intended to model *real* phenomena, we will proceed by guiding our development with the one-dimensional strain energy discussed in [47] which is based on the three-dimensional strain energy of linear elasticity for a homogenous isotropic medium [65].

The four strain measures in this theory are ${}^K\mu$, ${}_K\lambda$, ${}_K\varphi$, and ${}_K\vartheta$. These quantities are invariant under superposed rigid body motions. In the materially linear theory, a strain energy function that is quadratic in the strains is typically assumed. To allow the discrete directed curve to undergo large displacements, we adopt a material description that has nonlinear (non-quadratic) terms in order to preclude the possibility of the material passing through itself. To this end, we postulate the global strain energy for an isotropic, potentially

non-homogenous material of the form

$$
\begin{aligned}
2\Pi_{\mathrm{e}} &= 2\tilde{\Pi}_{\mathrm{e}}\big({}^{K}\mu, {}_{K}\mu, {}_{K}\lambda, {}_{K}\mu\, {}_{K}\kappa, {}_{K}\vartheta\big) \\
&= \sum_{K=0}^{N-2} {}^{K}k_1\big({}^{K}\mu^2 - {}^{K}\mu + {}^{K}\mu^{-1}\big)\big\|{}^{K}\mathbf{E}\big\| \\
&+ \sum_{K=0}^{N-1} {}_{K}k_2\big({}_{K}\lambda^2 - {}_{K}\lambda + {}_{K}\lambda^{-1}\big)\, {}_{K}L + \sum_{K=1}^{N-2} {}_{K}k_3({}_{K}\mu\, {}_{K}\kappa)^2\, {}_{K}L \\
&+ \sum_{K=0}^{N-1} {}_{K}k_4 \tan^2({}_{K}\vartheta)\, {}_{K}L + \sum_{K=0}^{N-2} {}^{K}k_5\left(\frac{{}_{K+1}\vartheta - {}_{K}\vartheta}{\big\|{}^{K}\mathbf{E}\big\|}\right)^2 \big\|{}^{K}\mathbf{E}\big\| \\
&+ \sum_{K=0}^{N-2} {}^{K}k_6\left(\frac{{}_{K+1}\lambda - {}_{K}\lambda}{\big\|{}^{K}\mathbf{E}\big\|}\right)^2 \big\|{}^{K}\mathbf{E}\big\| + 2\sum_{K=1}^{N-2} {}_{K}k_7({}_{K}\lambda - 1)({}_{K}\mu - 1)\, {}_{K}L. \qquad (3.4.11)
\end{aligned}
$$

The strain energy can be expressed as a function of the sets $\{{}_{K}\mathbf{x}\}$ and $\{{}_{K}\mathbf{d}\}$ through the use of Formulae $(3.3.4)_2$, $(3.3.6)_2$, $(3.3.7)_2$, (3.3.13), $(3.3.15)_2$, (3.3.19), (3.3.20), (3.3.21), $(3.3.23)_2$, $(3.3.24)_2$, and $(3.3.25)_2$ which relate the various strains to the position vectors:

$$
\begin{aligned}
&\hat{\Pi}_{\mathrm{e}}({}_{K}\mathbf{x}, {}_{K}\mathbf{d}) = \tilde{\Pi}_{\mathrm{e}}\big({}^{K}\mu, {}_{K}\mu, {}_{K}\lambda, {}_{K}\mu\, {}_{K}\kappa, {}_{K}\vartheta\big) = \\
&\tilde{\Pi}_{\mathrm{e}}\Big({}^{K}\hat{\mu}({}_{K}\mathbf{x}), {}_{K}\hat{\mu}({}_{K}\mathbf{x}), {}_{K}\hat{\lambda}({}_{K}\mathbf{d}), {}_{K}\hat{\mu}({}_{K}\mathbf{x})\, {}_{K}\hat{\kappa}({}_{K}\mathbf{x}), {}_{K}\hat{\vartheta}({}_{K}\mathbf{x}, {}_{K}\mathbf{d})\Big). \qquad (3.4.12)
\end{aligned}
$$

In order of appearance in Equation (3.4.11), this constitutive function accounts for:

$$
\begin{aligned}
\text{nonlinear centerline stretching :} &\quad \sum_{K=0}^{N-2} {}^{K}k_1\big({}^{K}\mu^2 - {}^{K}\mu + {}^{K}\mu^{-1}\big)\big\|{}^{K}\mathbf{E}\big\|, \\
\text{nonlinear cross-section stretching :} &\quad \frac{1}{2}\sum_{K=0}^{N-1} {}_{K}k_2\big({}_{K}\lambda^2 - {}_{K}\lambda + {}_{K}\lambda^{-1}\big)\, {}_{K}L, \\
\text{centerline bending :} &\quad \frac{1}{2}\sum_{K=1}^{N-2} {}_{K}k_3({}_{K}\mu\, {}_{K}\kappa)^2\, {}_{K}L, \\
\text{longitudinal shearing :} &\quad \frac{1}{2}\sum_{K=0}^{N-1} {}_{K}k_4 \tan^2({}_{K}\vartheta)\, {}_{K}L, \\
\text{longitudinal shearing gradients :} &\quad \frac{1}{2}\sum_{K=0}^{N-2} {}^{K}k_5\left(\frac{{}_{K+1}\vartheta - {}_{K}\vartheta}{\big\|{}^{K}\mathbf{E}\big\|}\right)^2 \big\|{}^{K}\mathbf{E}\big\|, \\
\text{cross-section stretch gradients :} &\quad \frac{1}{2}\sum_{K=0}^{N-2} {}^{K}k_6\left(\frac{{}_{K+1}\lambda - {}_{K}\lambda}{\big\|{}^{K}\mathbf{E}\big\|}\right)^2 \big\|{}^{K}\mathbf{E}\big\|, \\
\text{the Poisson effect :} &\quad \sum_{K=1}^{N-2} {}_{K}k_7({}_{K}\lambda - 1)({}_{K}\mu - 1)\, {}_{K}L.
\end{aligned}
$$

We note that the Poisson effect is sometimes referred to as "hourglassing." There is no possibility for the material to pass through itself *except* in the instance that shear gradients are large. However, we do not expect this to occur owing to the fact that shear deformation tends to be much smaller than bending and stretching deformation for a rod-like body's geometry. If one finds this behavior to occur, the term in the strain energy associated with the longitudinal shearing gradients must be modified so that

$$\Pi_{\mathrm{e}} \to \infty \quad \text{if} \quad \left\| {}_{K+1}\mathbf{d} + {}^{K}\mathbf{e} - {}_{K}\mathbf{d} \right\| \to 0,$$

or, for instance, if the centerline is chosen close to the upper lateral surface of the rod,

$$\Pi_{\mathrm{e}} \to \infty$$
$$\text{if}$$
$$\left\| \left({}_{K}H - \| {}_{K}\mathbf{D} \| \right) {}_{K}\mathbf{d} + {}^{K}\mathbf{e} - \left({}_{K+1}H - \left\| {}_{K+1}\mathbf{D} \right\| \right) {}_{K+1}\mathbf{d} \right\| \to 0.$$

The stretching terms are constructed so that $\Pi_e \to \infty$ as ${}_{K}\lambda \to 0, \infty$ and ${}^{K}\mu \to 0, \infty$

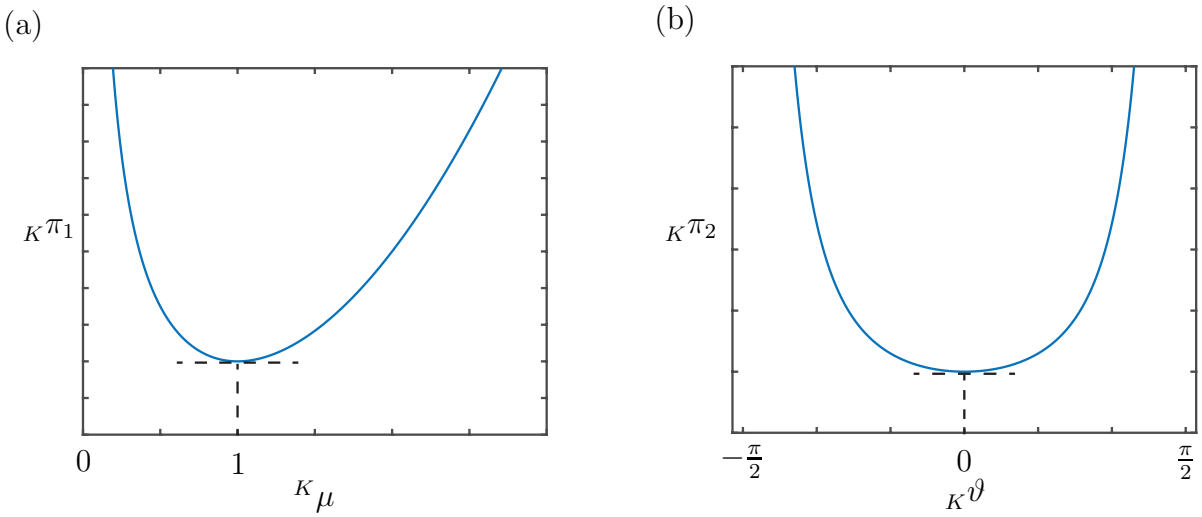

Figure 3.7: *Examples of partwise strain energy characteristics,* ${}_{K}\pi_1$ *and* ${}_{K}\pi_2$*, to prevent the discrete directed curve from passing through itself for (a) stretching and (b) shearing.*

while the shearing term is constructed so that $\Pi_e \to \infty$ as ${}_{K}\vartheta \to \pm\frac{\pi}{2}$ (see Figure 3.7). The centerline bending energy term is an extensible version of Euler's classic prescription. It is quadratic in the curvature ${}_{K}\mu\,{}_{K}\kappa$, which represents a change in turning angle per unit *reference* arc length. If the strain measure were a change in angle per unit *current* arc length, then the resulting forces on the centerline vertices would be such as to drive the current arc length to infinity (in an attempt to minimize the bending energy), an undesired effect. The bending energy is integrated only over the interior vertices of the discrete directed curve in order to prevent anomalous forces at the boundary vertices.

The shear and cross-section stretch gradients are necessary for transmission of shear strains through the medium, a characteristic of strain-gradient elasticity. These terms are required if we wish to model longitudinal and transverse shear pulses propagating through the rod. The final term of the elastic energy is the Poisson effect. By coupling cross-section stretch to centerline stretch, we ensure lateral contractions in the presence of centerline stretching and vice-versa, a behavior exhibited by incompressible materials. Like the bending energy, the Poisson effect energy is only integrated over interior vertices to prevent unrealistic forces at the boundary vertices.

Stiffnesses

The stiffnesses ${}^{K}k_1$, ${}_{K}k_2$, ${}_{K}k_3$, ${}_{K}k_4$, ${}^{K}k_5$, ${}^{K}k_6$, and ${}_{K}k_7$ should be such that, when confining ourselves to the class of motions that exhibit small deformations and small deformation gradients, we retain solutions from the continuous theory of linearly elastic rods. The strain measures established for the discrete theory are not entirely comparable to the strain measures used in the linear theory of elastic rods (cf. [47]). Furthermore, if the centerline is chosen so that ${}_{K}Y^{02} \neq 0$, then we stray even further from the elastic constants for the linear directed rod theory.[2] Therefore, the stiffnesses stated here will come with the calibration coefficients, ${}^{K}c_1$, ${}_{K}c_2$, ${}_{K}c_3$, ${}_{K}c_4$, ${}^{K}c_5$, ${}^{K}c_6$, and ${}_{K}c_7$. We obtain an order of magnitude estimate of the required stiffnesses from the continuous linear theory with the centerline chosen such that ${}_{K}Y^{02} = 0$:

$$
\begin{gathered}
{}^{K}k_1 = {}^{K}c_1 \frac{{}^{K}E\,{}^{K}A\big(1-{}^{K}\nu\big)}{(1+{}^{K}\nu)(1-2\,{}^{K}\nu)}, \\
{}_{K}k_2 = {}_{K}c_2 \frac{{}_{K}E\,{}_{K}A(1-{}_{K}\nu)}{(1+{}_{K}\nu)(1-2\,{}_{K}\nu)}, \\
{}_{K}k_3 = {}_{K}c_3\,{}_{K}E\,{}_{K}I, \qquad {}_{K}k_4 = {}_{K}c_4 k\,{}_{K}G\,{}_{K}A, \qquad {}^{K}k_5 = {}^{K}c_5\,{}^{K}E\,{}^{K}I, \\
{}^{K}k_6 = {}^{K}c_6 \frac{{}^{K}E\,{}^{K}I}{(1+{}^{K}\nu)}, \\
{}_{K}k_7 = {}_{K}c_7 \frac{{}_{K}E\,{}_{K}A\,{}_{K}\nu}{(1+{}_{K}\nu)(1-2\,{}_{K}\nu)},
\end{gathered}
\tag{3.4.13}
$$

where k is the shear correction factor and we have used material and geometric quantities from Table 3.1. Derivations of k values for various cross-sections may be found in [15].

The calibration coefficients are to be determined numerically by comparing with analytical solutions from the continuous linear theory. If the centerline is chosen so that ${}_{K}Y^{02} = 0$, then the first calibration coefficient for centerline stretching may be derived from the continuous theory. For example, the longitudinal stretching stiffness from the continuous linear

[2] These constants were established in a series of works by Green and Naghdi and are summarized in [47, 46].

theory is $\frac{EA(1-\nu)}{4(1+\nu)(1-2\nu)}$. The continuous analogue of the longitudinal stretching energy postulated in Equation (3.4.11) is $\frac{1}{2}k_1(\mu^2-\mu+\mu^{-1})$. If the nonlinear stretching energy is to coincide with the stretching energy of the linear theory for small deformations, we then require that

$$\left[\frac{d^2}{d\mu^2}\left(\frac{1}{2}k_1\big(\mu^2-\mu+\mu^{-1}\big)\right)\right]_{\mu=1}=\frac{EA(1-\nu)}{4(1+\nu)(1-2\nu)}. \tag{3.4.14}$$

This would yield a calibration coefficient ${}^{K}c_1=\frac{1}{2}$. Similar comparisons may be made for the lateral stretching stiffness and the Poisson effect stiffness. However, this procedure only applies when the centerline is chosen so that the first inertia is zero everywhere.

The internal forces

In taking gradients of $\hat{\Pi}_{\mathrm{e}}({}_K\mathbf{x},{}_K\mathbf{d})$ with respect to ${}_K\mathbf{x}$ and ${}_K\mathbf{d}$ it will be useful to record the following identities:

$$\begin{aligned}\frac{\partial}{\partial\mathbf{a}}\left(\mathbf{c}\cdot\frac{\mathbf{a}-\mathbf{b}}{\|\mathbf{a}-\mathbf{b}\|}\right)&=\mathbf{A}\left(\frac{\mathbf{a}-\mathbf{b}}{\|\mathbf{a}-\mathbf{b}\|}\right)\frac{\mathbf{c}}{\|\mathbf{a}-\mathbf{b}\|},\\ \frac{\partial}{\partial\mathbf{a}}\left(\frac{\mathbf{a}-\mathbf{b}}{\|\mathbf{a}-\mathbf{b}\|}\cdot\frac{\mathbf{c}-\mathbf{a}}{\|\mathbf{c}-\mathbf{a}\|}\right)&=\mathbf{A}\left(\frac{\mathbf{a}-\mathbf{b}}{\|\mathbf{a}-\mathbf{b}\|}\right)\frac{\mathbf{c}-\mathbf{a}}{\|\mathbf{c}-\mathbf{a}\|\|\mathbf{a}-\mathbf{b}\|}\\ &\quad-\mathbf{A}\left(\frac{\mathbf{c}-\mathbf{a}}{\|\mathbf{c}-\mathbf{a}\|}\right)\frac{\mathbf{a}-\mathbf{b}}{\|\mathbf{a}-\mathbf{b}\|\|\mathbf{c}-\mathbf{a}\|},\end{aligned} \tag{3.4.15}$$

where the projection operator $\mathbf{A}(\hat{\mathbf{a}})\mathbf{b}$ annihilates the component of $\mathbf{b}$ along the unit vector $\hat{\mathbf{a}}$:

$$\mathbf{A}(\hat{\mathbf{a}})\mathbf{b}=(\mathbf{I}-\hat{\mathbf{a}}\otimes\hat{\mathbf{a}})\mathbf{b}=\mathbf{b}-(\mathbf{b}\cdot\hat{\mathbf{a}})\hat{\mathbf{a}}. \tag{3.4.16}$$

To aid in listing the internal forces in a succinct way, we introduce the following functions:

$$
\begin{aligned}
{}^{K}f_1 = \widehat{{}^{K}f_1}\big({}^{K}\mu\big) &= \frac{{}^{K}k_1}{2}\big(2\,{}^{K}\mu - 1 - {}^{K}\mu^{-2}\big),\\
{}_{K}p_2 = \widehat{{}_{K}p_2}({}_{K}\lambda) &= \frac{{}_{K}k_2\,{}_{K}L}{2\|{}_{K}\mathbf{D}\|}\big(2\,{}_{K}\lambda - 1 - {}_{K}\lambda^{-2}\big),\\
{}_{K}f_3 = \widehat{{}_{K}f_3}({}_{K}\varphi) &= \frac{4\,{}_{K}k_3}{{}_{K}L}\frac{1}{(1+\cos({}_{K}\varphi))^2\|{}^{K-1}\mathbf{e}\|\|{}^{K}\mathbf{e}\|},\\
{}_{0}f_4 = \widehat{{}_{0}f_4}({}_{0}\vartheta) &= {}_{0}k_4\,{}_{0}L\frac{\tan({}_{0}\vartheta)\sec^3({}_{0}\vartheta)}{\|{}^{0}\mathbf{e}\|},\\
{}_{K}f_4 = \widehat{{}_{K}f_4}({}_{K}\vartheta) &= {}_{K}k_4\,{}_{K}L\frac{\tan({}_{K}\vartheta)\sec^3({}_{K}\vartheta)}{\|{}^{K-1}\mathbf{e}+{}^{K}\mathbf{e}\|},\\
{}_{N-1}f_4 = \widehat{{}_{N-1}f_4}\big({}_{N-1}\vartheta\big) &= {}_{N-1}k_4\,{}_{N-1}L\frac{\tan\big({}_{N-1}\vartheta\big)\sec^3\big({}_{N-1}\vartheta\big)}{\|{}^{N-2}\mathbf{e}\|},\\
{}_{K}p_4 = \widehat{{}_{K}p_4}({}_{K}\vartheta) &= {}_{K}k_4\,{}_{K}L\frac{\tan({}_{K}\vartheta)\sec^3({}_{K}\vartheta)}{\|{}_{K}\mathbf{d}\|},\\
{}^{0}p_5 = \widehat{{}^{0}p_5}({}_{0}\vartheta,{}_{1}\vartheta) &= \frac{{}^{0}k_5}{\big\|{}^{0}\mathbf{E}\big\|}({}_{0}\vartheta - {}_{1}\vartheta)\sec({}_{0}\vartheta),
\end{aligned}
$$

$$
\begin{aligned}
{}^{K}p_5 = \widehat{{}^{K}p_5}({}_{K}\vartheta) &= \frac{{}^{K-1}k_5}{\big\|{}^{K-1}\mathbf{E}\big\|}\big({}_{K}\vartheta - {}_{K-1}\vartheta\big)\sec({}_{K}\vartheta)\\
&\quad + \frac{{}^{K}k_5}{\big\|{}^{K}\mathbf{E}\big\|}\big({}_{K}\vartheta - {}_{K+1}\vartheta\big)\sec({}_{K}\vartheta),\\
{}^{N-1}p_5 = \widehat{{}^{N-1}p_5}\big({}_{N-1}\vartheta,{}_{N-2}\vartheta\big) &= \frac{{}^{N-2}k_5}{\big\|{}^{N-2}\mathbf{E}\big\|}\big({}_{N-1}\vartheta - {}_{N-2}\vartheta\big)\sec\big({}_{N-1}\vartheta\big),\\
{}^{0}p_6 = \widehat{{}^{0}p_6}({}_{0}\lambda,{}_{1}\lambda) &= \frac{{}^{0}k_6}{\|{}_{0}\mathbf{D}\|\big\|{}^{0}\mathbf{E}\big\|}({}_{1}\lambda - {}_{0}\lambda),
\end{aligned}
$$

$$
\begin{aligned}
{}^{K}p_6 = \widehat{{}^{K}p_6}({}_{K}\lambda) &= \frac{{}^{K-1}k_6}{\|{}_{K}\mathbf{D}\|\|{}^{K-1}\mathbf{E}\|}({}_{K-1}\lambda - {}_{K}\lambda) \\
&\quad + \frac{{}^{K}k_6}{\|{}_{K}\mathbf{D}\|\|{}^{K}\mathbf{E}\|}({}_{K+1}\lambda - {}_{K}\lambda), \\
{}^{N-1}p_6 = \widehat{{}^{N-1}p_6}({}_{N-2}\lambda, {}_{N-1}\lambda) &= \frac{{}^{N-2}k_6}{\|{}_{N-1}\mathbf{D}\|\|{}^{N-2}\mathbf{E}\|}({}_{N-2}\lambda - {}_{N-1}\lambda), \\
{}_{K}f_7 = \widehat{{}_{K}f_7}({}_{K}\lambda) &= \frac{{}_{K}k_7}{2}({}_{K}\lambda - 1), \\
{}_{K}p_7 = \widehat{{}_{K}p_7}({}_{K}\mu) &= \frac{{}_{K}k_7\,{}_{K}L}{\|{}_{K}\mathbf{D}\|}({}_{K}\mu - 1).
\end{aligned} \tag{3.4.17}
$$

The centerline vertex internal forces are derived using Equation $(3.4.7)_1$ as:

$$
\begin{aligned}
{}_{0}\mathbf{F}_{\text{int}} &= \left({}^{0}f_1 + {}_{1}f_7\right){}^{0}\mathbf{t} - {}_{1}f_3\mathbf{A}\left({}^{0}\mathbf{t}\right){}^{1}\mathbf{e} - {}_{1}f_4\mathbf{A}({}_{1}\mathbf{t})\,{}_{1}\hat{\mathbf{d}}, \\
{}_{1}\mathbf{F}_{\text{int}} &= \left(-{}^{0}f_1 - {}_{0}f_7 - {}_{1}f_7\right){}^{0}\mathbf{t} + \left({}^{1}f_1 + {}_{1}f_7 + {}_{2}f_7\right){}^{1}\mathbf{t} \\
&\quad + {}_{1}f_3\left(\mathbf{A}\left({}^{0}\mathbf{t}\right){}^{1}\mathbf{e} - \mathbf{A}\left({}^{1}\mathbf{t}\right){}^{0}\mathbf{e}\right) - {}_{2}f_3\mathbf{A}\left({}^{1}\mathbf{t}\right){}^{2}\mathbf{e} \\
&\quad + {}_{0}f_4\mathbf{A}({}_{0}\mathbf{t})\,{}_{0}\hat{\mathbf{d}} - {}_{2}f_4\mathbf{A}({}_{2}\mathbf{t})\,{}_{2}\hat{\mathbf{d}}, \\
{}_{J}\mathbf{F}_{\text{int}} &= \left(-{}^{J-1}f_1 - {}_{J-1}f_7 - {}_{J}f_7\right){}^{J-1}\mathbf{t} + \left({}^{J}f_1 + {}_{J}f_7 + {}_{J+1}f_7\right){}^{J}\mathbf{t} \\
&\quad + {}_{J-1}f_3\mathbf{A}\left({}^{J-1}\mathbf{t}\right){}^{J-2}\mathbf{e} + {}_{J}f_3\left(\mathbf{A}\left({}^{J-1}\mathbf{t}\right){}^{J}\mathbf{e} - \mathbf{A}\left({}^{J}\mathbf{t}\right){}^{J-1}\mathbf{e}\right) \\
&\quad - {}_{J+1}f_3\mathbf{A}\left({}^{J}\mathbf{t}\right){}^{J+1}\mathbf{e} + {}_{J-1}f_4\mathbf{A}\left({}_{J-1}\mathbf{t}\right){}_{J-1}\hat{\mathbf{d}} - {}_{J+1}f_4\mathbf{A}\left({}_{J+1}\mathbf{t}\right){}_{J+1}\hat{\mathbf{d}}, \\
{}_{N-2}\mathbf{F}_{\text{int}} &= \left(-{}^{N-3}f_1 - {}_{N-3}f_7 - {}_{N-2}f_7\right){}^{N-3}\mathbf{t} \\
&\quad + \left({}^{N-2}f_1 + {}_{N-1}f_7 + {}_{N-2}f_7\right){}^{N-2}\mathbf{t} \\
&\quad + {}_{N-3}f_3\mathbf{A}\left({}^{N-3}\mathbf{t}\right){}^{N-4}\mathbf{e} + {}_{N-2}f_3\left(\mathbf{A}\left({}^{N-3}\mathbf{t}\right){}^{N-2}\mathbf{e} - \mathbf{A}\left({}^{N-2}\mathbf{t}\right){}^{N-3}\mathbf{e}\right) \\
&\quad + {}_{N-3}f_4\mathbf{A}\left({}_{N-3}\mathbf{t}\right){}_{N-3}\hat{\mathbf{d}} - {}_{N-1}f_4\mathbf{A}\left({}_{N-1}\mathbf{t}\right){}_{N-1}\hat{\mathbf{d}}, \\
{}_{N-1}\mathbf{F}_{\text{int}} &= \left(-{}^{N-2}f_1 - {}_{N-2}f_7\right){}^{N-2}\mathbf{t} + {}_{N-2}f_3\mathbf{A}\left({}^{N-2}\mathbf{t}\right){}^{N-3}\mathbf{e} \\
&\quad + {}_{N-2}f_4\mathbf{A}\left({}_{N-2}\mathbf{t}\right){}_{N-2}\hat{\mathbf{d}}.
\end{aligned} \tag{3.4.18}
$$

At every directorline vertex ($J = 0, \ldots, N-1$), the internal director force is derived using Equation $(3.4.7)_2$:

$$
{}_{J}\mathbf{P}_{\text{int}} = \left({}_{J}p_4 + {}^{J}p_5\right)\mathbf{A}\left({}_{J}\hat{\mathbf{d}}\right){}_{J}\mathbf{t} + \left({}^{J}p_6 - {}_{J}p_2 - {}_{J}p_7\right){}_{J}\hat{\mathbf{d}}. \tag{3.4.19}
$$

The discrete directed rod theory presented in this chapter is now complete. It remains to integrate the equations of motion (3.3.50) given initial conditions. If it is desired to model boundary conditions, then they may be imposed as positional constraints.

3.5 Validation of the discrete theory

The model as it is presented in this section is to be simultaneously calibrated, validated, and demonstrated against four example problems from the continuous linear theory of elastic rods. Equilibrium deformations are calculated for the following examples illustrated in Figure 3.8:

(i) a clamped-free bar hanging under its own weight (Figure 3.8(a));

(ii) a clamped-free Timoshenko beam hanging under its own weight (Figure 3.8(b));

(iii) a clamped-clamped Timoshenko beam hanging under its own weight (Figure 3.8(c)); and

(iv) a clamped-clamped bar subject to uniform normal traction σ at both ends (Figure 3.8(d)).

The rods are released from rest in their reference configuration and allowed to vibrate about their equilibrium configurations. The displacement profiles are obtained by integrating numerically with a Runge-Kutta method and tuning the material damping towards critical damping such that, by the end of the simulation, the rod contains a negligible amount of kinetic energy and has converged to the equilibrium configuration.

In all four problems, properties of the discrete directed curve are assigned as follows: the rod is materially and geometrically homogeneous, the centerline (the dashed line in Figure 3.8) is chosen as the line of cross-sectional mass (and area) centers, the cross sections are rectangular, $N = 20$, $\mathcal{L} = 5$ m, ${}^{K}\mathbf{E} = \frac{\mathcal{L}}{N-1}\mathbf{E}_3$ identically, ${}_{K}H = 0.5$ m $= {}_{K}W$ identically, ${}_{K}E = 1$ GPa identically, ${}_{K}G = {}_{K}E/2/(1 + {}_{K}\nu)$, ${}_{K}\rho_0 = 250$ kg/m identically, $g = 9.81$ m/s^2, ${}_{K}\mathbf{F}_{\text{ext}} = {}_{K}\rho_0 g\, {}_{K}L\mathbf{E}_3$ for the hanging bar, and ${}_{K}\mathbf{F}_{\text{ext}} = -\,{}_{K}\rho_0 g\, {}_{K}L\mathbf{E}_2$ for the other three problems, identically. Thus, for the hanging bar we have chosen $\mathbf{E}_3$ to align with the direction of gravity.

We will make reference to continuous quantities in the following subsections, including: the centerline displacement, $\mathbf{u} = \mathbf{r} - \mathbf{R}$, the director displacement, $\boldsymbol{\delta} = \mathbf{d} - \mathbf{D}$, and the centerline stretch, μ. The directors from the continuous theory are not required to point to the lateral surface of the rod-like body. It is common in the continuous theory to choose $\|\mathbf{D}\| = 1$, indicating the use of Cartesian coordinates that carry a physical dimension of length. We will be comparing against solutions which have made this choice. Hence, the director displacement from the continuous theory is scaled according to the relationship

$$ {}_{K}\boldsymbol{\delta} = {}_{K}\mathbf{d} - {}_{K}\mathbf{D} = {}_{K}H(\mathbf{d}({}_{K}\xi) - \mathbf{D}({}_{K}\xi)) = {}_{K}H\boldsymbol{\delta}({}_{K}\xi) \tag{3.5.1} $$

to make a fair comparison. The "director displacement" in Figures 3.11 - 3.12 refers to the displacement of material points on the lateral surface of the rod-like body relative to the centerline displacement. The directors displayed in Figure 3.8 are those from the continuous theory, being unit length in the reference configuration.

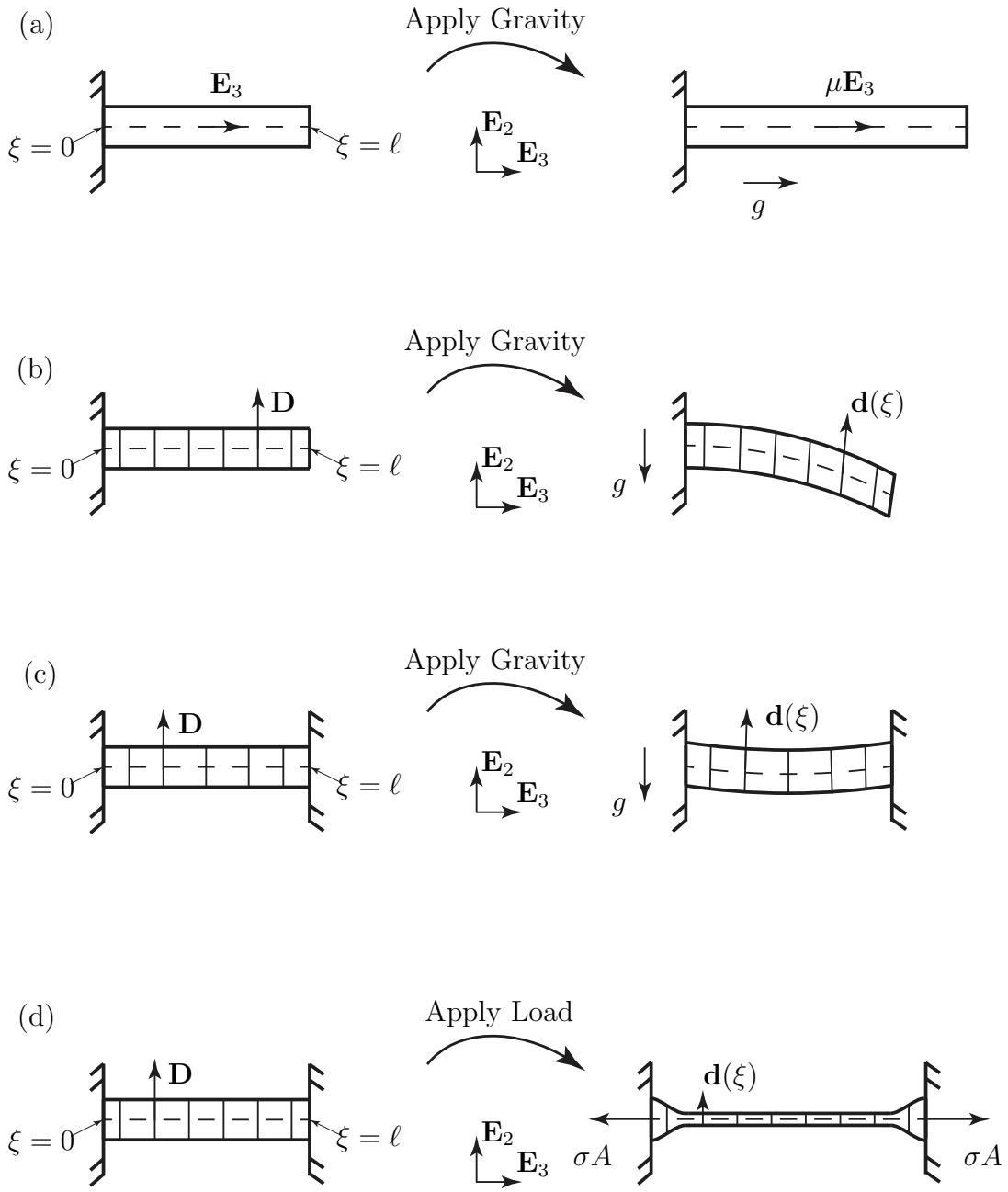

Figure 3.8: *Equilibrium configurations of four different problems involving a variety of deformations from the continuous theory of linear elasticity for rod-like bodies. These problems are used to determine the calibration coefficients* ${}^{K}c_1$, ${}_{K}c_2$, ${}_{K}c_3$, ${}_{K}c_4$, ${}^{K}c_5$, ${}^{K}c_6$, *and* ${}_{K}c_7$. *Note that the directors do not necessarily point to the lateral surface of the rod-like body in the continuous theory.*

A bar loaded under its own weight

We refer the reader to the situation pictured in Figure 3.8(a) where a bar is defined in its reference configuration. The constraint at the left end responsible for fixing the rod is expressed as ${}_0\mathbf{u} \cdot \mathbf{E}_3 = 0$ for the discrete rod. We apply a gravitational body force along the rod with the aim to find and validate the calibration coefficient ${}^K c_1$. We assume the bar to have zero Poisson's ratio everywhere so as not to activate other modes of deformation. Thus, we expect the director displacement to be zero. The resulting equilibrium centerline displacement is obtained from the continuous linear theory of elasticity for rods:

$$\mathbf{u} \cdot \mathbf{E}_3 = \frac{\rho_0 g \ell^2}{EA} \left(\frac{\xi}{\ell} - \frac{1}{2} \left(\frac{\xi}{\ell} \right)^2 \right). \tag{3.5.2}$$

In this experiment, we find the calibration coefficient for centerline stretching to be ${}^K c_1 = \frac{1}{2}$, which is in accordance with the discussion at the end of Section 3.4.

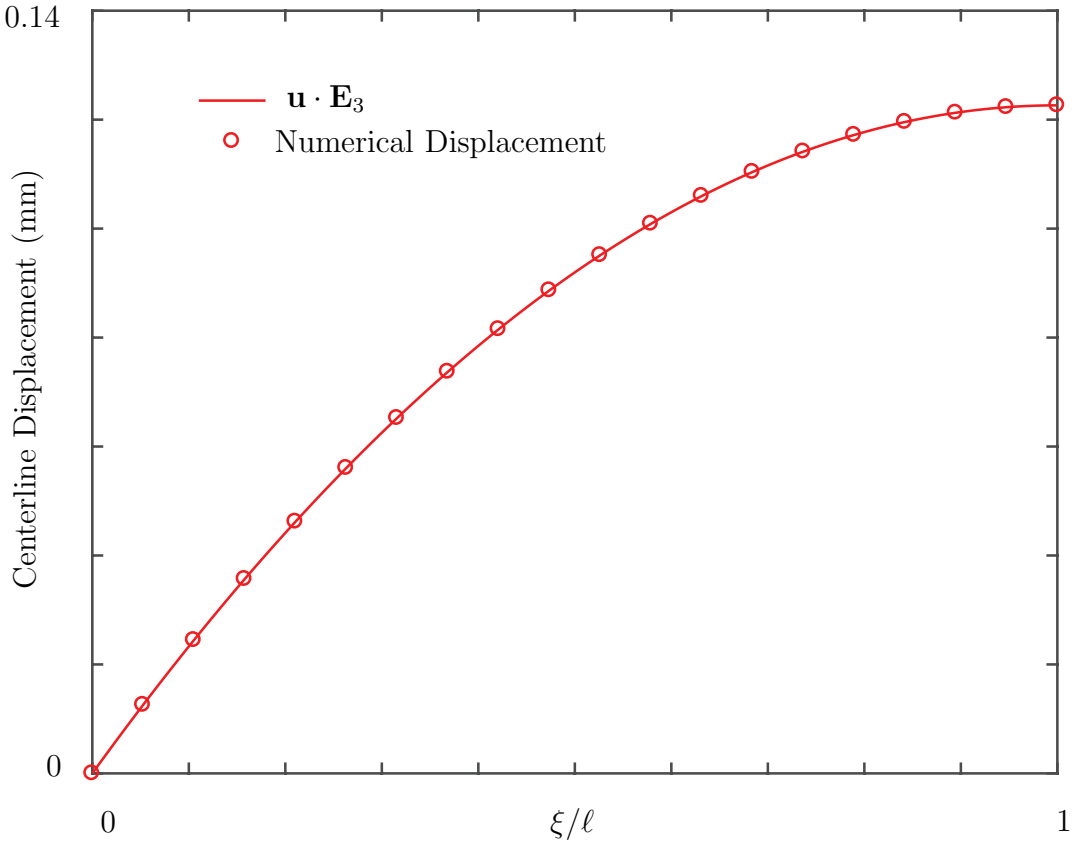

Figure 3.9: *Validation of the calibration coefficient* ${}^{K}c_1 = \frac{1}{2}$ *for a clamped-free rod deforming under its own weight (cf. Figure 3.8(a)).*

A clamped-free and clamped-clamped Timoshenko beam

We next consider the deformation of a Timoshenko beam under its own weight in two scenarios involving differing sets of supports: clamped-free and clamped-clamped, as in Figure 3.8(b)-(c). For the clamped-free beam, we have the following boundary conditions which are imposed as positional constraints in the discrete theory: ${}_0\mathbf{u} = \mathbf{0}$ and ${}_0\boldsymbol{\delta} = \mathbf{0}$. Once more, we demand a material in which Poisson's ratio is zero so that we may validate the coefficients ${}_{K}c_3$, ${}_{K}c_4$, and ${}^{K}c_5$ which calibrate the bending, shear, and shear gradient stiffnesses, respectively. The continuous theory predicts the centerline and director displacement as

$$\mathbf{u}\cdot\mathbf{E}_2 = \left(-\frac{\sigma_1}{24}\left(\frac{\xi}{\ell}\right)^3 + \frac{\sigma_1}{6}\left(\frac{\xi}{\ell}\right)^2 + \frac{2\sigma_2-\sigma_1}{4}\frac{\xi}{\ell} - \sigma_2\right)\xi, \tag{3.5.3}$$

and

$$\boldsymbol{\delta} \cdot \mathbf{E}_3 = \frac{\sigma_1}{6}\left(\frac{\xi}{\ell}\right)^3 - \frac{\sigma_1}{2}\left(\frac{\xi}{\ell}\right)^2 + \frac{\sigma_1}{2}\frac{\xi}{\ell}, \tag{3.5.4}$$

where

$$\sigma_1 = \frac{\rho_0 g \ell^3}{EI} \quad \sigma_2 = \frac{2(1+\nu)\rho_0 g \ell}{kEA}. \tag{3.5.5}$$

The resulting discrete centerline and director displacements are compared to the corresponding quantities of the continuous theory in Figure 3.10, where a choice of ${}_K c_3 = 0.99$, ${}_K c_4 = 2.01$, and ${}^K c_5 = 1$ is found to be suitable.

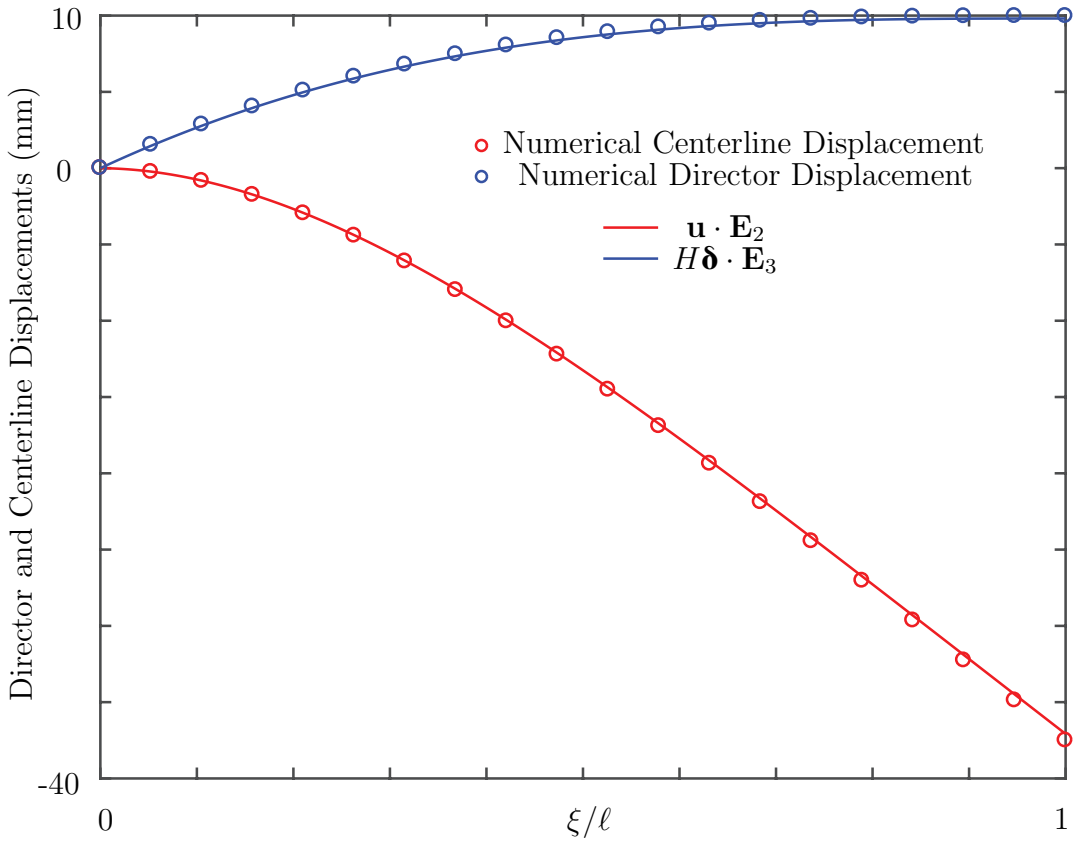

Figure 3.10: *Validation of the calibration coefficients* ${}_K c_3 = 0.99$, ${}_K c_4 = 2.01$, *and* ${}^K c_5 = 1$ *for a clamped-free Timoshenko rod deforming under its own weight (cf. Figure 3.8(b)).*

The clamped-clamped beam is constrained by ${}_{N-1}\mathbf{u} = \mathbf{0}$ and ${}_{N-1}\boldsymbol{\delta} = \mathbf{0}$ in addition to the constraints on the left side of the clamped-free beam. The solutions from the continuous

theory are

$$\mathbf{u}\cdot\mathbf{E}_2 = \left(-\frac{\sigma_1}{24}\left(\frac{\xi}{\ell}\right)^3 + \frac{\sigma_1}{12}\left(\frac{\xi}{\ell}\right)^2 + \frac{12\sigma_2-\sigma_1}{24}\frac{\xi}{\ell} - \frac{\sigma_2}{2}\right)\xi, \tag{3.5.6}$$

and

$$\boldsymbol{\delta}\cdot\mathbf{E}_3 = \frac{\sigma_1}{6}\left(\frac{\xi}{\ell}\right)^3 - \frac{\sigma_1}{4}\left(\frac{\xi}{\ell}\right)^2 + \frac{\sigma_1}{12}\frac{\xi}{\ell}, \tag{3.5.7}$$

where σ_1 and σ_2 are as in Equation (3.5.5). The findings for the clamped-clamped Timoshenko beam that are illustrated in Figure 3.11 fortify the calibration coefficients found for the clamped-free case.

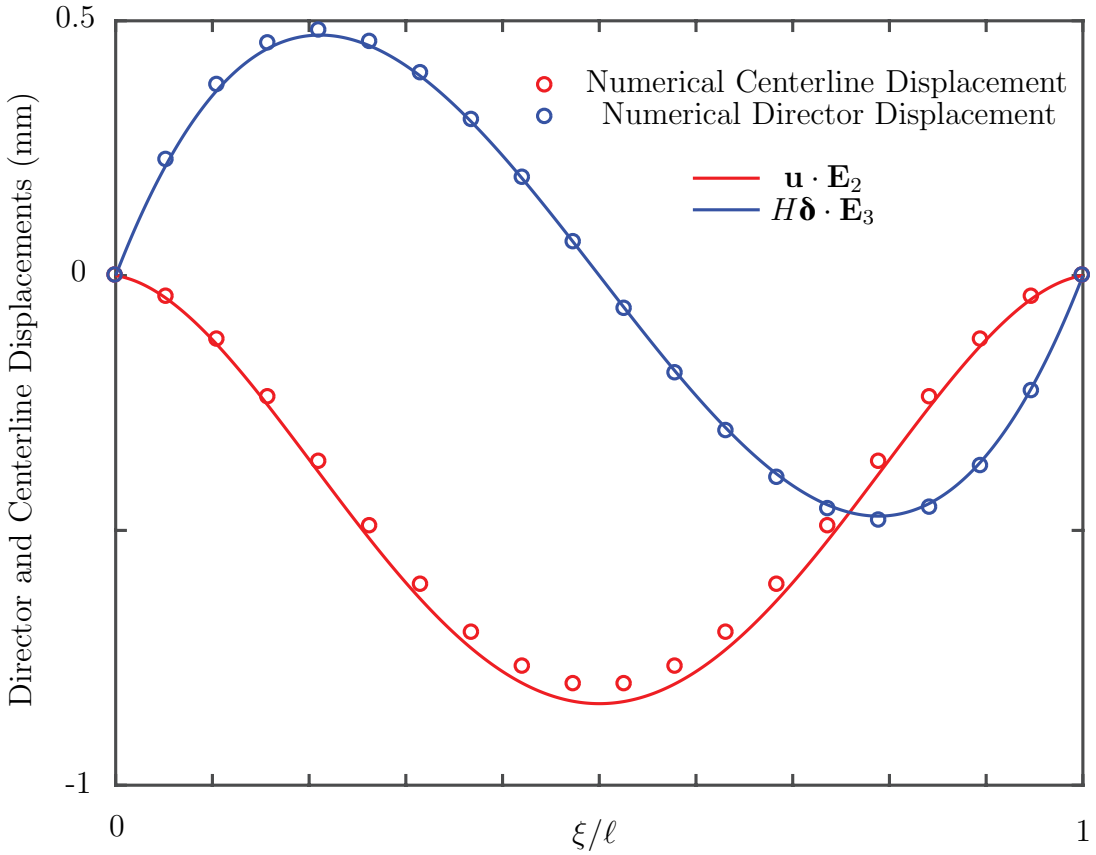

Figure 3.11: *Validation of the calibration coefficients* ${}_K c_3 = 0.99$, ${}_K c_4 = 2.01$, *and* ${}^K c_5 = 1$ *for a clamped-clamped Timoshenko rod deforming under its own weight (cf. Figure 3.8(c)).*

A necking problem

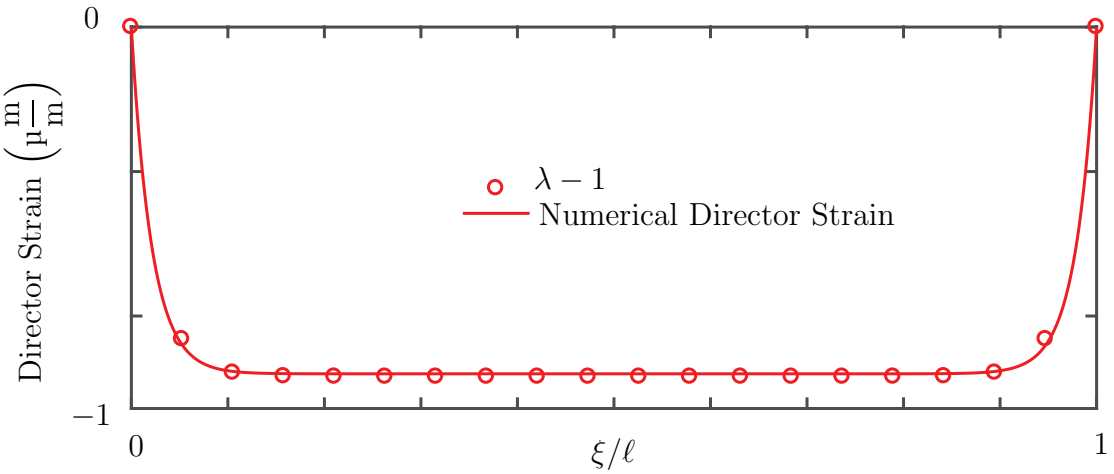

Figure 3.12: *Validation of the calibration coefficients* ${}_K c_2 = \frac{1}{2}$, ${}^K c_6 = \frac{1}{2}$, *and* ${}_K c_7 = 1.66$ *using a necking problem (cf. Figure 3.8(d)).*

Finally, to calibrate the remaining coefficients we consider a necking (or hourglassing) problem. Following [43] and [58], we choose a shear correction coefficient of $k = 5/6$ for a rectangular cross section. The rod is subject to the constraints: ${}_0\boldsymbol{\delta} = \mathbf{0}$ and ${}_{N-1}\boldsymbol{\delta} = \mathbf{0}$. We aim to validate the lateral stretch, lateral stretch gradient, and Poisson effect stiffnesses with the choices ${}_K c_2 = \frac{1}{2}$, ${}^K c_6 = \frac{1}{2}$, and ${}_K c_7 = 1.66$ identically. We do not concern ourselves with the centerline displacement since we already validated ${}^K c_1$ in the sagging problem. We choose a value of Poisson's ratio as ${}_K\nu = 0.3$, identically, and an applied load of $n = \sigma A = 1$ kN. An analytical solution for the director strain is found from the continuous theory to be

$$\lambda - 1 = \frac{\nu n}{EA}\left(\frac{1 - \cosh(\beta\ell)}{\sinh(\beta\ell)}\sinh(\beta\xi) + \cosh(\beta\xi) - 1\right), \tag{3.5.8}$$

where $\lambda = \frac{\|\mathbf{d}\|}{\|\mathbf{D}\|}$ is the director stretch and where

$$\beta^2 = \frac{A(1+\nu)}{I(1-\nu)}. \tag{3.5.9}$$

Note that we are comparing against a theory that allows for three-dimensional motions of the continuum. There is a lateral stretch due to Poisson's ratio not only in $\mathbf{E}_2$ direction but also the $\mathbf{E}_1$ direction. Despite this, the plane of material that intersects the $\mathbf{E}_1 - \mathbf{E}_3$ plane

remains in this plane and in a state of plane strain. Care should be taken in interpreting the results. We find the chosen calibration coefficients to be in agreement with the continuous theory upon inspection of Figure 3.12.

Dynamic validation: a clamped-free Bernoulli-Euler beam

Consider a clamped-free Bernoulli-Euler beam undergoing unforced linear vibration in its first mode shape. The governing equation of motion may be derived for a uniform beam as

$$EI\frac{\partial^4 w}{\partial \xi^4} + \rho_0 \frac{\partial^2 w}{\partial t^2} = 0, \tag{3.5.10}$$

where w is the vertical displacement of the beam. Assuming a separation of variables of the form

$$w(\xi, t) = W(\xi)T(t), \tag{3.5.11}$$

we obtain the two linear ODE's

$$\frac{d^4 W}{d\xi^4} + \beta W = 0, \quad \text{and} \quad \frac{\rho_0}{EI}\frac{d^2 T}{dt^2} + \beta T = 0, \tag{3.5.12}$$

where β, the wavenumber, is some unknown constant. By imposing the clamped-free boundary conditions, we find a transcendental equation for the wavenumber (see [52] for additional details) as

$$\cosh(\beta_n L)\cos(\beta_n L) + 1 = 0. \tag{3.5.13}$$

We may find the first root as

$$\frac{\beta_1 \pi}{L} = 0.59686. \tag{3.5.14}$$

Hence, the corresponding angular frequency of the vibration is

$$\omega_1 = \frac{3.5161}{L^2}\sqrt{\frac{EI}{\rho_0}}, \tag{3.5.15}$$

and the nth mode shape is

$$\hat{w}_n = A_1\left[\cosh(\beta_n x) - \cos(\beta_n x) + \frac{\cos(\beta_n L) + \cosh(\beta_n L)}{\sin(\beta_n x) + \sinh(\beta_n x)}(\sin(\beta_n x) - \sinh(\beta_n x))\right]. \tag{3.5.16}$$

Approximating the angle of the centerline as $\theta = \frac{d\hat{w}_n}{d\xi}$, two Timoshenko beams are simulated with ${}_K c_4 = 2.0$ and ${}_K c_4 = 20.1$. The stiffnesses are set with the validated calibration coefficients and the remaining problem parameters are as follows: $g = 9.81$ ms^{-2}, $N = 20$, $L = 1$ m, $W = 0.1$ m, $k = 5/6$, $E = 1$ GPa, $\rho_0^* = 10^3$ kg, $\rho_0 = \rho_0^* A$, and $\nu = 0$. A time history of the kinetic energies is plotted in Figure 3.13. We find that for a high shear stiffness, the period of vibration close to the first mode-shape of a Bernoulli-Euler beam is

approximately 0.03 s. Equation (3.5.15) predicts a period of vibration of 0.031 s. Therefore, we may consider the discretized theory to be dynamically validated, in addition to being statically valid.

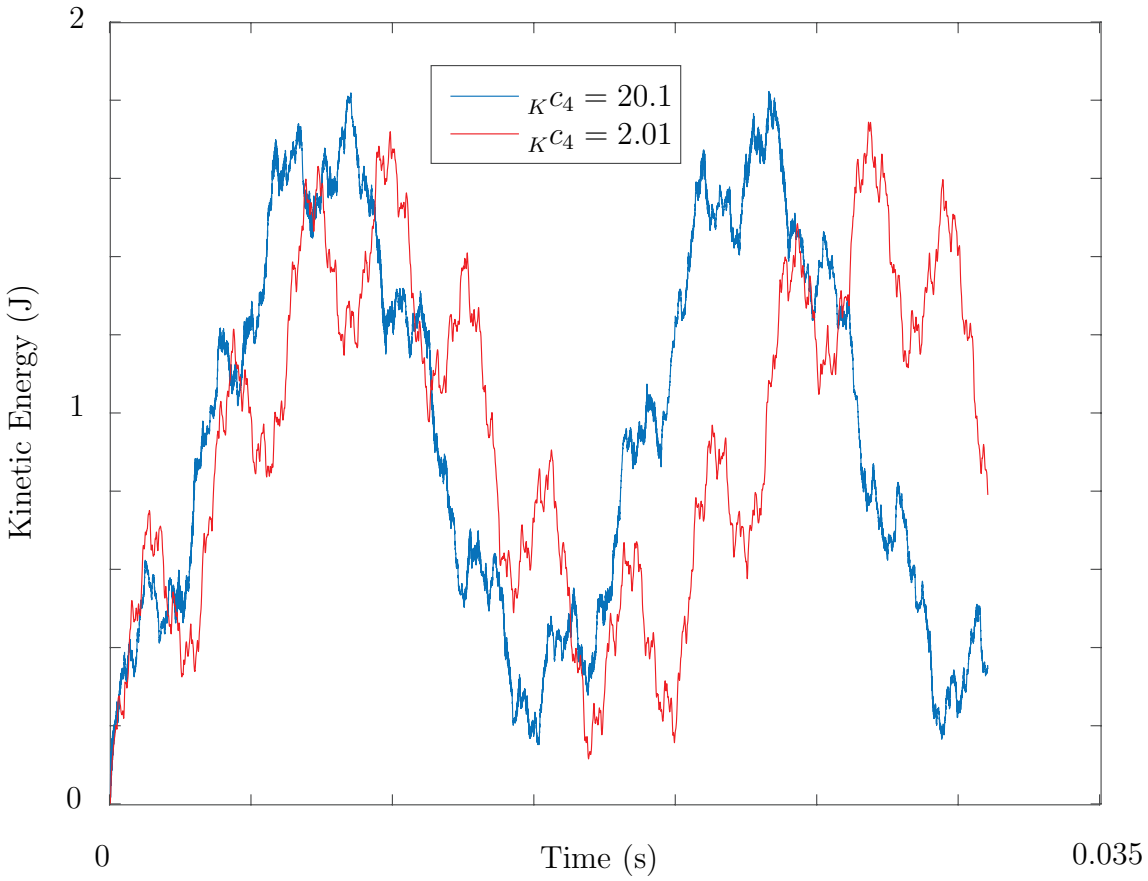

Figure 3.13: *Dynamic validation of a beam with high shear stiffness:* $_K c_4 = 20$. *The period of the vibration is found to be approximately 0.03 seconds, which reconciles well with that of the first mode of vibration for an Bernoulli-Euler beam which is calculated to have a period of 0.031 seconds for the given problem parameters.*

3.6 Conclusion

In this chapter, we have formulated a novel discretized directed rod theory that may be used to model nonlinear planar motions of a rod-like body. The theory is well-suited to analyzing the planar motions of locomoting and gripping soft robots. What has been developed can be considered a discretized approximation to a planar version of Green and Naghdi's theory of a directed rod and an extension to the planar theory of a discrete elastic rod developed

by Goldberg et al. [21]. The latter researchers' formulation is a planar version of Bergou et al.'s work [4, 6, 5] that is applicable to branched-like rod structures. In our formulation, we discussed the implications of an arbitrarily chosen centerline and the need for calibration coefficients in the stiffnesses of the postulated strain energy. The model was validated and calibrated against four classical problems from the continuous theory of linear elasticity for rods. An extension to three-dimensional motions will require the introduction of three new deformation measures: one due to torsion and two others due to additional modes of bending and shearing.

Bibliography

[1] G. Andrikopoulos, G. Nikolakopoulos, and S. Manesis. "A survey on applications of pneumatic artificial muscles". In: *2011 19th Mediterranean Conference on Control & Automation (MED)*. IEEE. 2011, pp. 1439–1446. URL: https://doi.org/10.1109/MED.2011.5982983.

[2] S. S. Antman. *Nonlinear Problems of Elasticity*. Second. Vol. 107. Applied Mathematical Sciences. New York: Springer-Verlag, 2005. URL: http://dx.doi.org/10.1007/0-387-27649-1.

[3] K. Arda et al. "Quantitative assessment of normal soft-tissue elasticity using shear-wave ultrasound elastography". In: *American Journal of Roentgenology* 197.3 (2011), pp. 532–536. URL: https://doi.org/10.2214/AJR.10.5449.

[4] B. Audoly et al. "A discrete geometric approach for simulating the dynamics of thin viscous threads". In: *Journal of Computational Physics* 253 (2013), pp. 18–49. URL: http://dx.doi.org/10.1016/j.jcp.2013.06.034.

[5] M. Bergou et al. "Discrete elastic rods". In: *ACM Transactions on Graphics (SIGGRAPH)* 27.3 (Aug. 2008), 63:1–63:12. URL: http://dx.doi.org/10.1145/1360612.1360662.

[6] M. Bergou et al. "Discrete viscous threads". In: *ACM Transactions on Graphics (SIGGRAPH)* 29.4 (2010), 116:1–116:10. URL: http://dx.doi.org/10.1145/1778765.1778853.

[7] R. L. Bishop. "There is more than one way to frame a curve". In: *The American Mathematical Monthly* 82.3 (1975), pp. 246–251. URL: http://dx.doi.org/10.2307/2319846.

[8] A. I. Bobenko. *Geometry II: Discrete Differential Geometry*. Berlin, 2015. URL: http://page.math.tu-berlin.de/~bobenko/Lehre/Skripte/DDG_Lectures.pdf.

[9] A. S. Boxerbaum et al. "Worms, waves and robots". In: *2012 IEEE International Conference on Robotics and Automation*. IEEE. 2012, pp. 3537–3538. URL: https://doi.org/10.1109/ICRA.2012.6224805.

[10] M. Brand and M. B. Rubin. "A constrained theory of a Cosserat point for the numerical solution of dynamic problems of non-linear elastic rods with rigid cross-sections". In: *International Journal of Non-Linear Mechanics* 42.2 (2007), pp. 216–232. URL: https://doi.org/10.1016/j.ijnonlinmec.2006.10.002.

[11] M. Bukowicki and M. L. Ekiel-Jeżewska. "Different bending models predict different dynamics of sedimenting elastic trumbbells". In: *Soft Matter* 14.28 (2018), pp. 5786–5799. URL: https://doi.org/10.1039/C8SM00604K.

[12] M. Calisti, G. Picardi, and C. Laschi. "Fundamentals of soft robot locomotion". In: *Journal of The Royal Society Interface* 14.130 (2017), p. 20170101. URL: https://doi.org/10.1098/rsif.2017.0101.

[13] D. Chalishajar, A. States, and B. Lipscomb. "On applications of generalized functions in the discontinuous beam bending differential equations". In: *Applied Mathematics* 7.16 (2016), pp. 1943–1970. URL: https://doi.org/10.4236/am.2016.716160.

[14] G. Chapman. "Of the movement of worms". In: *Journal of Experimental Biology* 27.1 (1950), pp. 29–39. URL: https://jeb.biologists.org/content/27/1/29.

[15] G. R. Cowper. "The shear coefficient in Timoshenko's beam theory". In: *ASME Journal of Applied Mechanics* 33.2 (1966), pp. 335–340. URL: http://dx.doi.org/10.1115/1.3625046.

[16] K. A. Daltorio et al. "Efficient worm-like locomotion: slip and control of soft-bodied peristaltic robots". In: *Bioinspiration & Biomimetics* 8.3 (2013), p. 035003. URL: https://doi.org/10.1088/1748-3182/8/3/035003.

[17] W. Driesen. *Concept, modeling and experimental characterization of the modulated friction inertial drive (MFID) locomotion principle*. Tech. rep. EPFL, Lausanne, Switzerland, 2008. URL: https://infoscience.epfl.ch/record/121454?ln=en.

[18] G. Falsone. "The use of generalised functions in the discontinuous beam bending differential equations". In: *International Journal of Engineering Education* 18.3 (2002), pp. 337–343. URL: https://www.ijee.ie/articles/Vol18-3/IJEE1303.pdf.

[19] G. Falsone. "The use of generalized functions modeling the concentrated loads on Timoshenko beams". In: *Structural Engineering and Mechanics* 67.4 (2018), pp. 385–390. URL: https://doi.org/10.12989/sem.2018.67.4.385.

[20] J. Gerstmayr, M. K Matikainen, and A. M. Mikkola. "A geometrically exact beam element based on the absolute nodal coordinate formulation". In: *Multibody System Dynamics* 20.4 (2008), p. 359. URL: https://doi.org/10.1007/s11044-008-9125-3.

[21] N. N. Goldberg et al. "On Planar Discrete Elastic Rod Models for the Locomotion of Soft Robots". In: *Soft Robotics* 6.5 (2019), pp. 595–610. URL: https://doi.org/10.1089/soro.2018.0104.

[22] J. Gray and H. W. Lissmann. "Studies In animal locomotion: VII. Locomotory reflexes in the earthworm". In: *Journal of Experimental Biology* 15.4 (1938), pp. 506–517. URL: https://jeb.biologists.org/content/15/4/506.

[23] A. E. Green, N. Laws, and P. M. Naghdi. "A linear theory of straight elastic rods". In: *Archive for Rational Mechanics and Analysis* 25.4 (1967), pp. 285–298. URL: http://dx.doi.org/10.1007/BF00250931.

[24] A. E. Green and P. M. Naghdi. "On thermal effects in the theory of rods". In: *International Journal of Solids and Structures* 15.11 (1979), pp. 829–853. URL: http://dx.doi.org/10.1016/0020-7683(79)90053-2.

[25] A. E. Green, P. M. Naghdi, and M. L. Wenner. "On the theory of rods. I Derivations from three-dimensional equations". In: *Proceedings of the Royal Society. London. Series A. Mathematical, Physical and Engineering Sciences* 337.1611 (1974), pp. 451–483. URL: http://dx.doi.org/10.1098/rspa.1974.0061.

[26] A. E. Green, P. M. Naghdi, and M. L. Wenner. "On the theory of rods. II Developments by direct approach". In: *Proceedings of the Royal Society. London. Series A. Mathematical, Physical and Engineering Sciences* 337.1611 (1974), pp. 485–507. URL: http://dx.doi.org/10.1098/rspa.1974.0062.

[27] A. E. Green and W. T. Zerna. *Theoretical Elasticity*. Second. Oxford: Clarendon Press, 1968.

[28] A. J Hanson and H. Ma. "Parallel transport approach to curve framing". In: *Indiana University, Techreports-TR425* 11 (1995), pp. 3–7. URL: ftp://ftp.cs.indiana.edu/pub/hanson/iucs-tr425.ps.

[29] T. Hidaka, H. Kuriyama, and T. Yamamoto. "The mechanical properties of the longitudinal muscle in the earthworm". In: *Journal of Experimental Biology* 50.2 (1969), pp. 431–443. URL: https://jeb.biologists.org/content/50/2/431.

[30] M. K. Jawed, A. Novelia, and M. O'Reilly O. *A Primer on the Kinematics of Discrete Elastic Rods*. SpringerBriefs in Applied Sciences and Technology. New York: Springer-Verlag, 2018. URL: http://dx.doi.org/10.1007/978-3-319-76965-3.

[31] Y. Kandhari A.and Wang, H. J. Chiel, and K. A. Daltorio. "Turning in Worm-Like Robots: The Geometry of Slip Elimination Suggests Nonperiodic Waves". In: *Soft Robotics* 6.4 (2019), pp. 560–577. URL: https://doi.org/10.1089/soro.2018.0080.

[32] J. B. Keller and M. S. Falkovitz. "Crawling of worms". In: *Journal of Theoretical Biology* 104.3 (1983), pp. 417–442. URL: https://doi.org/10.1016/0022-5193(83)90115-7.

[33] W. M. Kier. "The diversity of hydrostatic skeletons". In: *Journal of Experimental Biology* 215.8 (2012), pp. 1247–1257. URL: https://jeb.biologists.org/content/215/8/1247.

[34] W. T. Koiter. "Couple-stresses in the theory of elasticity, I & II". In: *Philosophical Transactions of the Royal Society of London B* (1969).

[35] J. A Kurth and W. M. Kier. "Scaling of the hydrostatic skeleton in the earthworm Lumbricus terrestris". In: *Journal of Experimental Biology* 217.11 (2014), pp. 1860–1867. URL: https://jeb.biologists.org/content/217/11/1860.

[36] C. Majidi. "Soft robotics: a perspective - current trends and prospects for the future". In: *Soft Robotics* 1.1 (2014), pp. 5–11. URL: https://doi.org/10.1089/soro.2013.0001.

[37] E. V. Mangan, R. D. Kingsley D. A .and Quinn, and H. J. Chiel. "Development of a peristaltic endoscope". In: *Proceedings 2002 IEEE International Conference on Robotics and Automation*. Vol. 1. IEEE. 2002, pp. 347–352. URL: https://doi.org/10.1109/ROBOT.2002.1013385.

[38] A. Menciassi et al. "Design, fabrication and performances of a biomimetic robotic earthworm". In: *2004 IEEE International Conference on Robotics and Biomimetics*. IEEE. 2004, pp. 274–278. URL: https://doi.org/10.1109/ROBIO.2004.1521789.

[39] M. Mofid and J. E Akin. "Discrete element response of beams with traveling mass". In: *Advances in Engineering Software* 25.2-3 (1996), pp. 321–331. URL: https://doi.org/10.1016/0965-9978(95)00099-2.

[40] P. M. Naghdi. "On the formulation of contact problems of shells and plates". In: *Journal of Elasticity* 5.3–4 (1975), pp. 379–398. URL: http://dx.doi.org/10.1007/BF00126998.

[41] P. M. Naghdi. "The Theory of Shells and Plates". In: *Linear Theories of Elasticity and Thermoelasticity: Linear and Nonlinear Theories of Rods, Plates, and Shells*. Ed. by C. Truesdell. Berlin, Heidelberg: Springer-Verlag, 1973, pp. 425–640. URL: http://dx.doi.org/10.1007/978-3-662-39776-3_5.

[42] P. M. Naghdi and M. B. Rubin. "Constrained theories of rods". In: *Journal of Elasticity* 14 (1984), pp. 343–361. URL: http://dx.doi.org/10.1007/BF00125605.

[43] P. M. Naghdi and M. B. Rubin. "On the significance of normal cross-sectional extension in beam theory with application to contact problems". In: *International Journal of Solids and Structures* 25.3 (1989), pp. 249–265. URL: http://dx.doi.org/10.1016/0020-7683(89)90047-4.

[44] S. Neukirch et al. "Vibrations of post-buckled rods: the singular inextensible limit". In: *Journal of Sound and Vibration* 331.3 (2012), pp. 704–720. URL: https://doi.org/10.1016/j.jsv.2011.09.021.

[45] G. E. Newell. "The role of the coelomic fluid in the movements of earthworms". In: *Journal of Experimental Biology* 27.1 (1950), pp. 110–122. URL: https://jeb.biologists.org/content/27/1/110.

[46] O. M. O'Reilly. *Modeling Nonlinear Problems in the Mechanics of Strings and Rods: The Role of the Balance Laws*. Interaction of Mechanics and Mathematics. New York: Springer International Publishing, 2017. URL: http://dx.doi.org/10.1007/978-3-319-50598-5.

[47] O. M. O'Reilly. "On constitutive relations for elastic rods". In: *International Journal of Solids and Structures* 35.11 (1998), pp. 1009–1024. URL: http://dx.doi.org/10.1016/S0020-7683(97)00100-5.

[48] A. A. Orzechowski G.and Shabana. "Analysis of warping deformation modes using higher order ANCF beam element". In: *Journal of Sound and Vibration* 363 (2016), pp. 428–445. URL: https://doi.org/10.1016/j.jsv.2015.10.013.

[49] R. H. Plaut. "Mathematical model of inchworm locomotion". In: *International Journal of Non-Linear Mechanics* 76 (2015), pp. 56–63. URL: https://doi.org/10.1016/j.ijnonlinmec.2015.05.007.

[50] K. J. Quillin. "Kinematic scaling of locomotion by hydrostatic animals: ontogeny of peristaltic crawling by the earthworm Lumbricus terrestris". In: *Journal of Experimental Biology* 202.6 (1999), pp. 661–674. URL: https://jeb.biologists.org/content/202/6/661.

[51] K. J. Quillin. "Ontogenetic scaling of hydrostatic skeletons: geometric, static stress and dynamic stress scaling of the earthworm Lumbricus terrestris". In: *Journal of Experimental Biology* 201.12 (1998), pp. 1871–1883. URL: https://jeb.biologists.org/content/201/12/1871.

[52] S. S Rao. *Vibration of Continuous Systems*. Vol. 464. Wiley Online Library, 2007.

[53] M. B. Rubin. *Cosserat Theories: Shells, Rods, and Points*. Dordrecht: Kluwer Academic Press, 2000. URL: http://dx.doi.org/10.1007/978-94-015-9379-3.

[54] M. B. Rubin. "Numerical solution of two-and three-dimensional thermomechanical problems using the theory of a Cosserat point". In: *Theoretical, Experimental, and Numerical Contributions to the Mechanics of Fluids and Solids*. Springer, 1995, pp. 308–334. URL: https://doi.org/10.1007/978-3-0348-9229-2_17.

[55] M. B. Rubin. "Numerical solution procedures for nonlinear elastic rods using the theory of a Cosserat point". In: *International Journal of Solids and Structures* 38.24-25 (2001), pp. 4395–4437. URL: https://doi.org/10.1016/S0020-7683(00)00271-7.

[56] M. B. Rubin. "On the numerical solution of one-dimensional continuum problems using the theory of a Cosserat point". In: *Journal of Applied Mechanics* 52.2 (1985), pp. 373–378. URL: https://doi.org/10.1115/1.3169056.

[57] M. B. Rubin. "On the theory of a Cosserat point and its application to the numerical solution of continuum problems". In: *Journal of Applied Mechanics* 52.2 (1985), pp. 368–372. URL: https://doi.org/10.1115/1.3169055.

[58] M. B. Rubin. "Restrictions on nonlinear constitutive equations for elastic rods". In: *Journal of Elasticity* 44.1 (1996), pp. 9–36. URL: http://dx.doi.org/10.1007/BF00042190.

[59] M. Runciman, A. Darzi, and G. P. Mylonas. "Soft Robotics in Minimally Invasive Surgery". In: *Soft Robotics* 6.4 (2019), pp. 423–443. URL: https://doi.org/10.1089/soro.2018.0136.

[60] D. W. Schuldt and B. Rife J.and Trimmer. "Template for robust soft-body crawling with reflex-triggered gripping". In: *Bioinspiration & Biomimetics* 10.1 (2015), p. 016018. URL: https://doi.org/10.1088/1748-3190/10/1/016018.

[61] S. Seok et al. "Meshworm: a peristaltic soft robot with antagonistic nickel titanium coil actuators". In: *IEEE/ASME Transactions on Mechatronics* 18.5 (2012), pp. 1485–1497. URL: https://doi.org/10.1109/TMECH.2012.2204070.

[62] S. Seok et al. "Peristaltic locomotion with antagonistic actuators in soft robotics". In: *2010 IEEE International Conference on Robotics and Automation*. 2010, pp. 1228–1233. URL: https://doi.org/10.1109/ROBOT.2010.5509542.

[63] M. K. Seymour. "Locomotion and coelomic pressure in Lumbricus terrestris L". In: *Journal of Experimental Biology* 51.1 (1969), pp. 47–58. URL: https://jeb.biologists.org/content/51/1/47.

[64] A. A. Shabana and M. Patel. "Coupling between shear and bending in the analysis of beam problems: planar case". In: *Journal of Sound and Vibration* 419 (2018), pp. 510–525. URL: https://doi.org/10.1016/j.jsv.2017.12.006.

[65] I. S. Sokolnikoff. *Mathematical Theory of Elasticity*. New York: McGraw-Hill, 1956.

[66] N. Tashiro. "Mechanical properties of the longitudinal and circular muscle in the earthworm". In: *Journal of Experimental Biology* 55.1 (1971), pp. 101–110. URL: https://jeb.biologists.org/content/55/1/101.

[67] N. Tashiro and T. Yamamoto. "The phasic and tonic contraction in the longitudinal muscle of the earthworm". In: *Journal of Experimental Biology* 55.1 (1971), pp. 111–122. URL: https://jeb.biologists.org/content/55/1/111.

[68] S. P. Timoshenko and J. N. Goodier. *Theory of Elasticity*. Third. New York: McGraw-Hill, 1970.

[69] C. Truesdell and W. Noll. *The Non-Linear Field Theories of Mechanics*. Third. Edited, and with a preface, by Stuart S. Antman. Berlin: Springer-Verlag, 2004.

[70] M. Wadepuhl and W.-J. Beyn. "Computer simulation of the hydrostatic skeleton. The physical equivalent, mathematics and application to worm-like forms". In: ().

[71] J. M. Winters. "Hill-Based Muscle Models: A Systems Engineering Perspective". In: *Multiple Muscle Systems: Biomechanics and Movement Organization*. Ed. by J. M. Winters and Savio L.-Y. Woo. New York, NY: Springer New York, 1990, pp. 69–93. URL: https://doi.org/10.1007/978-1-4613-9030-5_5.

[72] A. Yavari, M. Nouri, and M. Mofid. "Discrete element analysis of dynamic response of Timoshenko beams under moving mass". In: *Advances in Engineering Software* 33.3 (2002), pp. 143–153. URL: https://doi.org/10.1016/S0965-9978(02)00003-0.

[73] X. Zhou, C. Majidi, and O. M. O'Reilly. "Energy efficiency in friction-based locomotion mechanisms for soft and hard robots: Slower can be faster". In: *Nonlinear Dynamics* 78.4 (2014), pp. 2811–2821. URL: https://doi.org/10.1007/s11071-014-1627-3.